UNIVERSITA' DEGLI STUDI DELL'INSUBRIA

DOTTORATO DI RICERCA IN BIOTECNOLOGIE,
BIOSCIENZE E TECNOLOGIE CHIRURGICHE
Curriculum Biologia Cellulare e Molecolare
XXIX CICLO

Enzyme functionalized magnetic nanoparticles for biomedical and industrial applications

Nanoparticelle magnetiche funzionalizzate con enzimi per applicazioni biomediche ed industriali

Docente guida: Prof.ssa **Rosalba Gornati**
Tutor: Dott.ssa **Federica Rossi**

Tesi di dottorato di:
Riccardo Balzaretti
Matr. 706924

Dip. Biotecnologie e Scienze della Vita - Università degli Studi dell'Insubria

Anno accademico 2015-2016

TABLE OF CONTENTS

SUMMARY.....4

CHAPTER I – INTRODUCTION.....6

I.I BACKGROUND.....7

I.1 Nanotechnology, Nanomaterials and Nanoparticles.....7

I.2 Magnetic nanoparticles.....8

I.3 Surface Modification of NPs.....10

I.4 NP Interactions with Biological World.....14

I.5 NP Safety and Toxicity.....20

I.6 NP Applications.....23

I.II NP SYSTEMS FOR BIOMEDICAL AND INDUSTRIAL APPLICATIONS.....30

II.1 NP-Enzyme system for cancer therapy: NP-DAAO.....30

II.2 NP-Enzyme system for industry: NP-LASPO.....35

I.III INFLUENCE OF NPs ON STEM CELLS.....38

III.1 Adipose Stem Cells (ASCs).....38

III.2 Cobalt, Iron, Nickel zerovalent NPs.....41

CHAPTER II - SYNTHESIS OF MAGNETIC NP-ENZYME SYSTEM FOR CANCER THERAPY: AN UPGRADE OF THE NP-DAAO SYSTEM 43

II.I Materials and Methods 44

II.II Results and Discussion 55

II.III Conclusions 68

CHAPTER III - SYNTHESIS OF MAGNETIC NP-ENZYME SYSTEM FOR INDUSTRY: THE NP-LASPO SYSTEM 70

III.I Materials and Methods 71

III.II Results and Discussion 74

III.III Conclusions 78

CHAPTER IV - STUDY OF TOXICITY AND INFLUENCE ON DIFFERENTIATION IN ASCs EXPOSED TO NPs 80

IV.I Materials and Methods 81

IV.II Results and Discussion 84

IV.III Conclusions 93

BIBLIOGRAPHY 95

PAPERS 116

SUMMARY

In this work we designed two nanoparticle-enzyme (NP-enzyme) systems: one for medical and one for industrial applications.

The first NP-enzyme system, thought for medical purpose, especially for cancer therapy, is represented by the NP-DAAO system.

Briefly, D-amino acid oxidase (DAAO) is an enzyme that generates reactive oxygen species (ROS) and it is believed of having potential uses as a novel therapeutic molecule if internalized by cancer cells or just localized on their plasma membrane. When conjugated onto iron oxide nanoparticles (NP-DAAO), the enzyme can be magnetically directed to targeted locations with an increased efficacy. Subsequently, ROS production can be initiated by injection of DAAO substrate D-alanine inducing apoptosis of cells surrounding the NP-DAAO complex. Here we described a platform for optimal bioconjugation using monodisperse γ-Fe_2O_3 NPs (~10 nm) resulted in high DAAO loading (24 U/mg NPs), stable NP-DAAO dispersions and more than 90% enzymatic activity recovery, which is retained when NP-DAAO are exposed to human serum. Lastly, we proved its efficacy in killing different tumor cell lines (SKOV-3, U87, and HCT-116) compared to the free enzyme.

The second NPs-enzyme system designed in this study is conceived for industrial application. This NPs-system is composed of Fe_3O_4 NPs conjugated to L-aspartate oxidase (LASPO).

This NP-LASPO system will combine the catalytic activity of LASPO to resolve racemic solution of D,L-aspartate with the possibility to recover and reuse the system once the reaction in the bioreactor is over. Thanks to its magnetic feature, it will be possible to obtain pure end products without the enzyme contamination. In industrial applications this NP-LASPO system will

enable a simpler, faster and cheaper resolution of racemic mixtures of D,L-Aspartate. In this study, we optimized an existing protocol for the LASPO immobilization on NPs changing the parameters of the conjugation reaction. Finally, we improved the NP-LASPO conjugation process by increasing the enzymatic activity recovery from 37.5% up to 134.6%.

Since the application of these NP-enzyme systems, as well as the NPs, can be employed for biomedical and industrial applications, it is necessary to assess their possible toxicity.

In the last part of this work, we started a study on the toxicity of magnetic NPs. We focused on the toxicity of Cobalt, Iron, Nickel zerovalent NPs and the potential influence on the Adipose-derived Stem Cells (ASCs) differentiation process.

A population of hASCs was effectively isolated and characterized by flow cytometry: its stemness was proved by the positivity to CD44, CD90, CD105 and HLA-A,B,C and negativity to CD45 and HLA-DR. Afterwards, the cytotoxicity of CoNPs, FeNPs and NiNPs was assayed on hASCs: CoNPs and NiNPs exert a dose and time dependent cytotoxic effect which is higher compared to FeNPs. Finally, the possible hASCs Adipogenic differentiation induced by CoNPs was evaluated. The morphological analysis pointed out that both CoNPs and $CoCl_2$ were able to speed up the differentiation process. These are preliminary results and we need to investigate in more detail if this process is due to CoNPs or Co^{2+} ions or both these components.

CHAPTER I – INTRODUCTION

I.I BACKGROUND

I.1 Nanotechnology, Nanomaterials and Nanoparticles

In the last years, nanomaterials (NMs) have caught the interest of research communities all around the world. The *Official Journal of the European Union* defined Nanomaterial as "a natural, incidental or manufactured material containing particles, in an unbound state or as an aggregate or as an agglomerate and where, for 50% or more of the particles in the number size distribution, one or more external dimensions is in the size range 1 nm-100 nm"[1]. NMs are distinguished by the number of dimensions between the size range of 1 nm-100 nm: nanofilms (one dimension), nanofibers and nanotubes (two dimensions) and nanoparticles (three dimensions)[2].

Among all the NMs, nanoparticles (NPs) are the most popular. The origin of NPs is various and they can be grouped into two main classes: natural and anthropogenic NPs (Tab. 1).

Tab. 1: The main sources of nanoparticles[3].

Natural	**Anthropogenic**	
	Unintentional	Intentional
Gas-to-particle conversions Forest fires Volcanoes (hot lava) Viruses Biogenic magnetite: magnetotactic bacteria, mollusks, arthropods, fish, birds, human brain, Ferritin (12.5 nm) Microparticles (<100 nm; activated cells)	Internal combustion engines Power plants Incinerators Jet engines Metal fumes (smelting, welding, etc.) Polymer fumes Other fumes Heated surfaces Frying, broiling, grilling Electric motors	Controlled size and shape, designed for functionality Metals, semiconductors, metal oxides, carbon, polymers Nanospheres, -wires, -needles, -tubes, -shells, -rings, -platelets Untreated, coated (nanotechnology applied to many products: cosmetics, medical, fabrics, electronics, optics, displays, etc.)

The field that deals with the design, synthesis and characterization of NMs and nanostructures is called Nanotechnology. One of its purposes is to create new products with properties and functions that differ from the ones of their bulk materials. Such properties are attributable to the increased ratio between the surface area and the number, per given mass, of the NPs; this fact allows a greater chemical reactivity, a higher electrical resistance/conductivity and, potentially, a more pronounced biological activity[3]. NMs are now widespread from industrial applications, such as catalyst[4], sensors[5] and photovoltaic devices[6], to agriculture[7,8], food safety[9,10] and cosmetics[11,12]. Some of the numerous nanoparticles applications[13] are reported in Fig.1.

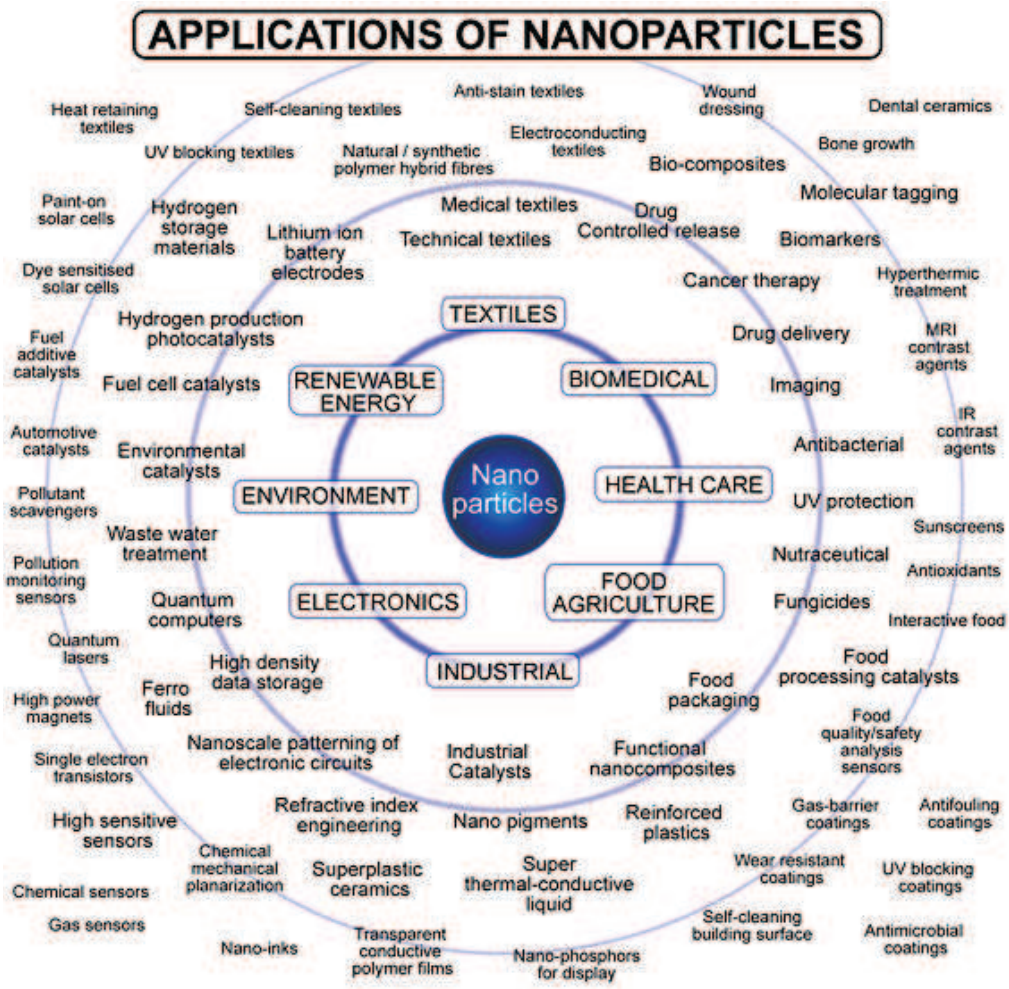

Fig. 1: **O**verview of the nanoparticle applications[13].

I.2 Magnetic nanoparticles

Besides their small size and different chemical activity from their bulk materials, NPs are very interesting also because of their magnetic properties. These particular properties, acquired when the particles size diminishes to the nano level, are due to an increased role of the surface spins. It was observed that some non-magnetic elements, such as Pd and Pt, present magnetic-like properties at the nano-size[14].

From the beginning of the new millennium, magnetic NMs are considered to overcome some technical limits like data recording and storage[15–17]. NMs helped also to update existing biomedical techniques such as magnetic resonance imaging (MRI), which exploits magnetic NPs as contrast agents to diagnosis[18,19], and more and more often for both diagnosis and therapy as theragnostic agents[20–22].

One of the most versatile groups of magnetic nanoparticles that can be employed in almost every application field is the one of the Iron Oxide Nanoparticles (IONPs). Among them, Superparamagnetic IONPs (SPIONs) are the leaders for biomedical applications mainly due to their biocompatibility and the large possibility of customization[23,24].

SPIONs present an iron oxide core that can be coated by either inorganic and/or organic materials. The most noticeable aspect that renders SPIONs a suitable candidate for numerous applications is their inducible high magnetization when exposed to an externally applied magnetic field: that allows heating or targeting them to the area of interest, for instance a tissue[25]. However, when exposed to the oxygen present in the air, these NPs can be oxidized resulting in a partial loss of their magnetic behaviour. Hence, it is necessary to create specific coatings to stabilize NPs to avoid their surface oxidation[26]. The coating molecules often merely act as a barrier to

protect the NPs against external agents; otherwise, it happens that they may drastically affect the electronic properties of the NPs. Therefore, the modification of the NP surface by covering their surface atoms with specific molecules plays a crucial role in the stabilization of the system by minimizing their energy[14].

I.3 Surface Modification of NPs

During the last decade researchers were pushed to study new structures of material and inorganic/organic compounds able to ensure more and/or new performance characteristics. These efforts resulted in several types of NP architectures with different core/shell arrangements, especially for IONP[24] (Fig.2) which meet the needs of almost every application.

Up to now, there is a very high number of organic and inorganic compounds for NP functionalization and coating. These compounds can be used to improve the NP biocompatibility and/or chemical stability but also to tune their dispersibility and solubility in water or other solvents. Especially for IONPs, these agents endow to iron oxide new physicochemical properties, such as magneto-optical, magnetic-electrical properties and magnetic-thermal properties[26].

Coating compounds can be divided in:

- Organic coatings like small organic molecules or surfactants, biomolecules and polymers.
- Inorganic coatings like silica layer, metal/non-metal elements and metal oxide/sulfide.

The protecting shells are often used not only to stabilize the NPs but also as a platform to further other functionalization processes in which, for instance, the NP core is covered by an inorganic coating and then again

functionalized with an organic one. These multiple functionalization processes are essentials to build up personalized NPs: that allows designing the suitable final NP for the task planned for it.

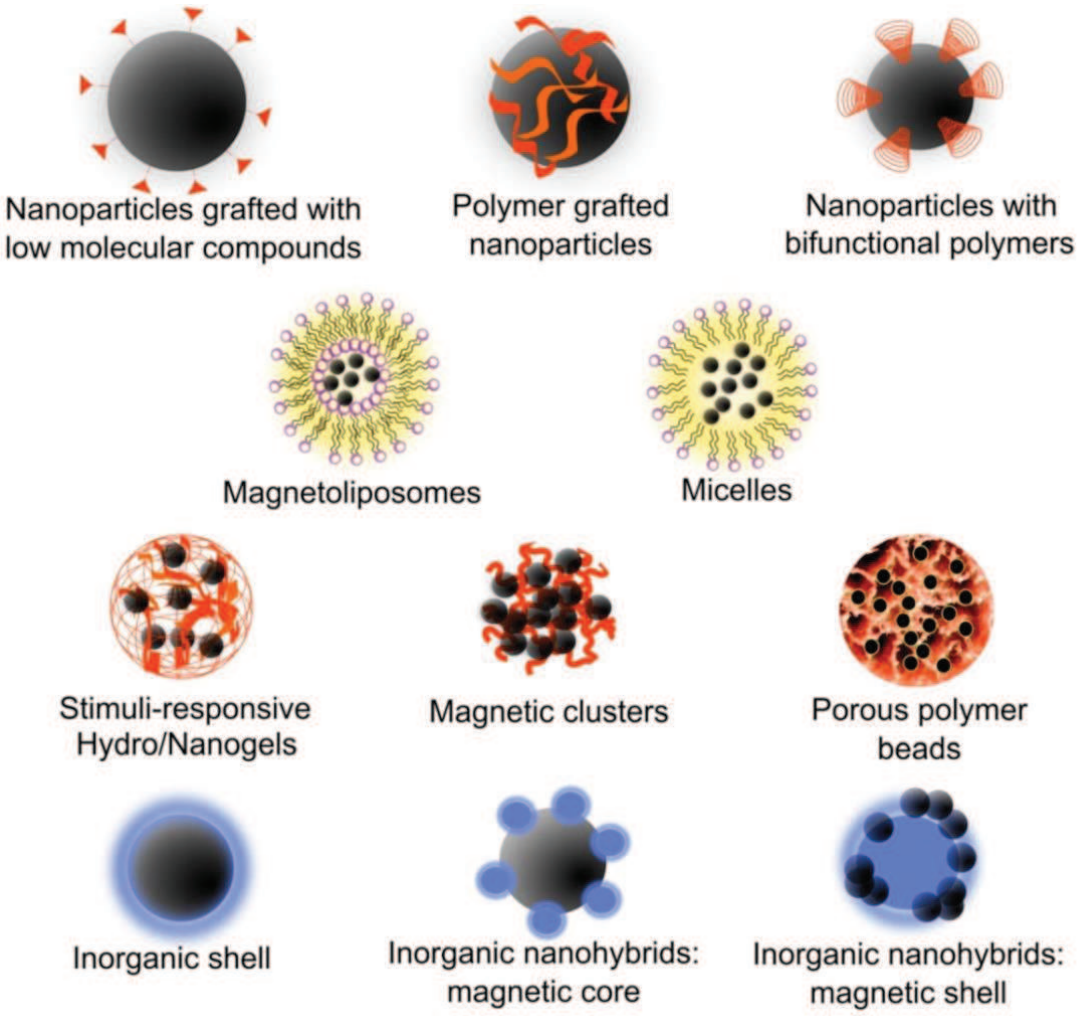

Fig.2: General types of IONP arrangements with molecules, polymers and inorganic chemicals (not in scale)[24].

Another helpful method to group IONPs for biotechnological application is to cluster them depending on the functional end-group they present on their surface. Some of the most used coating/functionalization compounds for IONPs are reported in Tab.2.

Tab.2: Polymers and organic molecules (sorted by functional group) typically used for the primary coating and/or stabilization of IONPs.

Chemical end-group	Compound
-OH	-Polyethylene glycol -Dextran -Polyvinylalcohol
-COOH	-Polyacrylic acid -Carboxymethylcellulose -Polyethylene glycol with terminal -COOH -Alginate -Polymethacrylic acid -Citrate
-NH_2	-Chitosan -Polyethylenimine -Poly(L-lysine) -Polyethylene glycol with terminal -NH_2 -Ethylenamine -Aminosilane

One of the most used functionalization compounds is the silane-like group. The hydrolysis/condensation reactions of these compounds lead to the formation of silane coating all around the NPs with their functional end-group oriented towards the external environment. The easy-controlled reaction, the large number of commercially available silane coupling agents and the well-documented chemistry represent three of the many advantages of the silane-like compounds; in addition, their high surfaces coverage and their strong binding, ensured by the functional groups, lead to a very stable core/shell structure. Among the silane compounds, the APTES (3-Aminopropyltriethoxysilane) is of great interest[27] (Fig.3).

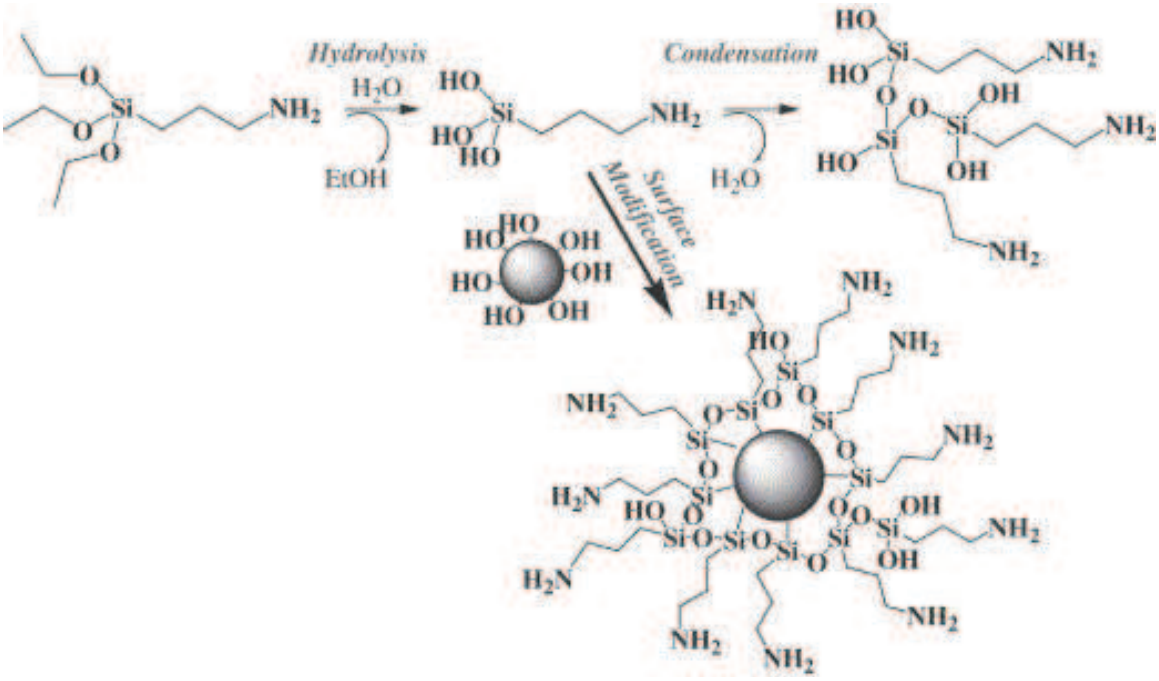

Fig.3: APTES structure. The APTES hydrolysis and condensation in water form a silane polymer that reacts with NPs.

When APTES is dissolved in water, with a little amount of ethanol, hydrolyzes and condensates to form a silane polymer. During the hydrolysis reaction, the alkoxide groups ($–OC_2H_5$) are replaced by hydroxyl groups (-OH) to form reactive silanol groups. These silanol groups condense one with the other to produce siloxane bonds (Si–O–Si) and in the meantime with the -OH present on the NPs surface to produce NP-O-Si bonds. Thus, the APTES amino group ($-NH_2$) remains free to bind other molecules[28].

Regarding the biomedical applications, in the past 30 years many biomolecules were conjugated to the functionalized NPs such as DNA, RNA and oligonucleotides (i.e. ssDNA/RNA, dsDNA/RNA), peptides, enzymes, carbohydrates, antibodies, tumor markers, fluorescent dyes, polymers (i.e., PEGs), drugs and so on[29] (Fig.4). Finally, one of the actual aims is to create innovative multifunctional NPs able to carry on their surface several biomolecules with different functions (i.e., theragnostic agents).

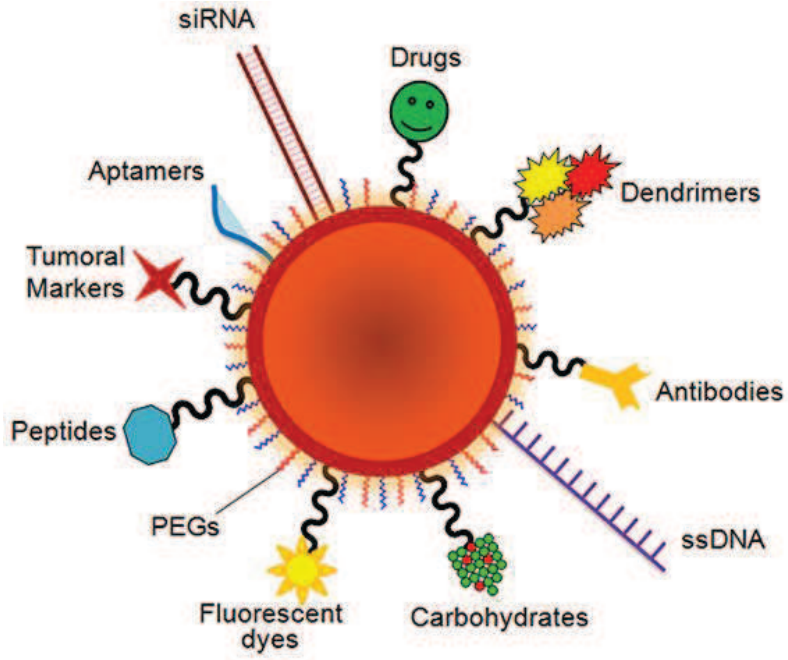

Fig 4: Schematic representation of a multifunctional NP able to act as a carrier of various biological molecules[29].

I.4 NP Interactions with Biological World

When NPs are spread into the surrounding environment, they are subject to an uncountable number of interactions with various chemical and physical agents that will sign their fate. It is evident how the aquatic and terrestrial environments are potentially endangered. Humic substance present in water and soil, also known as natural organic matter (NOM), is the one that most readily interact with the NPs released into the environment[30].

In order to prevent the damage to the ecosystems, we must be aware of the specific features of the NP released into the environment: each chemical/physical variable of the NP itself, or the media in which is exposed, can influence its integrity and finally the ability to interact with other molecules. Indeed, whilst molecules are metabolized in short or at least in long term exposure, non-stabilized NPs can rapidly form aggregates and, in

long term exposure, are able to dissolve themselves in ions or to lose their stabilizing coating[31] (Fig.5).

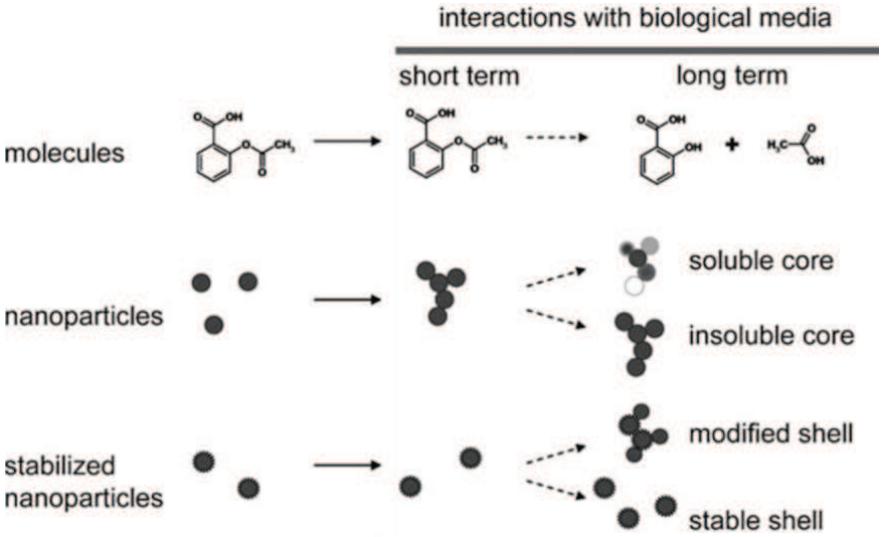

Fig.5: Inside the organism the fate of molecules is mainly signed by degradation and metabolism processes. Regarding NPs,it is difficult to predict it because of their agglomeration behaviour that affects the NP mobility, biodistribution, and clearance. Even stabilized NPs during long-term exposure in biological media can become unstable through chemical modification or loss of surface functionality[31].

There are many ways by which NPs may enter the human body[31]: inhalation, ingestion, penetration through the skin and injection into the blood stream. Once inside the body, NPs interact with the biomolecules present in biological fluids (interstitial fluid between cells, lymph or blood) resulting in the adsorption by most of them onto the NP surface in the so called "biomolecular corona". The structure and composition of that "biomolecular corona" depend on the nature of the physiological environment (blood, interstitial fluid, cell cytoplasm, etc.), the physicochemical properties of the NP (size, shape, composition, surface functionalization and charges) and the duration of exposure[32]. For instance, proteins followed by a small amount of

lipids mainly characterize the biomolecular corona composition of NPs exposed to blood plasma. This protein absorption is guided by the binding affinities between the NP and the proteins: that binding affinities can be very strong and stable leading to the formation of the “hard” corona or weak and loosely with the formation of the “soft” corona (Fig.6).

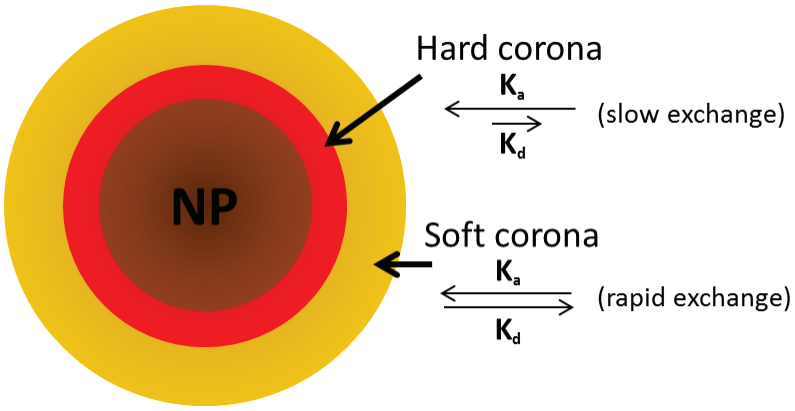

Fig.6: Simplified illustration of a NP with soft and hard protein corona. The exchange time and lifetime of the proteins in the corona is determined by their rate of adsorption (K_a) and desorption (K_d). The different protein composition forming the hard/soft corona often results in a very complex system of proteins.

Reassuming, the biomolecular corona is a highly variable platform of adsorbed biomolecules onto the NP surface: it represents, at the end, the peculiar biological "fingerprint" of each NP. As a consequence, the specific NP protein corona is responsible to interface towards the receptors located on the cell plasma membrane. This process is very important during the NPs cell uptake from the bloodstream and the following redistribution from one cellular compartment to another[33]. Once NPs are injected into the bloodstream they are immediately coated with blood plasma proteins enabling an opsonisation process that renders them more susceptible to be identified and removed by phagocytic cells of the reticuloendothelial system

(RES): that represents one of the most arduous hurdles to overcome for biomedical application. Hence, to elude the RES, the NP surfaces can be coated with natural or synthetic polymers allowing a prolonged circulation in the biological fluids[34]. A new and innovative approach, inspired by the concept of molecular biomimetism, is based on the self-recognition of homologous erythrocytes, red blood cells (RBCs), to bypass the RES checkpoints. This approach exploits the great variety of proteins residing on the RBCs membrane[35,36] to coat on the NPs surface making it similar to natural RBCs[37]: the main advantage is the possibility to escape the RES allowing a prolonged systemic circulation[38–40] (Fig.7).

The results obtained through the RBCs membrane coating for NPs functionalization have demonstrated their validity to connect the properties of natural cell membrane components with those of NPs.

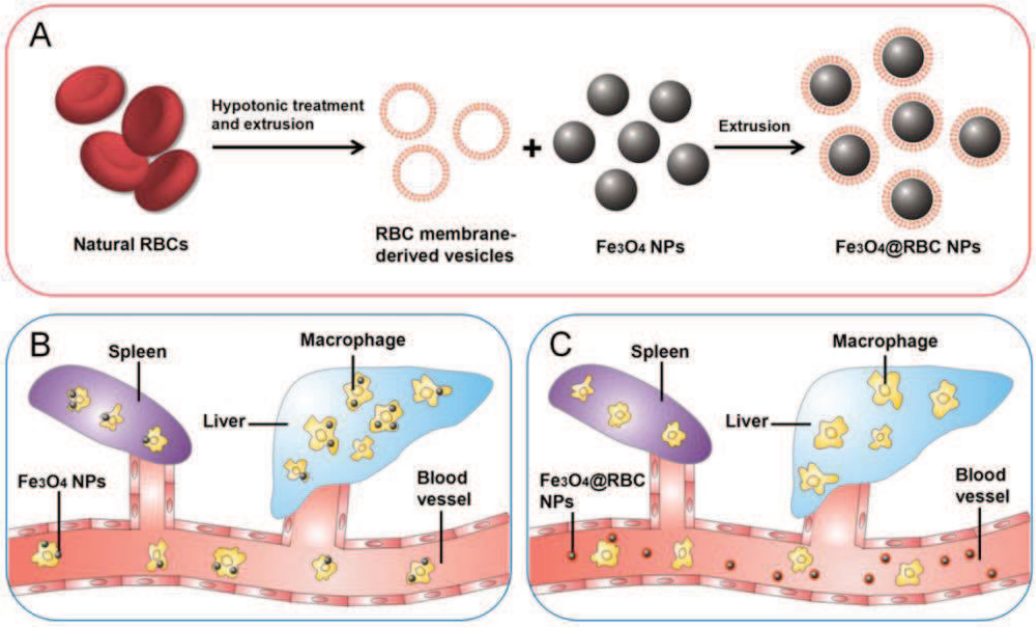

Fig.7: (A) Simplified preparation procedure of RBC membrane-camouflaged Fe_3O_4 NPs (Fe_3O_4@RBC NPs). (B) Uncoated Fe_3O_4 NPs are quickly removed by the RES (e.g., peripatetic macrophages and macrophage-rich organs: liver and spleen). (C) Fe_3O_4@RBC NPs can escape the RES uptake[41].

As previously reported, the NPs can enter the human body by different ways and eventually interact directly with cells. Thus, it is possible that NPs can cross the cell plasma membrane mainly by five different pathways: clathrin/caveolae-mediated endocytosis[42,43], phagocytosis[44], macropinocytosis[45], pinocytosis[44] and non-endocytic way[46,47]. Afterwards the internal vesicular transits, NPs can be exocyted via three pathways: lysosome secretion[48], vesicle-related secretion[49], and non-vesicle-related secretion[42,49]. These NPs endocytosis and exocytosis mechanisms are briefly resumed in Fig.8.

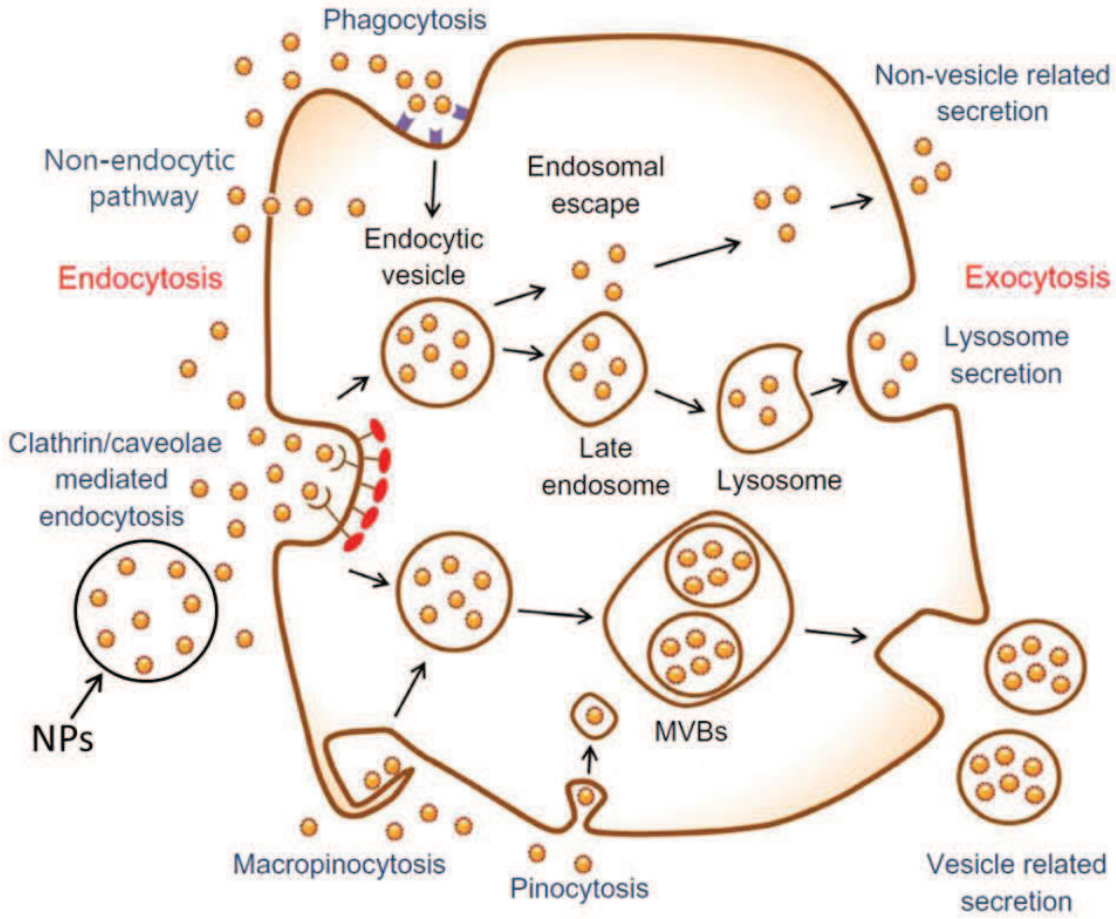

Fig. 8: Scheme of the endocytosis and exocytosis patterns of nanoparticles[42]. MVBs, multivesicular bodies.

Endocytosis, intracellular distribution and exocytosis are either modulated by the physicochemical properties of NPs such as size, shape, surface charge and functionalization[33], but also by cell-specific parameters such as cell type or cell cycle phase[50]. During the NP intracellular transit/storage it can happens that, depending on the NP feature[51,52], a part or the whole NP, including its core, the surface layer and the biomolecular corona, may be modified, removed or metabolized. The main mechanism through which the NPs are removed from the body is via the renal clearance pathway[53].

I.5 NP Safety and Toxicity

The NPs toxicity depends on their physicochemical features: size, composition, reactivity, mobility, stability, surface charge and chemistry, agglomeration/aggregation, storage medium and time[54,55].

As mentioned in the previous section, NPs can enter the body via different ways, reach and flow into the blood stream and, at the end, get into the cells. Moreover, it has been observed that NPs are also able to overcome biological barriers and to biodistribute among different organs based on their physicochemical nature[56] (Fig. 9).

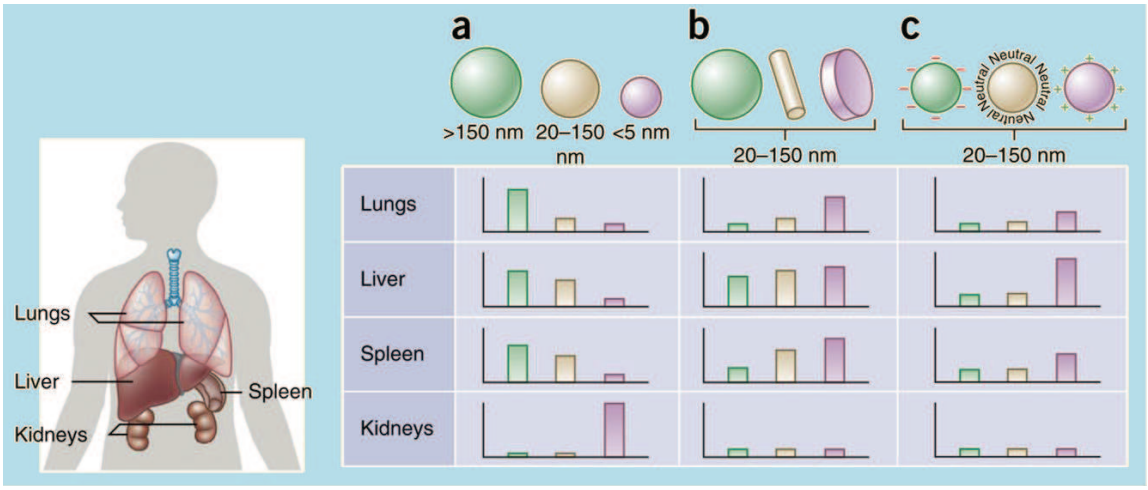

Fig.9 The size (a), shape (b) and surface charge (c) dictate the NPs biodistribution among different organs including the lungs, liver, spleen and kidneys[56].

Once inside the cell, NPs generally exert toxicity through two different, but sometime correlated, mechanisms: the generation of reactive oxygen species (ROS) and the NP dissolution into toxic ions[57,58]. Either the mechanisms are responsible for several cytotoxic effects such as DNA damaging and mitochondrial membrane disruption[57,59–61].

Iron

Many studies report IONPs as highly biocompatible with very low toxicity[62–67]. IONPs of 8.9 nm width assayed on two human epithelial cell lines (A549, Caco2) and murine fibroblasts (Balb/c 3T3) showed a very low cytotoxicity only at the highest concentration tested (100 µg/mL)[64]. In another study a similar cytotoxic results were observed exposing A549 cells to 80 µg/mL IONPs[65]. Furthermore, also some IONP surface coatings are helpful to reduce the NPs toxicity and promote cellular uptake[66].

An often ignored or underestimated aspect of IONPs is the surface passivation which incredibly reduces the NP toxicity by erasing the surface reactivity[67].

Although, some recent reviews place the doubt on IONPs safety because of their contradictory results[68–70], demanding more detailed analysis to assess deeper:

- *in vitro* aspects such as the cellular effects, ROS generation, ions release and genetic effects.
- *in vivo* aspects such as the toxicokinetics, acute toxicity, genotoxicity, neurotoxicity, immunotoxicity and reproductive toxicity.

These future studies will be helpful to fill the main gaps of knowledge in the IONP safety and toxicity fields.

Silver

Silver NPs (AgNPs) are the best example of NP toxicity related to ROS generation and ions release. It was demonstrated that small-size (15 nm) Silver NPs (AgNPs) generate 10 fold more ROS than large-size AgNPs (30-55 nm), that makes smaller NPs more toxic compared to larger ones [71]. Another

study proved that the size-dependent cytotoxicity of AgNPs in human lungs cells was due to the Ag ions release from the NPs into the culture media[72]. This study supported the theory of the so called 'Trojan horse effect' by which the NPs cellular uptake increases the concentration of toxic ions following the natural or enhanced by lysosome acid pH NP dissolution[73] (Fig.10). Other researchers observed that different-shaped AgNPs affect the cells viability in a different way[74]. Finally AgNPs were proved to induce inflammation, genotoxicity, cytotoxicity and developmental toxicity[57].

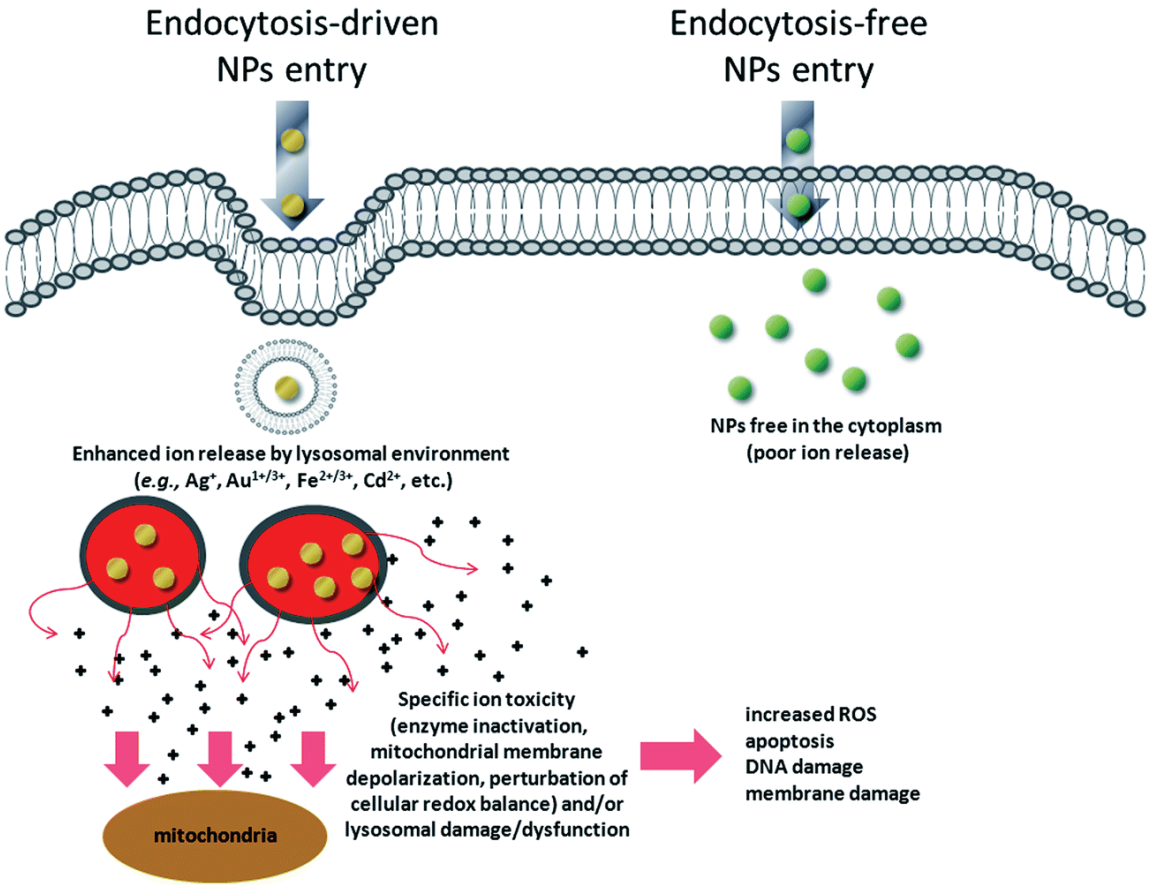

Fig. 10: Schematic representation of the Lysosome-Enhanced Trojan Horse effect (LETH effect) in which the active internalization mechanisms of NPs leads to an intracellular increase of toxic ions if compared to endocytosis-free NPs[73].

I.6 NP Applications

There are many fields in which NP applications thrive and most of them are listed in Fig.1. In biotechnology, a new branch of nanotechnology called nanobiotechnology has arisen to deals with the NP study and applications combined to biological world. The nanobiotechnology research aims to develop simple, safe and useful NP applications especially for biomedicine and industry.

Industrial Applications

NPs are employed in almost every industry fields from electronics to chemicals, from engineering to energy[75].

In construction industry, NPs are used to improve the mechanical features of many materials. For instance, the concrete can increase its compressive strength by more than 15% when nickel NPs are added. Another example are silica NPs which are employed as an antireflection coating on windows allowing to control the exterior light and to reduce the energy loss following air conditioning[76].

Among all these applications, in industry-related nanobiotechnology, the enzyme biocatalysis has elicited much interest. In particular NPs were seen as a solution to overcome the limitations of the enzyme-efficiency-determining factors[77].

Enzyme Biocatalysis

Enzymes are the most efficient and versatile catalyst[78]. They often win the challenge against chemical catalyst by offering more competitive processes.

Chemical and pharmaceutical industries use the enzymes biocatalysis to produce various chemical and biological substances because enzyme-based

processes usually lead to a reduction of reaction steps and, consequently, to a saving of time and waste[79].

The specific chemoselectivity, regioselectivity and stereoselectivity of enzymes demonstrate their superiority in the industrial production of enantiomerically pure compounds[80]. Besides organic synthesis, the enzyme biocatalysis is also helpful in many areas of research[81], including immunoassays[82] and substrate sensing[83].

However, despite the great potential in industrial applications, the use of free enzymes presents several drawbacks such as: thermal instability, activity inhibition, protease digestion, denaturing agents sensitivity and the impossibility of separating/reusing the enzyme at the end of a reaction. To overcome such limitations, researchers attempted parallel approaches like the screening of enzymes from natural sources, random mutations and immobilization on different substrates[84–86].

In this view, the enzyme immobilization for industrial applications aims to[87]:

- improve the enzyme overall stability
- increase the volume loading of specific biocatalyst
- simplify the biocatalyst recycling and the downstream processing

Immobilized enzymes have the advantages of a larger pH working range, an improved thermal stability and an easier separation from the bioreactor[88]. Other advantages are the enhanced enzyme activity, the modification of substrate selectivity/enantioselectivity and the multi-enzyme reaction[89–91]. Among all the various scaffolds used for enzyme immobilization, NPs provide interesting features (minimal diffusional limitation, maximum surface area and high effective enzyme loading) to be tailored combined with those of enzyme[91,92]. Such “nanobiocatalyst” can load a much higher

amount of enzyme, enhancing significantly the mass transfer efficiency, if compared to enzyme immobilized on micrometric supports[93].

During the last years, magnetic NPs have received increasing attention due to their magnetic characteristics which facilitate their recovery by using a magnetic field[94,95]. IONPs, for instance, have aroused great interest in biodiesel production[96] and food processing because of their biocompatibility and cheapness [97].

Medical Applications

The application of NPs in medicine is called Nanomedicine[98]. The NPs currently used in nanomedicine include liposomes, polymeric micelles, inorganic and polymeric NPs, nanorods and quantum dots. The medical applications of NPs range from diagnosis to drug/gene delivery, from therapy to tissue engineering[29,99,100]. As mentioned before, the customizable characteristics of NPs allow them to cross biological barriers such as the blood brain barrier (BBB) that is impermeable to almost every drugs but not to the ones conjugated to NPs[101–103].

Once injected into the blood stream, the NPs have to be attracted to the target tissue in order to carry out their tasks.

There are three ways to localize IONPs into the cancer tissue [21]:

- Passive Targeting: this strategy takes advantage of the peculiar physiology of tumor in respect of normal tissue (Fig.11 A). The passive targeting requires NPs with a diameter below the 200 nm able to accumulate into the tumor tissues exploiting their enhanced permeability and retention (EPR). Tumors often present an enhanced permeability of vessels with a little lymphatic drainage, leading to a passive accumulation and retention of NPs with prolonged

circulation times (EPR effect). The disadvantage of this strategy is that it is possible to be applied only in certain types of tumors.

- Active Biological Targeting: this procedure involves the NP surface functionalization with specific biomarkers able to recognise the tumors by targeting tumor cells (Fig.11 A). These biomarkers include small organic molecules, peptides, proteins and antibodies that are complementary to unique receptors, present or overexpressed, on the external surface of tumor cells plasma membrane. However, the synthesis of these targeting agents is expensive and needs high knowledge in chemistry.
- Active Magnetic Targeting: this technique enables the NPs accumulation by applying external magnetic field on the target site (Fig.11 B). Unfortunately, since the magnetic field strength decreases with the distance from the magnet, the efficacy of this kind of targeting is limited to the tissues close to the body's surface.

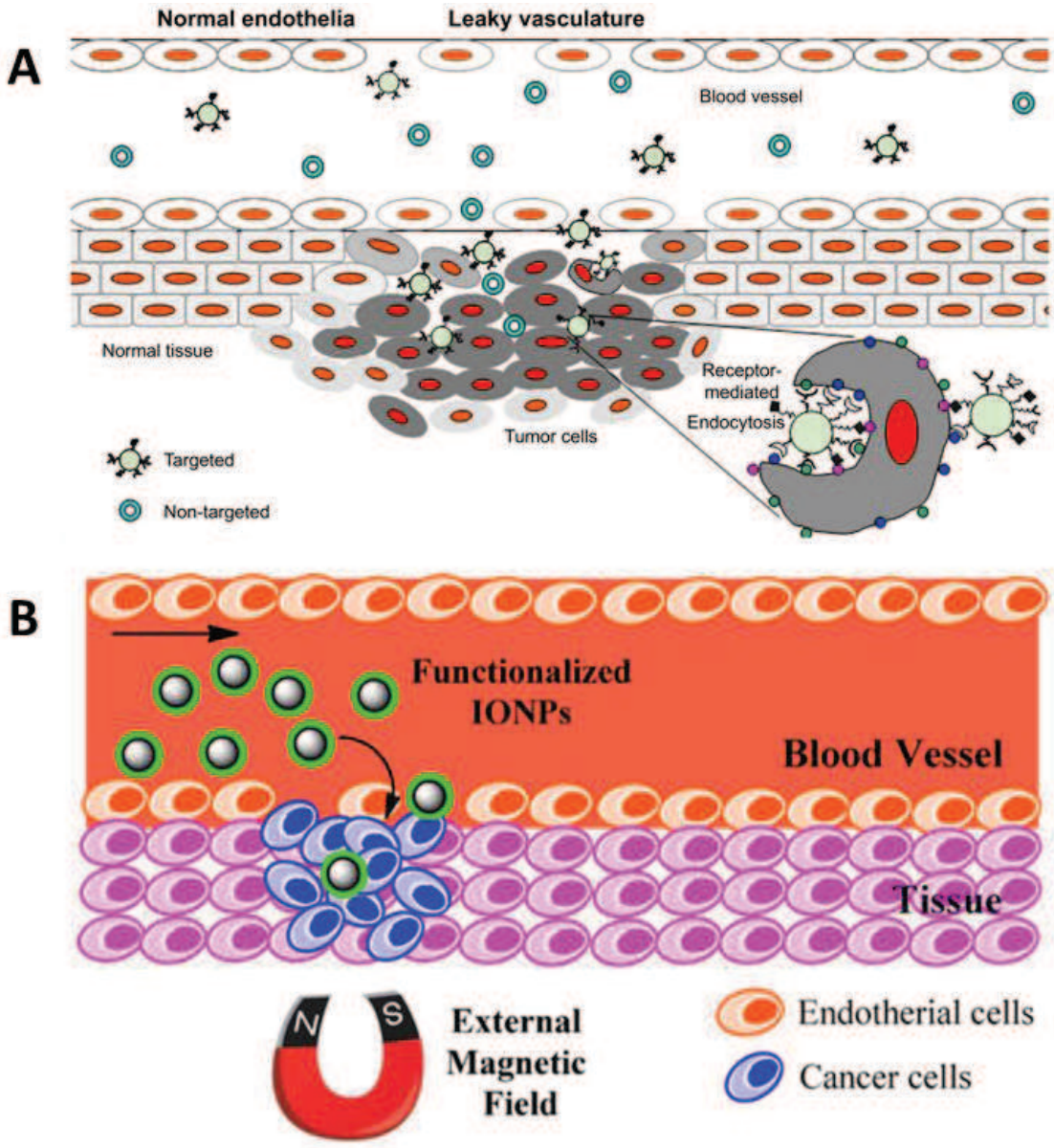

Fig.11: Different modalities of IONPs tumor targeting: passive and active biological targeting[104] (A) and active magnetic targeting[105] (B).

Unfortunately, despite the mechanism of targeting, about the 99% of all administered NPs are sequestered and/or eliminated by the RES and the renal system[53]. During the last 30 years, only few strides were made to solve this problem suggesting to give priority on the NP delivery studies before undergoing to the clinical testing[53]. Hence, the NP targeting and delivery to

malignant tissue (e.g. tumours) still remain a great challenge in nanomedicine.

Theragnosis

Among the different medical applications, the possibility given by magnetic NPs to combine diagnosis with therapy has led to the development of theranostic agents[106]. In this regard, gadolinium-based NPs, that were used as positive contrast agents for MRI, now may act as therapeutic agent for neutron capture therapy or radiosensitization[18]. Beside gadolinium-based NPs, the IONPs are widely used as theranostic agents thanks to their magnetic features and the availability of many functionalization biomolecules allowing to pursue different aims[24,107,108]. Especially for *in vivo* treatments, IONPs magnetic properties can be employed in three main groups of applications[105]: drug delivery, MRI contrast agents, hyperthermic/photoresponsive agents. For cancer theranostic applications of IONPs these three groups are often enclosed in a single and multitasking system[20] as shown in Fig.12. IONPs can act as an effective anticancer loading platform for targeted drug delivery (TDD) to carrier a wide range of molecules[109–111]. Furthermore, the IONPs magnetic aspects make them perfect for hyperthermia and thermoablation[105,112]. In these two techniques, the heat produced by IONPs when exposed to an external alternating magnetic field is used to induce necrosis in cancer cells. Together with hyperthermia, IONPs find also application as a photo-thermal therapeutic agent (PTA) in NIR photothermal therapy for efficient ablation of tumors[113].

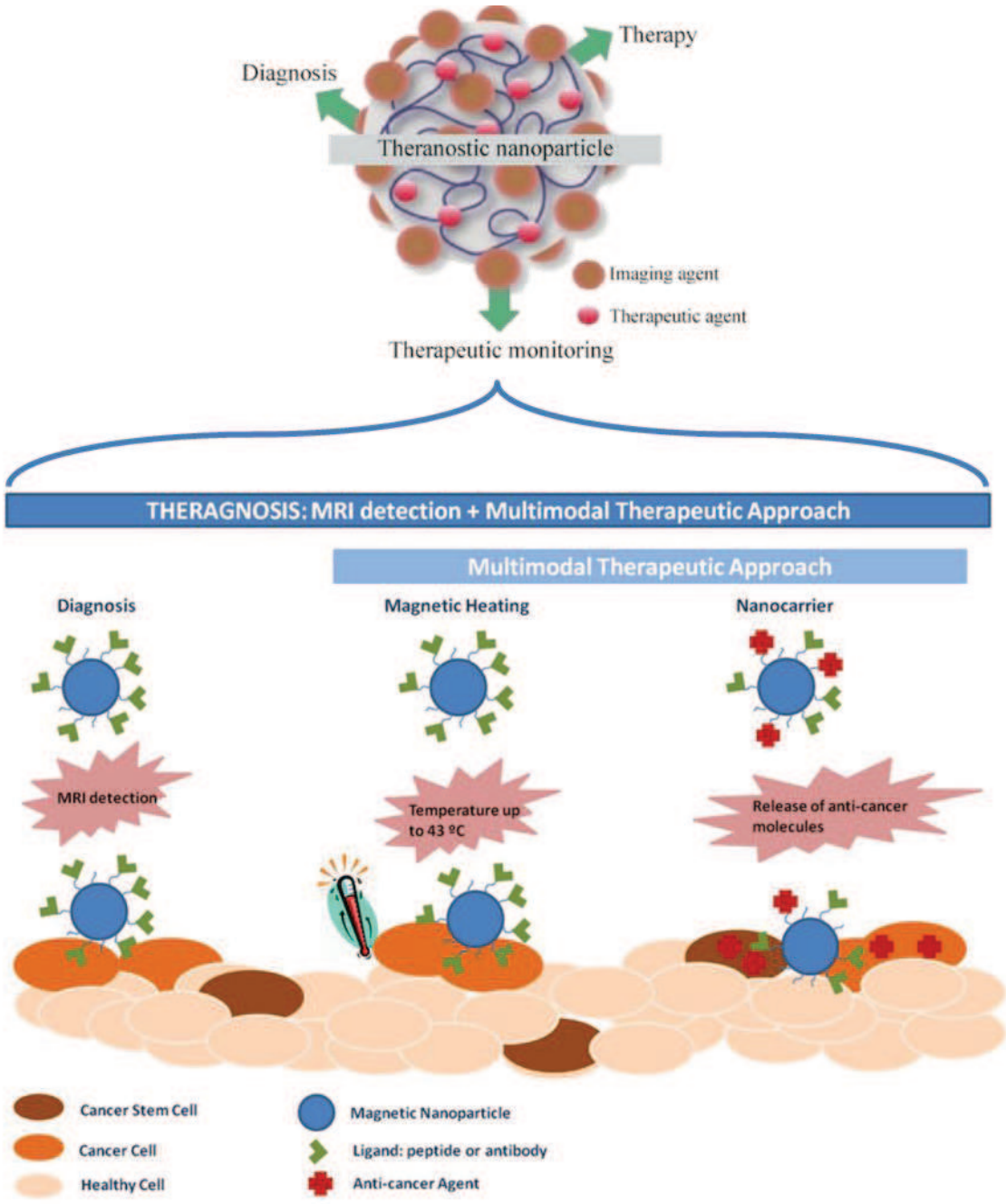

Fig.12: Example of magnetic nanoparticle for theranostic applications[20,114]

I.II NP SYSTEMS FOR BIOMEDICAL AND INDUSTRIAL APPLICATIONS

II.1 NP-Enzyme system for cancer therapy: NP-DAAO

The first part of this work proposes an improvement of the magnetic nanoparticle-enzyme system (NP-DAAO) preparation previously proposed by *Bava et al.*[115] and subsequently upgraded by *Cappellini et al.*[116]. This magnetic nanoparticle-enzyme system, thought for cancer therapy, utilizes magnetic IONPs conjugated with the enzyme D-amino acid oxidase (DAAO) to produce reactive oxygen species directly in a tumor, with the aim of reducing side effects and improving the patient's life quality.

What we tried to do in this study is to combine the advantages of IONPs with those of DAAO, minimizing their disadvantages such as the low preservation of DAAO activity and storage instability at 4°C. Thanks to the magnetic characteristics of the IONPs and their ability to cross biological barriers[103], it will be possible to localize this system, after injection into the blood stream, directly into the cancer mass with the help of an external magnetic field given by a powerful magnet (Fig.12 b). Once there, the injection of D-Alanine (one of the DAAO substrates) will produces H_2O_2 that will cause the death of the surrounding tumorigenic cells via apoptosis. In order to understand whether these particles can be used for nanomedicine purposes, it is important to optimize their synthetic route and to evaluate their toxicity on different cell lines.

DAAO

DAAO (EC 1.4.3.3) is a FAD-dependent enzyme that catalyzes with a high stereospecificity the oxidative deamination of D-amino acids to give α-keto acids and ammonia. Then oxygen, the terminal redox acceptor, reoxidizes the FAD cofactor previously reduced giving hydrogen peroxide[117](Fig.13). Putative DAAO genes are present in all kingdoms but not in the plants, among which *Chlorella vulgaris* represents the only exception[117].

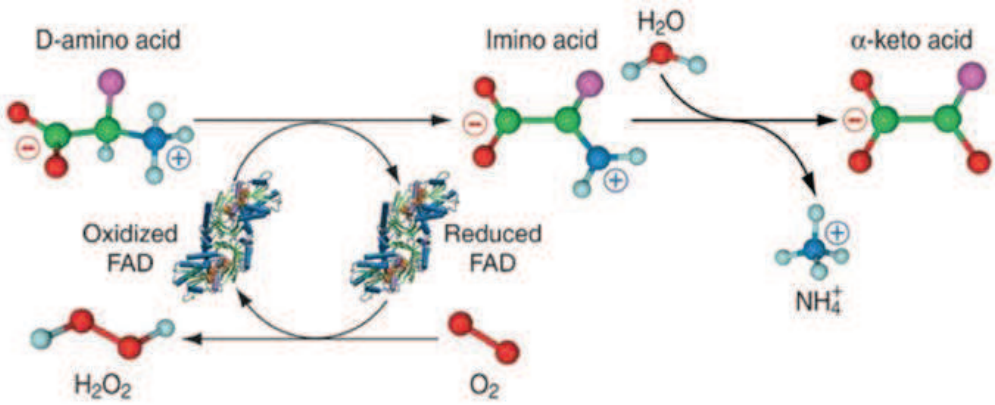

Fig. 13: Scheme of the DAAO reaction with D-amino acids to give α-keto acids, ammonia and H_2O_2[117].

DAAO in Prokaryotes

In prokaryotes, it has been found a similar DAAO enzyme called D-amino acid dehydrogenase (DAAdH EC 1.4.99.1). DAAdH is a flavoenzyme that oxidizes neutral D-amino acids, in particular D-Ala, into the corresponding α-keto acids. The DAAdH of *E. coli* is a heterodimer with two different subunits: the smaller one of about 45-kDa contains the FAD as coenzyme that transfers the two electrons received from the substrate to the sulfur-iron centre of the larger one of 55-kDa that eventually reduces the coenzyme Q. One interesting feature of DAAdH is that its oxidation processes do not involve the O_2 reduction to avoid a dangerous ROS

overproduction. The DAAdH is located in the periphery and is considered associated with the bacterial inner cell membrane. In bacteria, its known roles are mainly two: the first regards the energetic metabolism and the second involves the prevention of the inhibitory effect given by overconcentration of D-amino acids on bacterial growth[117].

DAAO in Eukaryotes

In eukaryotic organism, DAAO is a peroxixomal enzyme involved in the D-amino acids metabolism. Its peroxisomal location allows an efficient scavenging of the H_2O_2 produced during the oxidation reaction of D-amino acids. The D-amino acids may come from endogenous or exogenous sources and, once oxidized in the corresponding α-ketoacids, they can be used directly for the cell energetic metabolism or converted into L-amino acids and integrated into the proteins. However, if the D-amino acids are present in high concentration (>1 mM), the DAAO metabolic ability is not fast enough to prevent their accumulation into the tissues: that causes an extensive and serious damage e.g. the suppression of synthesis of some important enzymes and retardation of growth[118]. A very important DAAO role is to maintain physiological D-serine levels in the different brain tissues. D-serine is one of the most important regulators of the N-methyl-D-aspartate (NMDA) receptors whose dysfunction, due to erroneous DAAO gene expression, is one of the multiple causes that lead to schizophrenia disease[117]. Furthermore, a low DAAO activity was found in kidney and liver tumor cells if compared to healthy ones: that parameter could result useful for the early detection of tumors in these organs[119].

Among all the eukaryotic DAAO, the one from the yeast *Rhodotorula gracilis* (RgDAAO) represents a very interesting protein because of its high turnover

rate and FAD binding stability[120]. RgDAAO is a quite stable homodimer in which each subunit binds non-covalently the FAD cofactor. The primary structure of the single monomer consists in 368 amino acids corresponding to 40076 Da[117]. The secondary structure is composed by 11 α-helices and 13 β-sheets. At the N-terminus, there is the FAD-binding domain consisting in a βαβ motif that envelops the FAD and buries it inside the protein. The C-terminus, involved in the head-tail monomer dimerization, contains a unique loop of 21 amino acids that is not found in other known DAAO sequences. The dimerization occurs through the electrostatic interactions between the positively charged residues on the βF5-βF6 loop of one monomer and the negatively charged ones belonging to the α-helices I3' and I3'' of the other monomer[117] (Fig. 14) leading to a dimer of 80 kDa.

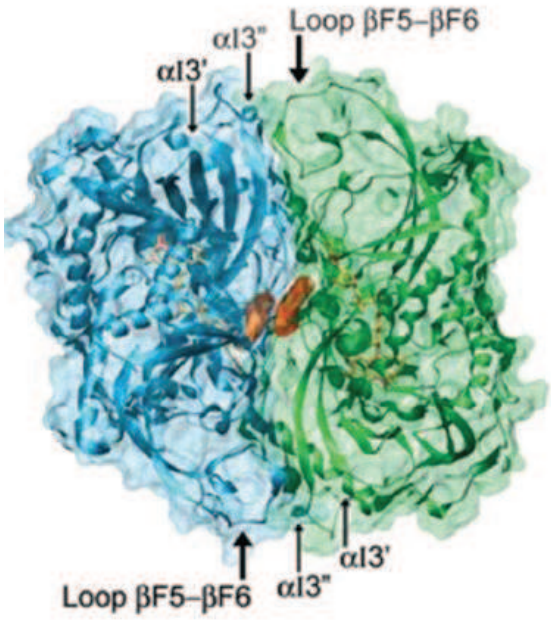

Fig. 14: RgDAAO homodimer with the typical head-to-tail interaction of the two monomers. The thick arrows identify the βF5-βF6 loop whilst the thin arrows identify the α-helices αI3' and αI3'' [117].

The RgDAAO active site is situated in a cavity delimited by two couples of β-strands: the first couple (I4 and I8) is bent around the isoalloxazine ring of

the flavin whilst the second one (I5 and I6) is situated close to the substrate-binding site. The flavin constitutes the "bottom" of the cavity. All the β-strands present in the structure of the active site have an antiparallel orientation and are connected to each other by hydrogen bond which stabilize and stiffen the structure[121].

Industrial application of DAAO

Industrial applications of the RgDAAO concern primarily the production of the 7-(5-oxoadipoamido)cephalosporanic (7-ACA) acid through the enzymatic deamination of the cephalosporin C. The 7-ACA is then used as a starting molecule to produce more than 50 semi-synthetic cephalosporins[122]. Since the production of 7-ACA without DAAO is very laborious and expensive, the use of this enzyme permits to save money and time allowing a better purification of the final products if bound to magnetic NPs[120]. Besides the 7-ACA production, DAAO is also used to resolve racemic solution of D,L-amino acids, obtaining optically pure solution of L-amino acids[123].

Medical applications of DAAO

In the medical field, the DAAO is used for the production of α-keto acids, which are consequently administered as food additive to treat patients with chronic uremia[124]. A new and emerging DAAO medical application concerns cancer therapy by exploiting its H_2O_2 production following D-amino acids oxidation. The H_2O_2-induced apoptosis[125] is made possible by different ROS generating enzymes like glucose oxidase (GO), xanthine oxidase (XO) and DAAO. The use of exogenous GO is tricky and can't be modulated because of the widespread and uncontrollable presence of its substrates (oxygen and

glucose)[126]. Similarly, XO, because of its enzymatic promiscuity, can't control its ROS production since it has a wide range of ubiquitous substrates[127]. On the contrary, DAAO is the optimal candidate to perform the H_2O_2-induced apoptosis of cancer cells because of the very low presence of D-amino acids in humans and the absolute stereoselectivity of RgDAAO. With RgDAAO it is possible to regulate strictly the ROS production by the exogenous administration of D-amino acids[127].

II.2 NP-Enzyme system for industry: NP-LASPO

The second part of this work focuses on the development of a magnetic nanoparticle-enzyme system designed for industrial application. This system utilizes a commercial Fe_3O_4 NPs (IONPs) that, once functionalized with APTES (IO-APTES), are conjugated with the L-aspartate oxidase (LASPO) giving the IO-APTES-LASPO system (NP-LASPO). This NP-LASPO system will combine the catalytic activity of LASPO to resolve racemic solution of D,L-aspartate with the possibility to recover and reuse the system when the reaction in the bioreactor is over. Thanks to its magnetic feature, it will be possible to obtain pure end products without the enzyme contamination. In industrial applications that NP-LASPO system will enable a simpler, faster and cheaper resolution of racemic mixtures of D,L-Aspartate. In this study the protocol for the LASPO immobilization on NP-APTES was optimized.

LASPO

LASPO (EC 1.4.3.16) is a prokaryotic and FAD-dependent enzyme that catalyzes with a high stereospecificity the oxidative deamination of L-aspartate and L-asparagine to give α-keto acids and ammonia. Then, similarly to DAAO, the oxygen reoxidizes the FAD cofactor previously

reduced giving hydrogen peroxide. In prokaryotes, LASPO has a fundamental role in the *de novo* biosynthesis of nicotinamide adenine dinucleotide (NAD^+) by catalyzing the first reaction step. *In vivo*, the iminosuccinate produced by using L-aspartate as substrate is then condensed with dihydroxyacetone phosphate resulting in the production of quinolinate and, eventually, NAD^+. *In vitro,* LASPO is able to use both O_2 and fumarate in FAD re-oxidation, allowing to perform its catalytic reaction in aerobiosis and anaerobiosis: under aerobic condition, the LASPO oxidizes L-aspartate to iminosuccinate, which is then hydrolyzed to oxaloacetate through a non-enzymatic pathway[128](Fig. 15).

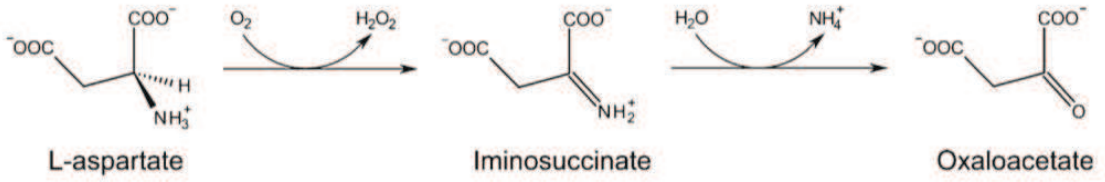

Fig. 15: Catalytic reaction of LASPO: the L-aspartate is oxidized to iminosuccinate followed by a nonenzymatically hydrolyzation to oxaloacetate[128].

Among all the studied LASPO, the one isolated from the thermophilic microorganism *Sulfolobus tokodaii* (StLASPO) is of potential interest for industrial applications. StLASPO is a monomeric (52 kDa) enzyme formed by a single polypeptide chain composed by 472 residues organized into three distinct folding domains: a FAD-binding domain, a capping domain, and a C-terminal domain[129] (Fig.16). One of the most interesting and attractive features of StLASPO is the high thermal stability: StLASPO is stable up to 80 °C where no remarkable changes in its activity were observed during an incubation of 400 min at pH 7.5. Besides the high thermal stability and high temperature optimum, StLASPO arouses interest also because of the stable

activity in a wide range of pH (7.0-10.0), the tight interaction with FAD and the weak inhibition caused by D-aspartate and by the final product(s) (i.e., iminosuccinate or oxaloacetate)[130].

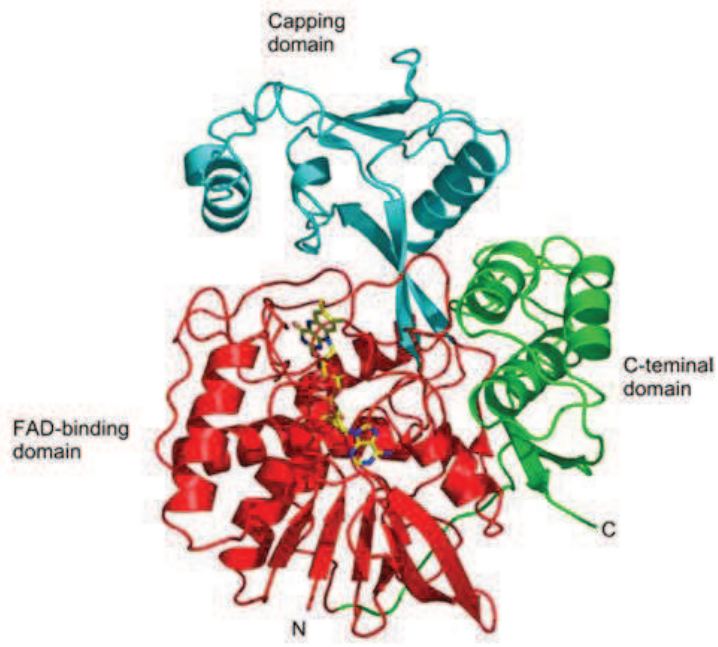

Fig. 16: StLASPO overall structure: the FAD-binding, capping and C-terminal domains are shown respectively in red, cyan and green. The FAD cofactor is represented as a stick model in yellow with oxygen and nitrogen atoms in red and blue, respectively[129].

Recombinant StLASPO was efficiently used for the resolution of a racemic mixture of D,L-aspartate and, thanks to its high stability, the enzyme was effectively reused for one more bioconversion cycle obtaining the same conversion yield[130]. Moreover, StLASPO was successfully immobilized on various supports reaching in terms of activity about 50-100% of yield[131]. These results suggest a very interesting perspective for the StLASPO conjugation on different supports (i.e. magnetic NPs) aiming to improve the enzyme qualities.

I.III INFLUENCE OF NPs ON STEM CELLS

Stem cells play an important role in several processes such as recovery of functional absences in diseases, homeostasis of healthy tissues, regeneration of damaged tissues and, unfortunately, in tumor formation. Therefore, it is evident how dangerous could be the perturbation of the stem cell homeostasis. When NPs enter, intentionally or not, the body may encounter stem cells and upset their physiology, for instance, unbalancing their differentiation process. Although several studies have demonstrated the toxic effects of NPs on cultured cell lines, up to now there are no clear data describing the overall molecular changes induced by them.

In this third and last part of my work I present a preliminary study of the toxicity and influence of Cobalt, Iron, Nickel zerovalent NPs on the differentiation process of Adipose-derived Stem Cells (ASCs).

III.1 Adipose Stem Cells (ASCs)

ASCs are a subgroup of Mesenchimal Stem Cells (MSCs) derived from adipose tissue firstly isolated and described as a new source of adult stem cells in 2001 by Zuk et al.[132]. Since the discovery, ASCs attracted more and more interest especially in regenerative medicine because of their peculiar features such as:

- The abundance of adipose tissue from which they are extracted that is easily recoverable through liposuction, a non-invasive surgery, as well as in the context of surgical interventions in which adipose tissue is removed due to aesthetic and/or functional reasons.
- The high differentiation potential among MSCs.

- The low immunogenicity that renders them suitable for allotransplant.
- The simplicity in setting ASCs cultures without the need of specific and expensive compounds that otherwise can affect their differentiation processes.
- The overcome of ethical issues still present for the use of Embryonic Stem Cells (ESCs).

Several studies proved the multipotency of ASCs (Fig.17). *In vitro* it is possible to induce the ASCs differentiation mainly by culturing cells in culture media supplemented with specific growth factors; indeed, by using the right mixture of growth factors, ASCs are able to differentiate following the mesodermal lineage into adipocytes, chondrocytes, osteoblasts and myocytes[133,134]. Furthermore, many studies demonstrated the potential ability of ASCs to transdifferentiate toward cell lines of both the ectodermal and the endodermal lineages like neurons, motor neurons, Schwann cells, keratinocytes, hepatocytes and pancreatic cells[135].

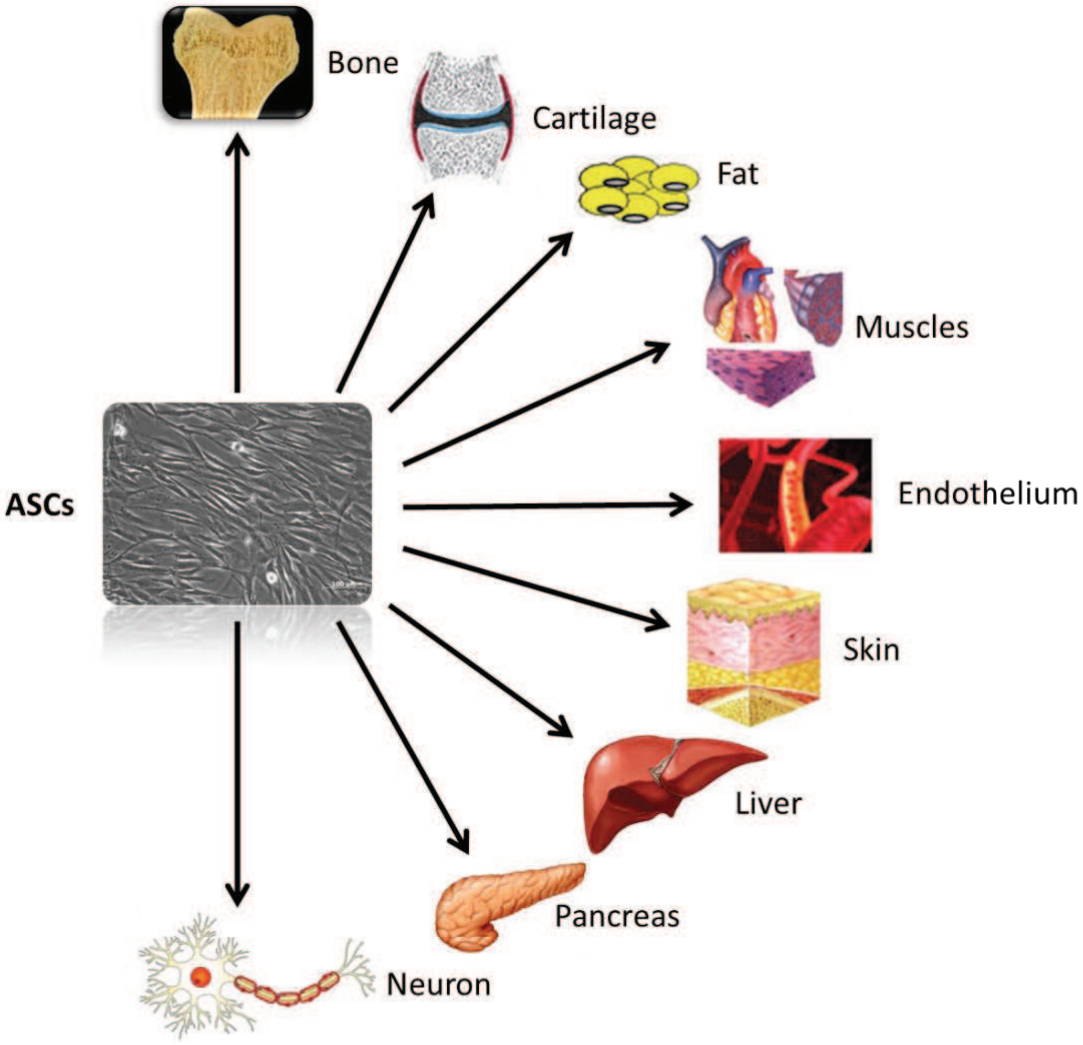

Fig.17: Schematic resume of ASCs multipotency.

Moreover, ASCs can support hematopoiesis, angiogenesis and vascularization, by participating in the blood vessels formation[136] and/or differentiating toward endothelial cells[137].

Another distinctive characteristic of ASCs is the lack of HLA-DR expression that allows them to evade the host's immune system. ASCs can inhibit the production of pro-inflammatory cytokines whilst stimulating the generation of anti-inflammatory IL-10 cytokine[138]. Their immunosuppressive properties result also from the production of prostaglandin E2 and 2,3 dioxygenase indole[139]. Hence, ASCs are able to protect against organ rejection and prevent from the Graft-Versus-Host-Disease (GVHD) after allogeneic stem

cell transplantation[140]. Thanks to their immune "stealth" abilities, ASCs could be a very interesting opportunity for therapeutic purposes in allogeneic transplantation in which it will be possible to collect from a suitable donor and standardize different ready-to-use ASCs cell lines[141].

Finally, ASCs are preferred to the golden standard of the Bone Marrow-derived Stem Cells (BMSCs) because of the easier and safer sample collection from the donor, the more abundance of stem cells up to 500 fold[142], the simple cell culture with a rapid cell growth[143].

III.2 Cobalt, Iron, Nickel zerovalent NPs

Cobalt, Iron and Nickel are three transition metals belonging to the VIIIb group of the periodic table. The choice to investigate the zerovalent NPs of Co, Fe and Ni aims to fill some knowledge gaps related to the present lack of the literature data about the toxicity and biological interactions of these three elements in the form of NPs.

Cobalt NPs

Cobalt NPs (CoNPs) are one of the most promising materials for nanotechnological applications ranging in different industrial sectors such as the production of pigments, catalysts and sensors, as well in electrochemistry, magnetism, memory storage, magnetic fluids[144–146]. CoNPs are used also in nanomedicine as a highly sensitive contrast agent in MRI[147,148]. However, it was proved that CoNPs aggregates are toxic on different cell lines: that toxicity was mainly due to Co ion dissolution from the CoNPs[149].

Iron NPs

Iron NPs (FeNPs) are widely used for the groundwater and soil remediation from pollutants such as phenanthrene and chlorinated ethanes/ethenes[150] as well as heavy metals[151]. Nevertheless, to reduce the environmental risks linked to the FeNPs dispersion, it is of use their immobilization on supports such as alginate beads or activated carbon; this strategy allows to retrieve and store the NPs[146,152]. However, many concerns remain about their fate and toxicity[153,154].

Nickel NPs

Nickel NPs (NiNPs) find application in modern industry as catalysts, sensors and in electronics[155,156]. However, their usage is creating concerns due to the potential risk associated to the toxicity of Ni-derived compounds that may be released from NiNPs into the environment. The International Agency for Research on Cancer (IARC) has classified the Ni-derived compounds as "carcinogenic to humans" (Group 1) while metallic Ni as "possible carcinogenic to humans" (Group 2B) with genotoxic and mutagenic activities[157]. Finally, NiNPs were proved capable of inducing lung epithelial and respiratory pathologies in human[158,159], embryotoxicity in zebrafis[160] and spermiotoxicity in Ciona intestinalis[161].

CHAPTER II - SYNTHESIS OF MAGNETIC NP-ENZYME SYSTEM FOR CANCER THERAPY: AN UPGRADE OF THE NP-DAAO SYSTEM

II.I MATERIALS AND METHODS

DAAO enzyme

The D-Amino Acid Oxidase (DAAO) used in this work is the wild type from *Rhodotorula gracilis* that was produced as recombinant proteins in *E. coli* and purified as stated in Fantinato et al.[162]. The final stock DAAO solutions were equilibrated in 50 mM potassium phosphate buffer at pH 7.5, 2 mM EDTA, 10% v/v glycerol and 5 mM 2-mercaptoethanol. MilliQ Ultrapure Water System (Millipore, MA, USA) was used. The DAAO enzyme was provided by the laboratory of Prof. Loredano Pollegioni of the Biotechnology and Life Sciences Department of Università degli Studi dell'Insubria, Varese.

IONPs

Two different types of Iron Oxide Nanoparticles (IONPs) were used:

1. The first type was γ-Fe_2O_3 synthetized *de novo* (dIONPs) following a protocol based on Bee et al.[163] and Geppert et al.[164]. The detailed synthesis process is reported below.
2. The second type was a commercial Fe_3O_4 nanopowder (cIONPs) acquired from Sigma (n.cat: 637106) with the particle size < 50 nm. These Fe_3O_4 NPs were the same utilized by Bava et al.[115] and Cappellini et al.[113].

The synthesis of dIONPs was performed in an Erlenmeyer flask positioned on a heating plate with a magnetic stirrer. Because of the risk of production of nitrous gases in the heating steps, the synthesis was conducted under a working fume-hood. The here described synthesis will yield approximately 50 mL of aqueous dIONPs dispersion with a total iron concentration of 500-700 mM. Nevertheless, it is possible to up- or downscale this method.

Preparation of dIONPs:

1. Weigh in 8.89 g $FeCl_3$ * 6 H_2O (Sigma-Aldrich n. cat: 31232) and 3.28 g $FeCl_2$ * 4 H_2O (Sigma-Aldrich n. cat: 44939) and dissolve it in 380 mL H_2O (in a 500 mL Erlenmeyer flask) on a magnetic stirrer for 30 min. While stirring add slowly 1.5 mL of 37% HCl to dissolve iron salts completely.
2. Add slowly and under strong stirring 25 mL of 25% NH_4OH to iron solution: a black precipitate will appear. Stir for additional 10 min.
3. Remove flask from magnetic stirrer and let particles precipitate by placing a permanent magnet (NdFeB-magnet) under the flask and wait until all the NPs are collected to the bottom (that happens after 10-20 min.). Be careful working with NdFeB-magnet since their magnetic field is very strong.
4. Remove the supernatant (aqueous media) by decantation and wash twice the NPs with 100 mL of H2O MilliQ, leaving them 10 min on magnetic stirrer for each washing. During the last washing steps, transfer the suspension into a smaller Erlenmeyer flask (100 mL).
5. After the transfer, add 40 mL of 2 M HNO_3 and heat up to 90 °C for a 5 min. The suspension will turn colour from black to dark brown.
6. Isolate particles again with the magnet and add 60 mL of 0.34 M solution of $Fe(NO_3)_3$ * 9 H_2O (Sigma-Aldrich n. cat: 216828). Heat up to 90 °C and stir for 30 min.
7. Cool down to RT and remove supernatant (NdFeB-magnet).
8. Add 50 mL of H_2O (can be more) on the particles and stir properly. The particles will now “dissolve” leading to a magnetic fluid containing a well dispersion of iron oxide nanoparticles.

9. Filter NPs through 0.2 µm syringe filters for removal of larger aggregates. If dispersion cannot be filtered well, add more water to dilute the ferrofluid and use new filter.
10. Pipette into a glass bottle and store at 4 °C. If needed the IONPs solution can be dialyzed to remove any Iron salts still present after the last steps.

IO-APTES NPs (NP-APTES)

IONPs were functionalized with APTES (Sigma n. cat: A3648) following two methods depending on the type of IONPs used.

NP-APTES from de novo synthesis (dNP-APTES)

Since dIONPs were suspended in aqueous media, the corresponding of 150 mg of NPs was added to 1 mL of a solution composed by 975.4 µL of EtOH and 24.6 µL of APTES. The right amount of APTES was calculated from the total NPs surface area to have enough APTES to coat each NP whilst EtOH was added up to the volume of 1 mL. The reaction was maintained under mechanical stirring for 1 h at RT and for 1 h at 90 °C. Then, the synthetized dNP-APTES were washed three times with H_2O MilliQ by centrifugation 5 minutes at 10000 x g and resuspended in H_2O MilliQ by ultrasonication. The centrifugation washing passages were necessary because the collection with the magnet used for the Sigma NPs would have required too much time.

NP-APTES from Sigma NPs (cNP-APTES)

150 mg of cIONPs were ultrasonicated with Ultrasonic Cleaner M S3 (Soltec, Milan, Italy) in 10 ml of H_2O MilliQ for 20 min. To start the functionalization reaction, a solution of 5 mL APTES (2% w/v) in H_2O MilliQ was added to NPs

and maintained under mechanical stirring for 5 h at 50 °C, according to del Campo et al.[27]. The Fe_3O_4-APTES (cNP-APTES) were then separated from unbound APTES by a commercial parallelepiped neodymium magnet (Webcraft GmbH, Uster, Switzerland; Ni-Cu-Ni plated; magnetization: N45; size: 30x30x15 mm), washed with 5 mL of H_2O MilliQ until pH 7 was reached. Afterwards, cNP-APTES were washed twice with 5 mL of EtOH and resuspended in 10 mL of EtOH. Then, they were ultrasonicated for 20 min and left in EtOH overnight. The day after, cNP-APTES were collected with the magnet and washed twice with 10 mL of H_2O MilliQ, ultrasonicated for 30 min and left at room temperature for 1 h. Hence, the water was removed and the cNP-APTES were dried at 50°C overnight.

IO-APTES-DAAO NPs (NP-DAAO)

NP-APTES NPs were conjugated with different amount of *Rg*DAAO depending on the free surface area presented by 4 mg of NP-APTES.

NP-DAAO from dNP-APTES (dNP-DAAO)

For 1 mL of reaction, 4 mg of dNP-APTES were activated in NaPPi buffer 5 mM pH 8.5 by adding EDC (1-Ethyl-3-(3-dimethylaminopropyl) carbodiimide hydrochloride, Sigma n.cat: 03450) and NHS (N-hydroxysulfosuccinimide, Sigma, n.cat: 130672) in the ratio 3:2 w/w. Then, 1786 µg of DAAO were added and NaPPi buffer 5 mM pH 8.5 up to a final reaction volume of 1 mL. The reaction was carried out for 4 h at 4 °C using a rotating plate tube stirrer. Eventually, the dNP-DAAO were collected by placing the sample on a magnet in ice (~4 °C) and washed twice with 1ml of NaPPi buffer 5 mM pH 8.5. The supernatant was stored for further analysis.

The choice of the suitable amount of DAAO for the conjugation was done starting from the fixed ratio used for cNP-DAAO between the μg of DAAO per the total surface area given by 4 mg of cNP-APTES, and then moving to the surface saturation by increasing the amount of enzyme. The total surface area of 4 mg NP-APTES was calculated from the average particle diameter, assuming spherical particles, by DLS analysis. For 4 mg of dNP-APTES were successfully loaded up to 1786 μg of DAAO.

NP-DAAO from cNP-APTES (cNP-DAAO)

According to the method used by Cappellini et al.[116], 4 mg of cNP-APTES were suspended by ultrasonication for 15 min with the same activation solution of EDC/NHS solution as previously described. Then, 250 μg of DAAO were added and NaPPi buffer 5 mM pH 8.5 up to a final reaction volume of 1 mL. The reaction was carried out for 4 h at 4 °C using a rotating plate tube stirrer. Subsequently, cNP-DAAO were collected through the magnet and washed twice with 1 mL of NaPPi 5 mM pH 8.5. The supernatant was stored for further analysis. The 250 μg of DAAO were chosen as the maximum loading capability per 4 mg of cNP-APTES as reported by Cappellini et al.[116].

A general and schematic representation of the whole NP-DAAO system formation is resumed in Fig. 18.

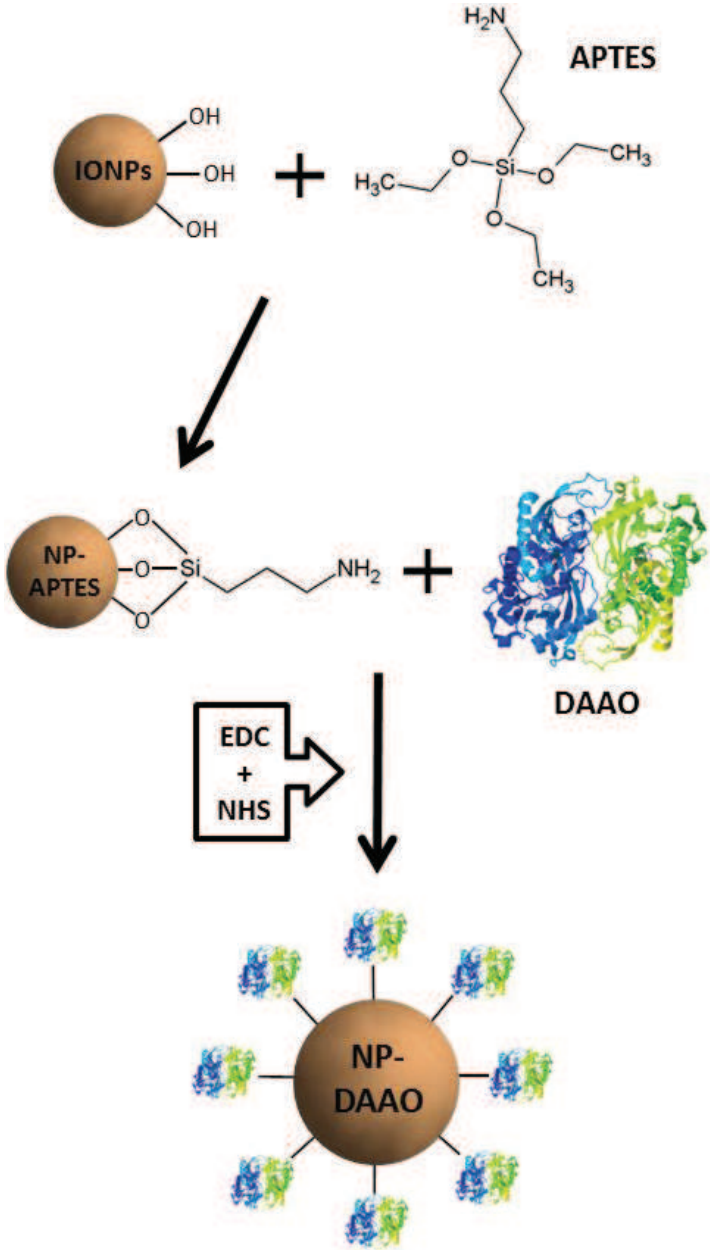

Fig. 18: Schematic representation of the NP-DAAO system formation process.

Transmission Electron Microscopy (TEM) Pictures and Analysis

dIONPs, dNP-APTES and dNP-DAAO were observed with a JEOL 1010 electron microscope (JEOL, Tokyo, Japan). Each sample was diluted in H_2O MilliQ and deposed onto a 200 nm mesh Formvar/carbon-coated copper grid. The NPs size distribution graphs were carried out by counting 100 NPs

per picture. Statistical analysis was performed using one way ANOVA with Scheffè test among the three groups of NPs.

Dynamic Light Scattering (DLS) Analysis

NP size measurements by DLS were carried out in H_2O MilliQ. NP dispersions were prepared by diluting the NP stock (25 mg/mL) to the required concentration (0.075 mg/mL). Measurements were performed at 25 °C using a Malvern Zetasizer Nano ZS90 (Worcestershire, UK). DLS results are reported as the average of at least 3 runs, each containing 13 individual measurements.

Zeta Potential (Z-pot) Analysis

Zeta potential (Z-pot) measurements were performed with the samples diluted to 0.075 mg/mL in 0.1% PBS at 25 °C using a Malvern Zetasizer Nano ZS90 (Worcestershire, UK).

Differential Centrifugal Sedimentation (DCS) Analysis

DCS experiments were performed with a CPS Disc Centrifuge DC24000. The analyzer measures the particle size distribution using centrifugal sedimentation within an optically clear spinning disk filled with fluid. The measurements were conducted in a sucrose gradient of 8−24% in H_2O MilliQ at 19000 rpm of speed. The concentration of the samples analyzed was 0.075 mg/mL.

Spectra Analysis

The amount of DAAO bound on the NP surface was determined by considering the difference between the starting amount of DAAO and the

protein recovered in the supernatant at the end of the conjugation reaction. The quantification of conjugated DAAO was performed using the extinction coefficient at 455 nm (~12.6 $mM^{-1}cm^{-1}$) and an UV-Vis V-560 Spectrophotometer (JASCO, MD, USA).

dNP-DAAO enzyme activity assay

The NP-DAAO activity was determined by measuring the absorbance increase accompanying the H_2O_2-induced oxidation of O-dianisidine. One DAAO unit corresponds to the amount of enzyme that converts 1 µmol of substrate per min at 25°C and at 0.253mM oxygen concentration.

The standard assay mixture contained 890 µL of 100 mM D-Ala in NaPPi buffer 100 mM pH 8.5, 100 µL 3.2 mg/mL O-dianisidine in H_2O MilliQ, 10 µL of 0.4 mg/mL horseradish peroxidase in NaPPi buffer 100 mM pH 8.5 and, eventually, 10 µL of 0.4 mg/mL NP-DAAO in the same buffer. The reaction starts by adding the enzyme and the absorbance increase is monitored at 440 nm (~13 mM-1cm-1) for 1 min at 25 °C using an UV-Vis Jasco V-560 Spectrophotometer (JASCO, MD, USA).

dNP-DAAO Yield and Activity Recovery

The immobilization yield was calculated as the percentage of the ratio between the Immobilized enzymatic Activity of DAAO on NP-DAAO (IA) and the Starting enzymatic Activity of DAAO added to the conjugation reaction (SA):

$$Yield\ (\%) = \frac{IA}{SA} \times 100$$

The IA refers to the difference between the SA and the DAAO enzymatic activity retained by the supernatant at the end of conjugation reaction.

Finally, to describe how much enzymatic activity is retained by the immobilized DAAO, it was calculated the Activity Recovery as the percentage of the ratio between the Observed enzymatic Activity of the DAAO loaded on NP-DAAO (OA) and the SA:

$$Activity\ recovery\ (\%) = \frac{OA}{SA} \times 100$$

This parameter gives an overall idea of the success of the total immobilization process.

dNP-DAAO storage stability

The dNP-DAAO were stored at 4 °C in NaPPi buffer 5 mM pH 8.5 and assayed after 1, 2, 4 and 8 months. Three different dNP-DAAO batches were analyzed and the results were normalized against the dNP-DAAO activity recorded the day of the DAAO conjugation to dNP-APTES.

dNP-DAAO activity in presence of human serum

The dNP-DAAO activity was investigated at different time (5, 30, 60 min.), temperature (20, 25, 30, 37 °C) and with or without the addition of human Serum (hS) at the final concentration of 10%.

The incubation solution with 10% hS was prepared by adding: 890 µL of NaPPi buffer 100 mM pH 8.5, 100 µL of hS and 10 µL of dNP-DAAO (stock sol. 4 mg/mL). The dNP-DAAO activity was determined as reported previously.

The 10% hS concentration was chosen on the basis of pilot experiments carried out with dNP-DAAO NPs incubated at 37 °C within the range 0.1-50% of hS.

Statistical analysis was performed using one way ANOVA with Scheffè test among the three groups of NPs.

Cell culture

Four different cell lines were used to evaluate the dNP-DAAO *in vitro* cytotoxicity and capability to kill human cancer cells. As a tumor model, three different human cell lines were used: SKOV-3 from ovary adenocarcinoma, U87 from glioblastoma and HCT116 from colorectal carcinoma. As non-tumor cell line, the hASCs (human Adipose-derived Stem Cells) cell line was used.

RPMI1640 medium was employed to maintain SKOV-3 and HCT116 cell lines as adherent cells while DMEM medium was used for U87 cell line and a 1:1 DMEM/DMEM-F12 medium for hASCs. Every cell line was incubated at 37 °C in a humidified 5% CO_2 atmosphere. RPMI1640, DMEM and DMEM/DMEM-F12 medium were supplemented with 10% fetal bovine serum, 1% L-Glutamine and 1% penicillin/streptomycin solution; DMEM medium was supplemented with also 1% sodium pyruvate and DMEM/DMEM-F12 medium with 0.1% gentamicin. Cells were passaged as needed using a solution at 0.25% trypsin–EDTA.

Cell viability test

Cell viability was determined as ATP content by using the CellTiter-Glo Luminescent Cell Viability Assay (Promega) according to the manufacturer's instruction. In detail, 200 µL of cell suspension containing 10000 cells were seeded into 96-well plates and cultivated for 24 h at 37 °C in 5% CO_2 to equilibrate and become attached prior the treatment. Then, cells were exposed for 24 h to 3.5, 7 and 14 mU of free DAAO and dNP-DAAO with or without 1 mM of D-Alanine (one of the DAAO substrates). The choice of this specific range of Units was based on the current literature[115].

Following the treatment, the plates were equilibrated for 30 min at room temperature and after the medium was replaced with 100 µL of new one plus 100 µL of CellTiter-Glo Reagent was then added to each well. Plates were shaken for 2 min and left at room temperature for 10 min to equilibrate the luminescent signal that eventually was recorded by using the Infinite F200 plate reader (Tecan Group, Männedorf, Switzerland). For all the cell lines, the experiments were performed in triplicate and repeated three times. Cell viability, expressed as ATP content, was normalized against control values.

Comparison between dNP-DAAO and cNP-DAAO

The whole dNP-DAAO system (dIONPs, dNP-APTES and dNP-DAAO) was then compared to one obtained from the Cappellini et al[116] procedure that represents the updated NP-DAAO system in literature (cNP-DAAO). Hence, cIONPs, cNP-APTES and cNP-APTES were synthesized and characterized by DLS and DCS analysis to highlight the differences among dNP-DAAO and cNP-DAAO. For DLS and DCS analysis, each sample of the cNP-DAAO system was processed alike the one of the dNP-DAAO system.

Furthermore, the yield, the activity recovery and the intrinsic cytotoxicity of the dNP-DAAO were compared to cNP-DAAO to have an overall outlook of any improvements. Regarding the intrinsic cytotoxicity comparison, it was used as a model the SKOV-3 cell line.

II.II RESULTS AND DISCUSSION

Samples characterization by TEM, DLS, DCS and Zeta-potential analysis

In this work, different techniques were used for a full NPs characterization.

TEM characterization is necessary to obtain a direct particles imaging on dried NPs and to provide a quantitative measure of the NPs size, size distribution and morphology.

TEM pictures and analysis (Fig. 21) show that dIONPs (Fig. 19a), dNP-APTES (Fig. 19b) and dNP-DAAO (Fig. 19c) possess an average size, expressed in nm, of respectively 8.5, 10.3 and 11.0. These results suggest a slight increase but statistically significant ($P < 0.002$) from the bare NPs towards the dNP-APTES. However, any statistical significance is observed among dNP-APTES and dNP-DAAO ($P < 0.341$). These results might be explained by the formation of dNP-DAAO aggregates during the DAAO conjugation reaction that cannot be well distinguished with TEM analysis.

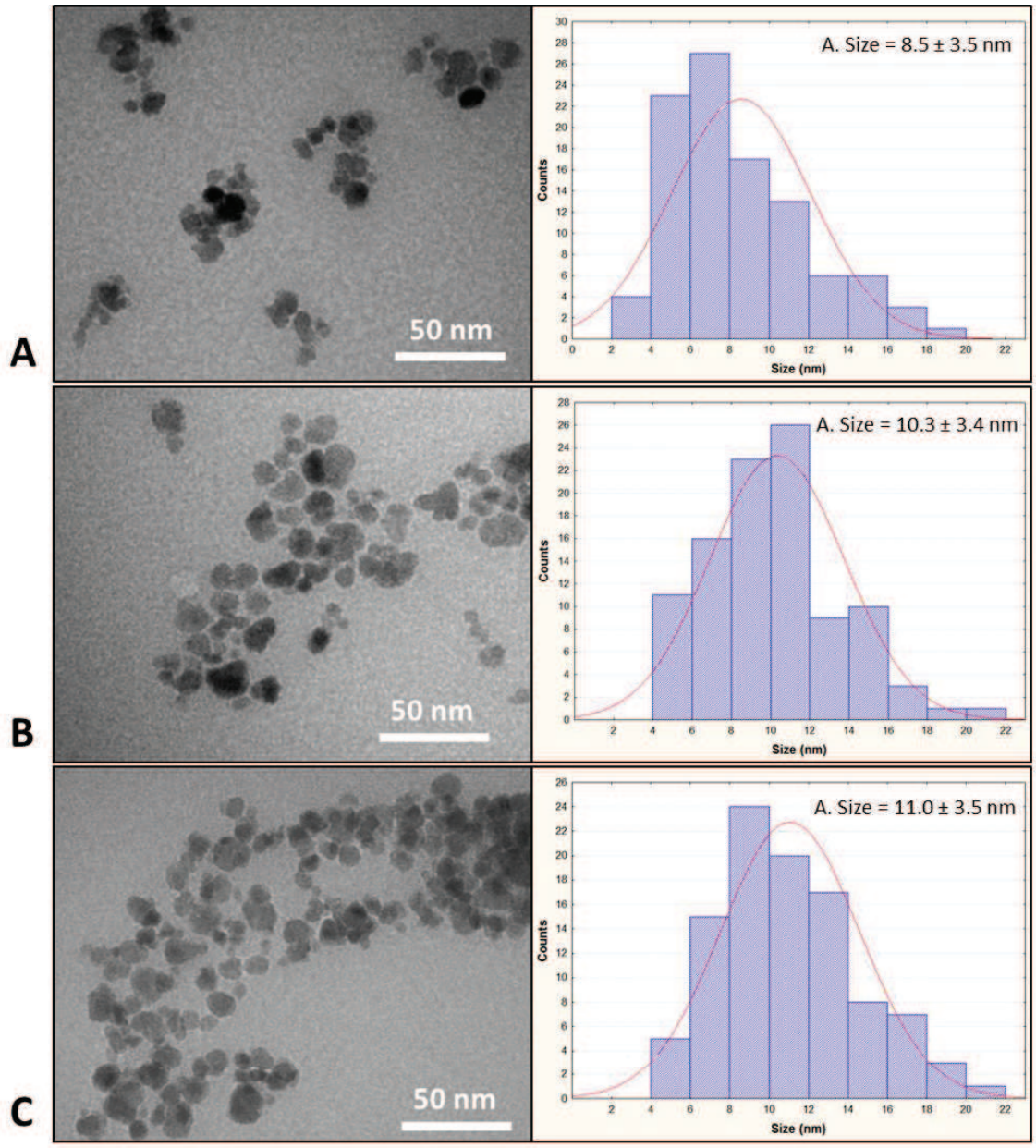

Fig. 19: TEM analysis dIONPs (a), dNP-APTES (b) and dNP-DAAO (c). The NPs size is expressed in nm as the average size ± standard deviation. 100 counts for each sample were measured.

DLS characterization is used to get information about the hydrodynamic radius of NPs dispersed in a liquid solution. The DLS analysis allows to observe the changes occurred in the NP size and size distribution when exposed to different solvents.

The DLS characterization analysis (Fig. 20a) reports a diameter of about 38 nm for the dIONPs and about 47 nm for the dNP-APTES. After conjugation with the DAAO enzyme, dNP-DAAO acquire a wider diameter of approximately 185 nm. Although the low PDI of both dIONP and dNP-APTES indicates the presence of monodisperse particles, the high PDI of dNP-DAAO suggests the probable formation of aggregates.

DCS characterization exploits the NP density and sedimentation time to calculate the NP size. This technique is very sensible and can detect more NP subpopulations within the same NP solution, highlighting also the presence of agglomerates and or aggregates.

The DCS analysis (Fig. 20b) of dIONPs results in a NPs average diameter of about 34.5 nm. As expected, the surface functionalization with APTES and DAAO results in a change of the particle sedimentation time. The dNP-APTES and dNP-DAAO have respectively an apparent size of 24 nm and 76 nm: this is due to a change in the sample density as also reported in other publications[165–167]. The narrow peaks present in each of the sample tested indicate a well-defined population of particles.

Under the best experimental condition, the still presence of dNP-DAAO aggregates is probably due to a slight aggregation process during DLS and DCS analysis. However, further analysis will be conducted to better understand the dNP-DAAO behavior in aqueous buffers.

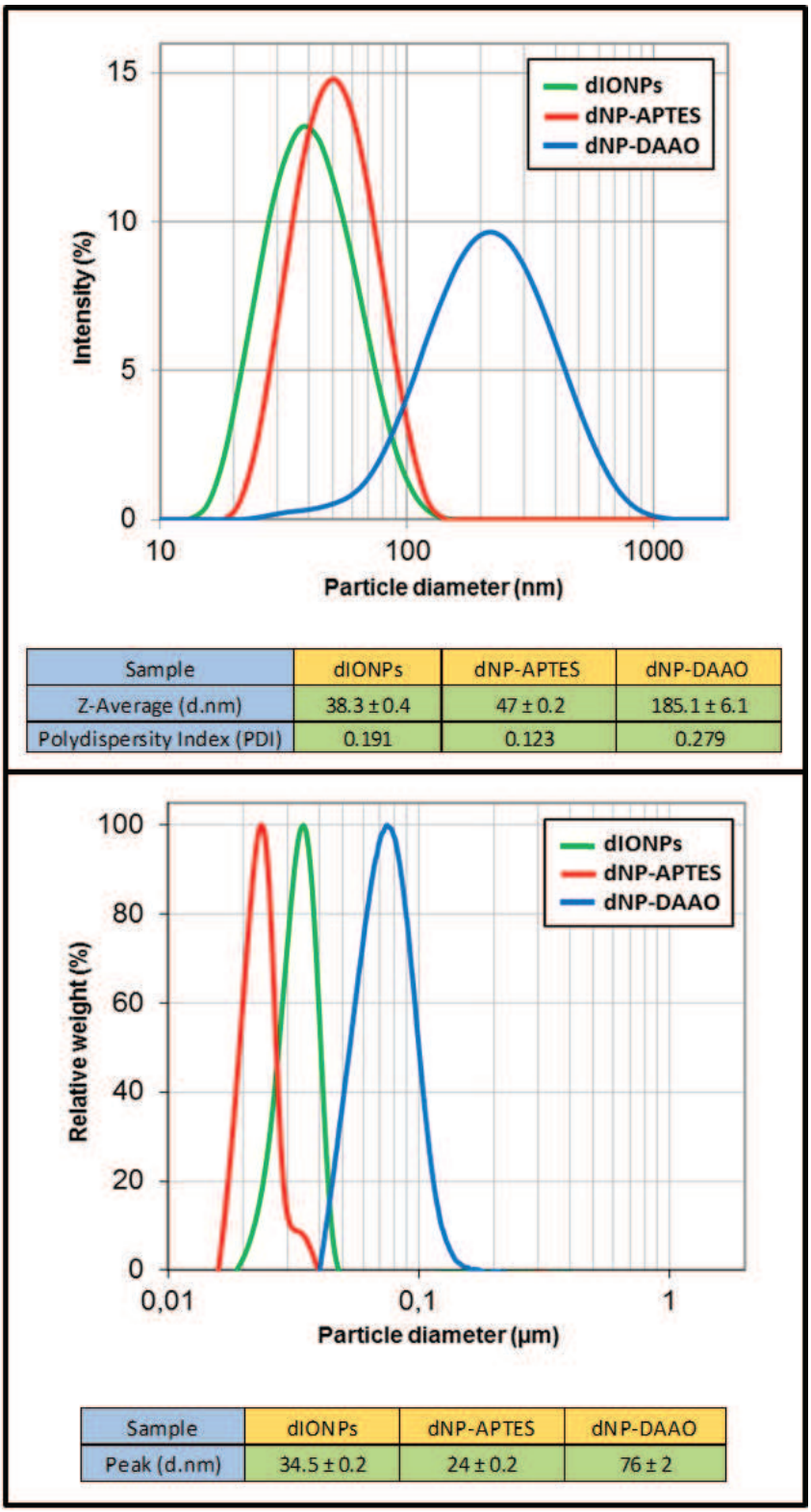

Sample	dIONPs	dNP-APTES	dNP-DAAO
Z-Average (d.nm)	38.3 ± 0.4	47 ± 0.2	185.1 ± 6.1
Polydispersity Index (PDI)	0.191	0.123	0.279

Sample	dIONPs	dNP-APTES	dNP-DAAO
Peak (d.nm)	34.5 ± 0.2	24 ± 0.2	76 ± 2

Fig. 20: DLS (a) and DCS (b) analysis of dIONPs, dNP-APTES NPs and dNP-DAAO NPs. The NPs size is expressed in nm as the average size ± standard deviation. The Polydispersity index is from cumulant fitting.

The Z-pot represents a very important analysis to record the surface charge of NPs. This analysis is to know the charge changes on the NP surface following the functionalization reaction.

The Z-potential analysis (Fig.21) shows a negative Z-pot for both dIONPs and dNP-DAAO of respectively -35.6 and -11.3 mV whilst dNP-APTES is positive at 9.8 mV. These measurements were performed in 0.1% PBS because the ones in H_2O MilliQ did not possess a suitable grade of salinity to allow stable and reproducible results. The negative Z-pot of the dNP-DAAO suggests a lower toxicity profile if compared to positively charged NPs[54,55]. Furthermore, it was proved that slightly negatively charged NPs might be highly up taken by tumor due to their prolonged blood circulation[167]. These results are very promising for the ultimate goal of using dNP-DAAO in cancer therapy.

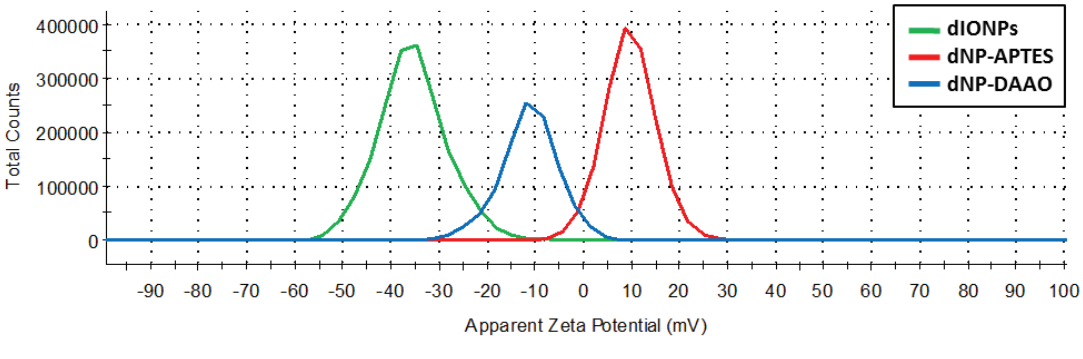

Sample	dIONPs	dNP-APTES	dNP-DAAO
Z-potential (mV)	-35.6 ± 0.6	9,8 ± 0.1	-11.3 ± 0.1

Fig. 21: Z-potential of dIONPs, dNP-APTES and dNP-DAAO. The Z-pot is expressed in mV as the average Z-pot ± standard deviation.

In Tab. 3 all the results of the analysis performed for the dNP-DAAO system characterization are resumed .

Tab. 3: dNP-DAAO system characterization by TEM, DLS, DCS and Z-pot analysis.

Sample	dIONPs	dNP-APTES	dNP-DAAO
size (d.nm)^{TEM}	8.5 ± 3.5	10.3 ± 3.4	11.0 ± 3.5
Z-Average (d.nm)^{DLS}	38.3 ± 0.4	47 ± 0.2	185.1 ± 6.1
PDI^{DLS}	0.191	0.123	0.279
Peak (d.nm)^{DCS}	34.5 ± 0.2	24.0 ± 0.2	76.0 ± 2.0
Z Potential (mV)	-35.6 ± 0.6	9,8 ± 0.06	-11.3 ± 0.06

DAAO conjugation to dNP-APTES

The DAAO enzyme was successfully conjugated up to 446 µg per mg of dNP-APTES with a maximum of 1786 µg per reaction (4 mg of dNP-APTES).

As shown in Tab. 4, the dNP-DAAO conjugation Yield and the Activity recovery were stable respectively at the 100% and 91%. Since it was employed a stock RgDAAO solution of about 59 U/mg, the units of enzyme loaded were about 24 U per mg of dNP-APTES up to 96 U per whole reaction.

Tab. 4: dNP-DAAO system features. Amount of enzyme loaded per mg of dNP-APTES; yield and activity recovery expressed in percentage; enzymatic Units (U) per mg of dNP-DAAO.

Sample	µg of DAAO/ mg NPs	% Yield	% Activity recovery	U/mg NPs
dNP-DAAO	446	100	91 ± 2	24 ± 0.5

dNP-DAAO storage stability

The dNP-DAAO activity was checked up to 8 months (Fig. 22). The dNP-DAAO activity shows a very low but constant decrease that after 8 months of storage at 4 °C reaches about the 16% activity loss. These results permit to store the entire batch on dNP-DAAO at 4 °C for at least 8 months without a great loss of enzymatic activity of the DAAO loaded. Compared to one of the previous NP-DAAO system[115] the storage stability is improved greatly going from the 20% of activity loss at two months to 6% and not more the 17% after 8 months.

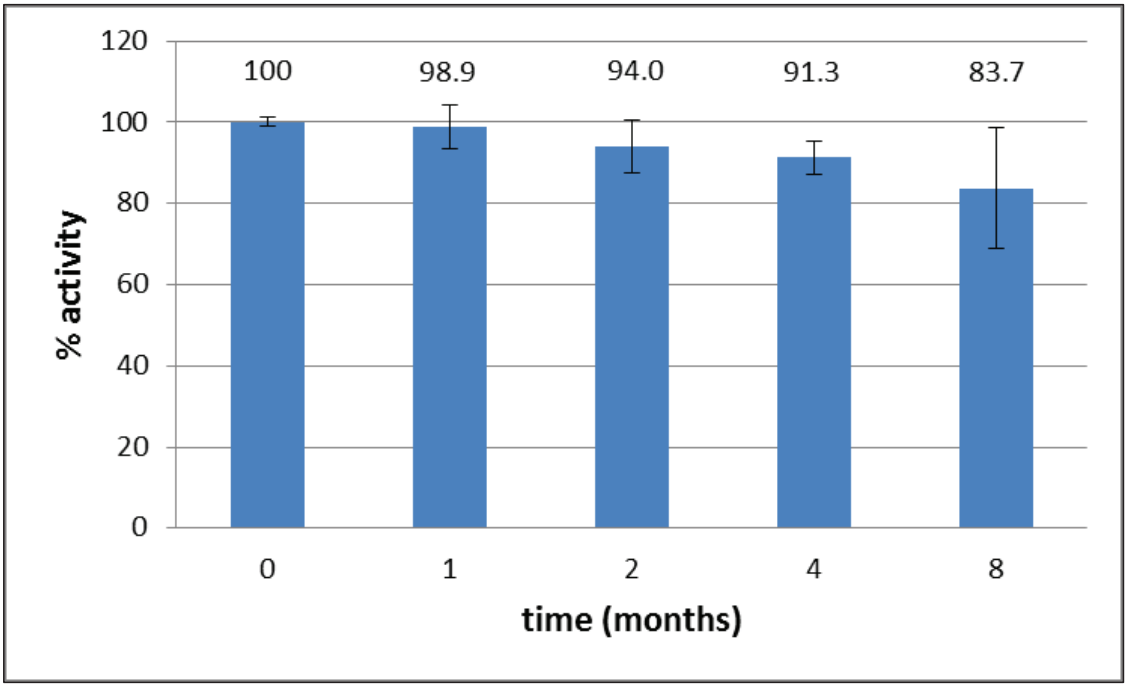

Fig. 22: dNP-DAAO storage stability from the day of the DAAO conjugation up to 8 months. The dNP-DAAO was stored at at 4 °C in NaPPi buffer 5 mM pH 8.5. Over each column is reported the percentage of retained activity normalized to Day 1 (shown as time "0").

dNP-DAAO thermal stability in presence of hS

As Fig. 23 suggests, the DAAO and dNP-DAAO enzymatic activity decreases with the increase of either the time and the temperature of incubation. From 20 to 30 °C no significant differences were observed in term of activity loss between the DAAO and dNP-DAAO. However, when incubated at 37 °C for 1 h, the dNP-DAAO retain about the 80% more of enzymatic activity compared to the DAAO alone ($P < 0.0005$). The enzymatic activity is an index of the overall enzymatic stability, therefore we can assume that the DAAO loaded on dNP-DAAO possess an enhanced thermal stability when compared to the DAAO alone.

Since the dNP-DAAO, thought for cancer therapy, have to be injected intravenously to perform its activity, it was assessed the influence of human Serum (hS) on the dNP-DAAO enzymatic activity.

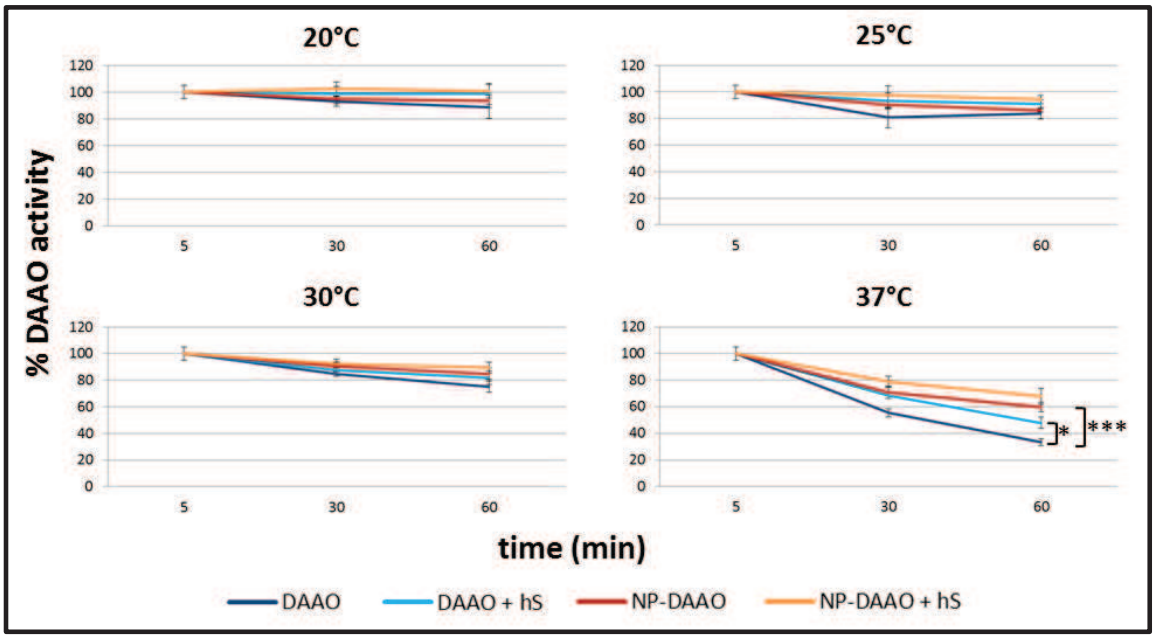

Fig. 23: Thermal stability of DAAO and dNP-DAAO during 5, 30, 60 minutes of incubation with/without 10 % human Serum (hS) at different temperatures (20, 25, 30 and 37 °C).

Interestingly, the incubation with hS 10% retains the enzymatic activity of dNP-DAAO as well as of DAAO. The results show that especially at 37 °C after 1 h of incubation, the hS positively affect the DAAO activity retention ($P < 0.022$) but not the dNP-DAAO ($P < 0.24$).

The results obtained by Z-pot analysis and by the dNP-DAAO activity assay when incubated with hS are preliminary but promising: they can indicate the NPs possible long-term stability into biological fluids, allowing their accumulation in a specific area of the body. Human serum plays an active role in preserving the DAAO activity through the formation of a protein corona able to protect the enzyme from the denaturation processes caused by the temperature increase. The next experiments will be conducted in order to characterize the peculiar dNP-DAAO protein corona. Once injected into the blood stream, the dNP-DAAO will be covered by many different biomolecules that finally give a specific fingerprint to the NP that will be used by the cells to define their fate.

Cell viability test

The efficacy of the dNP-DAAO was tested on different cell lines (Fig. 24). The overall results for all the concentration tested indicate that, without the substrate (D-Ala), the dNP-DAAO toxicity is similar to those of DAAO alone in each cell line. When D-Ala is added, the H_2O_2 produced by both dNP-DAAO and DAAO causes cell death. The dNP-DAAO exert a higher cytotoxic effect compared to DAAO alone that is dependent by the mU of enzyme present into the plate well. This is probably due to the tendency of dNP-DAAO to sediment at the bottom of the well where the consequent H_2O_2 production is localized near to the cells enhancing its toxicity. The maximum toxicity of dNP-DAAO occurs at 7 mU on all the three tumor cell lines; however, on

hASCs, a complete cell death is not fully reached even at 14 mU, leaving 2.5% of cells alive. These results, together with the ones observed at 3.5 mU for both dNP-DAAO and DAAO, could reflect a higher tolerance of hASCs toward the oxidative stress caused by H_2O_2. In fact, it was observed that hASCs have a strong antioxidant activity given by the secretion into the cell culture media of SOD2[168] that reduces the toxicity induced by oxidative stress.

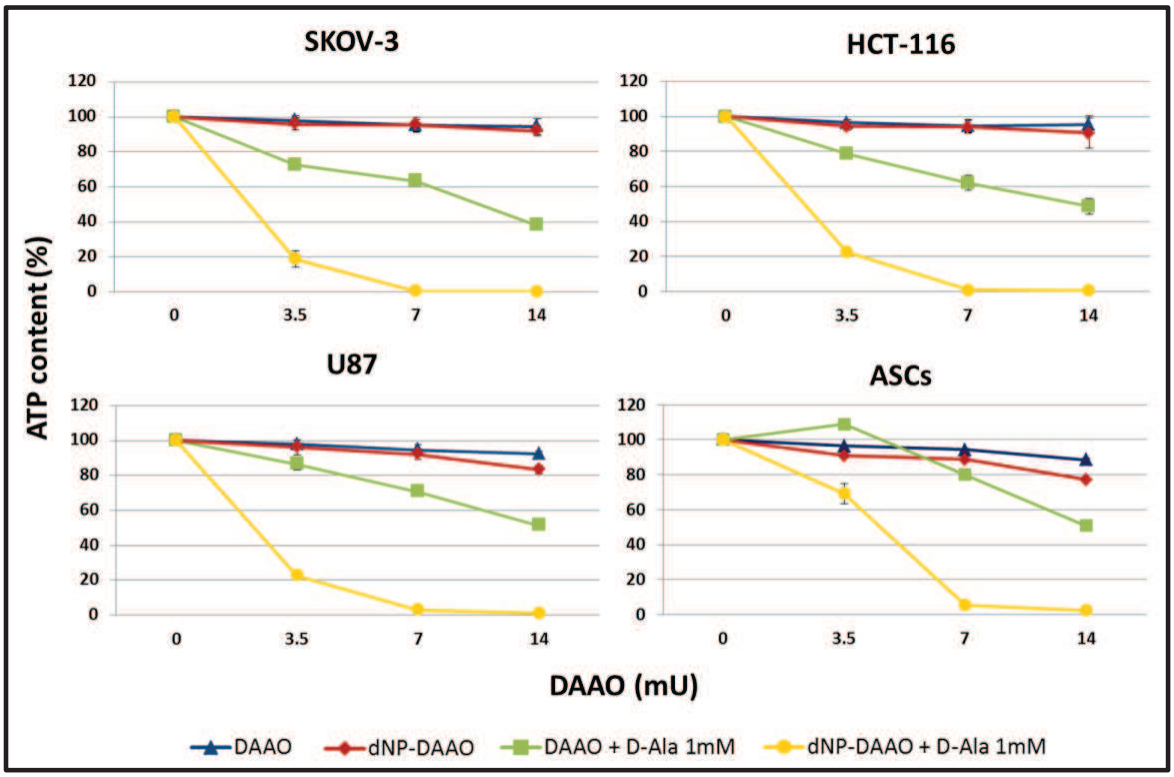

Fig.24: Cell viability is expressed as a percentage of ATP content after 24 h exposure to 3.5, 7 and 14 mU of dNP-DAAO and stock DAAO, with and without the substrate D-Ala 1 mM.

Although tumor cells of all the three cell lines were completely killed by dNP-DAAO with D-Ala, the human Adipose Stem Cells (hASCs) showed a certain grade of tolerance to H_2O_2. In a wider view, these results could be helpful to understand the processes at the base of the higher resistance to

oxidative stress presented by cancer stem cells[169]. Furthermore, from the cytotoxicity tests it can be highlighted the lack of target specificity of the dNP-DAAO toxicity: though this could be seen as a weak point, it gives the possibility to kill a huge variety of cell types through the NPs magnetic targeting towards the tissue of interest. Hence, this system could represent a very versatile tool to track (through MRI), target and kill tumor cells.

Comparison between the dNP-DAAO and cNP-DAAO systems

DLS and DCS analysis of the cNP-DAAO system were acquired and eventually compared to dNP-DAAO in Tab. 5.

Tab. 5: Comparison between the DCS and DLS analysis of dNP-DAAO (light green) and cNP-DAAO (light red) systems

Sample	*dIONPs*	*cIONPs*	*dNP-APTES*	*cNP-APTES*	*dNP-DAAO*	*cNP-DAAO*
Peak (nm)^{DCS}	34.5 ± 0.2	176 ± 0.5	24 ± 0.2	83.5 ± 0.4	76 ± 2	351 ± 3.5
Z-Average (nm) ^{DLS}	38.3 ± 0.4	1585 ± 81.1	47.0 ± 0.2	142.9 ± 2.4	185.1 ± 6.1	2043 ± 192.6
Polydispersity Index (PDI) ^{DLS}	0.191	0.353	0.123	0.197	0.279	0.690

As the Tab. 5 shows, the two systems are completely different. DLS and DCS analysis together indicate that the cNP-DAAO system is unstable in H_2O MilliQ as attested by the presence of a wide aggregation process. Although the dNP-DAAO system was successfully characterized in the same H_2O MilliQ, further analysis will be performed in different buffer solutions to assess the true characterization of the cNP-DAAO system.

The comparison of the DAAO binding efficiency between the two NP-DAAO systems is reported in Tab. 6. The dNP-DAAO were able to load up to 7.1 more DAAO than the cNP-DAAO. The yield and activity recovery remain unchanged for both the NP-DAAO system. The Units of DAAO found on dNP-DAAO are about 6.9 times more than the ones present on cNP-DAAO, these

results are coherent with the previous results of DAAO loading per mg of NPs[116]. However, according to Cappellini et al[116], the cNP-DAAO synthesized by us showed different Units per mg of NPs. This fact can be explained by the lower enzymatic activity of our RgDAAO stock batches.

Tab.6: Comparison of the DAAO binding efficiency between the cNP-DAAO (light red) and dNP-DAAO (light green) systems.

Sample	µg DAAO / mg NPs	% Yield	% Activity recovery	U / mg NPs
cNP-DAAO	62.5	100	90 ± 2	3.5 ± 0.1
dNP-DAAO	446	100	91 ± 2	24 ± 1

The last aspect that was compared between these two systems was their intrinsic cytotoxicity (Fig.25). The cytotoxicity exerted on the SKOV-3 cell line by the dNP-DAAO is extremely low if compared to cNP-DAAO. However, when D-Ala is added both the systems show similar results though the dNP-DAAO at 3.5 mU result less toxic than cNP-DAAO. This is due to the higher intrinsic toxicity of the cNP-DAAO that can be summed to the oxidative stress caused by the H_2O_2 production. These results obtained on SKOV-3 cell line are almost identical to U87 and HCT-116 cell lines (data not shown).

Notwithstanding the fact that dNP-DAAO are better than cNP-DAAO regarding the overall aspects assayed, the smaller size and the γ-Fe_2O_3 core composition of dNP-DAAO render them less susceptible to the influence of magnetic fields[170]. Therefore, this characteristic has to be taken in consideration when the NPs will be injected in the blood stream because it will be difficult to target the dNP-DAAO towards the tissue of interest.

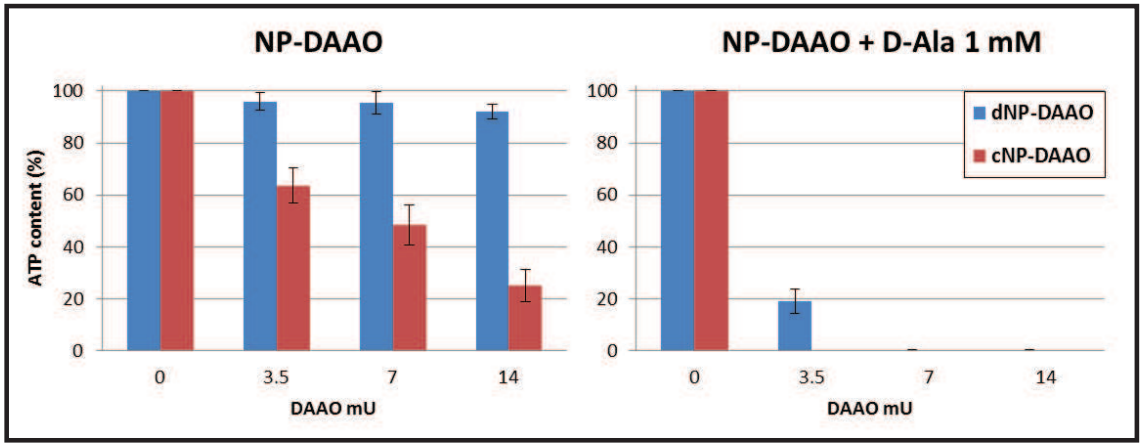

Fig. 25: Cytotoxicity of both cNP-DAAO and dNP-DAAO systems on SKOV-3 cell line. Cytotoxicity was performed in presence / absence of the substrate D-Alanine (D-Ala) 1 mM.

II.III CONCLUSIONS

We have synthesized and analyzed a magnetic NP-enzyme system for cancer therapy: dNP-DAAO. Under our best experimental condition, we have successfully immobilized up to 446 μg of RgDAAO enzyme per mg of NPs, obtaining a yield of 100%, more than 90% of the enzymatic activity recovery and finally a DAAO enzymatic activity of 24 U/mg of NPs.

The dNP-DAAO system characterization by TEM, DLS, DCS and Z-potential techniques indicated overall system stability.

The dNP-DAAO incubated at 37 °C showed a higher enzymatic activity than the DAAO alone. Furthermore, the presence of human serum in the incubation solution seems to slightly preserve over the time the DAAO enzymatic activity.

The *in vitro* cytotoxicity tests on different cell lines demonstrated an increased efficacy of dNP-DAAO compared to DAAO alone.

The dNP-DAAO system was partially compared to the one (cNP-DAAO) obtained from the Cappellini et al[116] procedure, showing three main remarkable improvements:

- A higher amount of DAAO loaded up to 7 times more due to the smaller size and the consequent higher surface area of the dIONPs compared to cIONPs.
- A better system stability in aqueous solution given by DLS and DCS analysis.
- A lower intrinsic toxicity of the system given by the reduced amount of NPs required for the same DAAO enzymatic activity.

Future aims will be to evaluate:

- The magnetic properties of the dNP-DAAO system.
- The role of the protein corona in dNP-DAAO activity, kinetic properties and cellular uptake.
- The dNP-DAAO biodistribution through the body with/without an eternal magnetic field with particular care of the ability to cross blood-barriers.
- The dNP-DAAO efficacy in destroying cancer cell in *in vivo* experiments.

CHAPTER III - SYNTHESIS OF MAGNETIC NP-ENZYME SYSTEM FOR INDUSTRY: THE NP-LASPO SYSTEM

III.I MATERIALS AND METHODS

Enzyme

The L-Aspartate oxidase (LASPO) used is this work is the wild type from *Sulfolobus tokodaii* that was overexpressed in E. coli cells and purified to > 95% purity as described by Bifulco et al[130]. The purified batch of StLASPO (2,255U/mL; 0,37U/mg) was stored in 20 mM Tris–HCl buffer at pH 7.5 and 10% glycerol. The LASPO enzyme was provided by the laboratory of Prof. Loredano Pollegioni of the Biotechnology and Life Sciences Department of Università degli Studi dell'Insubria, Varese.

IONPs and IO-APTES NPs

The Iron Oxide Nanoparticles (IONPs) and the functionalized IO-APTES NPs (NP-APTES) were the same commercial NPs (cIONPs and cNP-APTES) used for the synthesis of the cNP-DAAO system (see the “Material and Methods” section in “Chapter II”).

IO-APTES-LASPO (NP-LASPO)

According to a protocol previously developed in our laboratory, 4 mg of NP-APTES were ultrasonicated for 15 min in NaPPi buffer 5 mM pH 8.0, then 6 mg of EDC (1-Ethyl-3-(3-dimethylaminopropyl) carbodiimide, Sigma n.cat: 03450) and 8 mg of NHS (N-Hydroxysuccinimide, Sigma, n.cat: 130672) were added under sonication. Then, 100 µg of LASPO were added and NaPPi buffer 5 mM pH 8.0 up to a final reaction volume of 1 mL. The reaction was carried out for 2 h at room temperature on a rotating plate tube stirrer. Subsequently, NP-LASPO were collected using a magnet and washed twice

with 1 mL of NaPPi 5 mM pH 8.0. The supernatant was stored for further analysis.

These conditions of reaction represented the starting point of the optimization process done in this work. In order to establish the best conditions for LASPO conjugation to NP-APTES, four main parameters were considered: pH, NP-APTES amount, EDC:NHS concentration/ratio and reaction time. In the Tab. 7 the conditions at which the reactions were carried out are indicated.

Tab. 7: Different conditions for the LASPO conjugation reaction: the modified parameters for each reaction are indicated in bold.

NP-APTES (mg)	LASPO (µg)	EDC:NHS	EDC (mg)	pH	Time (h)
8	100	3:2	6	**8.0-9.0**	2
4 **5** **6** **7** **8**	100	3:2	6	8.5	2
4	100	**3:2**	**6** **5** **4** **3**	8.5	2
4	100	**1:1**	**3** **4** **6**	8.5	2
4	100	**2:3**	**4** **3.3** **2.7** **2**	8.5	2
4	100	2:3	2	8.5	**0.5** **1** **1.5** **2** **2.5** **4**

At the end of each series of conjugation reactions, the best condition (reflected by the higher activity recovery) was used as the starting point for the next optimization step.

NP-LASPO Enzyme Activity Assay

The NP-LASPO activity was assayed by measuring the initial rate of production of H_2O_2 with a coupled peroxidase/dye assay. The H_2O_2 reacts with phenol and 4-aminoantipyrine (4-AAP) by the catalytic action of peroxidase to form a red colored quinoamine dye complex. The dye produced was detected with a spectrophotometer at 505 nm (ε = 6.58 mM-1 cm-1) and 25 °C. According to Bifulco et al. [130], the standard assay mixture contained: 50 mM of Sodium Pyrophosphate, 1.5 mM 4-AAP, 2 mM Phenol, 20 µM FAD (flavin adenine dinucleotide), 10 mM L-Aspartate, 2.5 U of POD (horseradish peroxidase), in a final volume of 1mL. 40µl of NP-LASPO were assayed with a fixed wavelength measurement: the blank was read at λ=505 nm, NP-LASPO were added and incubated for 5 minutes at RT. Then, NP-LASPO were collected with the magnet and the supernatant was read.

NP-LASPO Yield and Activity Recovery

The yield and the activity recovery of each different NP-LASPO conjugation reaction were calculated as previously described for the NP-DAAO (see the “Material and Methods” section in “Chapter II”).

III.II RESULTS AND DISCUSSION

pH range

Several reactions were carried out to evaluate the effect of pH on the immobilization St-LASPO, varying the pH range from 8.0 to 9.0 (Tab. 8).

Tab. 8: Yield and activity recovery of the conjugation reactions performed at different pH. The best condition is indicated in underlined bold.

pH	Yield (%)	Activity Recovery (%)
8	99.7	37.5
8.1	99.7	30.1
8.3	99.6	37.2
8.5	**99.9**	**43.5**
8.7	99.6	34.0
8.9	99.5	30.0
9	99.4	42.1

The data suggest that the best reaction was the one conducted at pH 8.5 as shown by both the yield and the activity recovery.

NP-APTES amount

NP-APTES at different concentrations were tested on the updated reactions at pH 8.5 (Tab. 9).

Tab. 9: Yield and activity recovery of the updated conjugation reaction performed with different amount (mg) of NP-APTES. The best condition is indicated in underlined bold.

NP-APTES (mg)	Yield (%)	Activity Recovery (%)
4	**74.7**	**125.4**
5	54.5	85.9
6	49.0	82.4
7	63.7	63.9
8	99.9	43.5

From the reaction results listed in Tab. 9, the best activity recovery was obtained by using 4 mg of NP-APTES whilst the best yield with 8 mg. Although the yield, the best conjugation reaction was carried out with 4 mg of NP-APTES as reported by the highest activity recovery. Hence, since the yield is lower than the activity recovery, we can assume that the LASPO immobilized possess a higher enzymatic activity compared to free one.

Amount and ratio of EDC:NHS

Different concentrations and ratio of EDC and NHS were assayed during the enzyme conjugation reaction at pH 8.5 with 4 mg of NP-APTES (Tab. 10). The ratio of EDC:NHS was also subdivided in the molarity of each single chemical to have a better idea of the total moles occurring in the reaction.

Tab. 10: Yield and activity recovery of the updated conjugation reaction performed with different amount (mg) and ratio EDC:NHS (the w/w is expressed in mg). The molarity of both the EDC and NHS in the reaction is reported respectively in the second and third column. The best condition is indicated in underlined bold.

EDC:NHS (w/w)	EDC (mM)	NHS (mM)	Yield (%)	Activity Recovery (%)
6/4	39	35	74.7	125.4
5/3,3	32	29	90.7	70.7
4/2,7	26	23	94.5	81.6
3/2	19	17	87.8	105.4
3/3	19	26	88.1	116.3
4/4	26	35	81.3	124.4
6/6	39	52	77.5	119.4
4/6	26	52	93.6	87.0
3,3/5	21	43	80.9	106.5
2,7/4	17	35	85.7	113.1
2/3	**13**	**26**	**85.6**	**134.6**

The results show that the best condition for the LASPO conjugation was reached by using 2 mg of EDC and 3 mg of NHS per reaction. Looking at the molar ratio of the best reaction condition, the number of the NHS moles has to be double the EDC ones.

Reaction time

To check the optimum time needed for the LASPO conjugation onto NP-APTES, the reactions were conducted from 30 to 240 minutes (Tab. 11).

Tab. 11: Yield and activity recovery of the updated conjugation reaction carried out at different times. The best condition is indicated in underlined bold.

Time (min)	Yield (%)	Activity Recovery (%)
30	83.8	70.4
60	84.3	84.0
90	84.9	82.7
120	**85.6**	**134.6**
150	85.5	95.0
240	78.6	99.0

The results reported in Tab. 11 confirm that the best condition of reaction was the one already used in the previous method, namely at 120 minutes.

The case of the enzymatic activity increase

The final activity recovery suggests that, despite the decrease of the yield, the LASPO immobilized presents a higher activity: indeed, as previously reported, enzymes conjugated to NPs may present an enhanced activity, a better specificity, a prolonged half-life, an enhanced thermal stability and, in some cases, even an enzymatic acceleration[89,171,172].

Studying NP-enzyme conjugates, Ding et al[89] identified five physicochemical mechanisms that most contribute to higher the enzymatic activity:

1- A higher enzyme density;
2- An enhanced mass transport of incident substrate due to the attraction of substrate to the NP-enzyme surface as well as to the movement of the NP–enzyme complex;
3- The NP curvature/morphology and surface chemistry;
4- The NP surface chemistry;
5- A favourable enzyme orientation leading to an increased the enzyme–substrate interactions;

III.III CONCLUSIONS

Several reactions were performed to reach the best condition for LASPO conjugation to NP-APTES. In Fig. 26 each optimization step occurred from the starting NP-LASPO conjugation protocol is summarized.

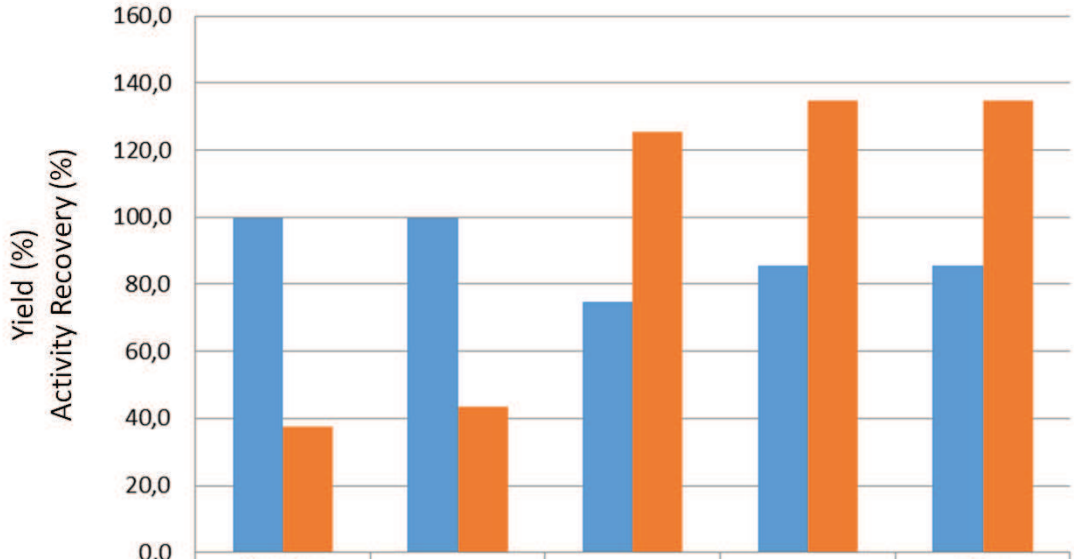

	Starting conjugation protocol	pH 8.5	NP-APTES 4 mg	EDC:NHS 2/3	Final conjugation protocol
Yield (%)	99.7	99.9	74.7	85.6	85.6
Activity Recovery (%)	37.5	43.5	125.4	134.6	134.6

Fig. 26: Optimization steps from the starting NP-LASPO conjugation protocol to the final improved one.

Among the four parameters analysed, only the reaction time confirmed its validity remaining stable at 2 hours. However, the updated optimal conjugation protocol switched the reaction pH from 8.0 to 8.5, the amount of NP-APTES from 8 mg to 4 mg and finally the EDC:NHS amount (mg) and ratio from 6:4 to 2:3.

The overall percentages of yield and activity recovery of the optimized conjugation protocol are respectively the 85.6% and the 134.6%: if these

values are normalized to those of the starting conjugation protocol, we obtain correspondingly the 85.7% and the 359%.

In biocatalysis, the susceptibility of the NP-LASPO to a magnetic field would allow its efficient recovery enabling also the reuse for several times and prevention of the final products contamination.

Future goals will be to repeat the experiments with different StLASPO batches in order to confirm the results. The kinetic properties of the immobilized enzyme will be characterized investigating via HPLC analysis the range of temperature and pH with higher performances in terms of activity and stability. Moreover, it will be checked the NP-LASPO ability to resolve racemic solution of D,L-Aspartate. Finally, it will be investigated the mechanisms that cause the enhanced enzymatic activity of the immobilized LASPO.

CHAPTER IV - STUDY OF TOXICITY AND INFLUENCE ON DIFFERENTIATION IN ASCs EXPOSED TO NPs

IV.I MATERIALS AND METHODS

hASCs isolation and culture

hASCs were isolated from mammary adipose tissue after surgical intervention due to breast hypertrophy (gigantomastia). The stromal cellular fraction, obtained according to Gronthos & Zannettino protocol[173], was seeded in T75 flask with 15 mL of cell culture medium and, after 6 h, the medium was replaced with the fresh one in order to remove unattached cells.

The hASCs cell culture medium was a 1:1 DMEM/DMEM-F12 supplemented with 10% fetal bovine serum (FBS), 1% L-Glutamine, 1% penicillin/streptomycin solution, 0.1% gentamicin and 0.04% fungizone. hASCs were passaged as needed using a solution at 0.25% trypsin–EDTA.

hASCs characterization by flow cytometry

The cell surface phenotype was assessed by flow cytometry analysis using a FACSAria II apparatus (BD, NJ, USA). To typify the hASCs population, a series of monoclonal antibodies (mAb) was used against the following specific cell surface markers: CD44, CD90, CD105 as a nominal staminal markers, CD45 as a differentiation marker and lastly HLA-A,B,C and HLA-DR respectively to check the HLA class I and class II molecules of the major histocompatibility complex. Anti-CD44, -CD45, -CD105 mAbs were fluorescein isothiocyanate (FITC) labeled whilst anti-CD90 was phycoerythrin (PE) labeled. Anti-HLA class I and class II mAbs were unlabeled and revealed by second-step incubation with goat antimouse IgG FITC-labeled. After antibody staining, cells were washed with PBS at 4 °C and fixed with 150 µL of PBS 4% paraformaldehyde for 30 min before the flow cytometry analysis.

Nanoparticles

The zerovalent nanoparticles (NPs) of Cobalt (CoNPs), Iron (FeNPs) and Nickel (NiNPs) were purchased from American Elements (Los Angeles, CA, USA):

- FeNPs: Product Code: FE-M-03M-NP.025N CAS #: 7439-89-6 APS*: ~25nm; 99.9% purity.
- NiNPs: Product Code: NI-M-03M-NP.020N CAS #: 7440-02-0 APS*: ~20nm; 99.8% purity.
- CoNPs: Product Code: CO-M-0251M-NP.030N CAS #: 7440-48-4 APS*: ~30nm; 99.5% purity.

*APS = Aerodynamic Particle Sizer

Cell viability test

In 96-well plates about 1000 hASCs were seeded and cultivated for 24 h at 37 °C in 5% CO_2 to equilibrate and become attached prior the treatment. Then, the cells were exposed for 24, 48, 72 and 96 h to increasing amount of NPs (0.3125 - 100 µg) resuspended in a final medium volume of 200 µL. NPs were previously ultrasonicated with the Ultrasonic Cleaner M S3 (Soltec, Milan, Italy) for at least 20 minutes to break any NPs agglomerates. Cell viability was determined by measuring cellular ATP content using the CellTiter-Glo Assay (Promega, Milan, Italy). The procedure is the same previously reported in the “Cell viability test” paragraph of the “Materials and methods” in Chapter II.

Adipogenic differentiation after hASCs exposure to CoNPs and $CoCl_2$

1000 cells were seeded on coverslips placed in a 6-well plate and left in the cell incubator for 24 h at 37 °C in 5% CO_2. Then, hASCs were treated with 2 mL of CoNPs 4.6 μg/mL and observed after 4, 7 and 10 days with an Inverted Contrast-Phase Microscope (ICPM) and an optical microscope respectively prior and after the cell staining. To highlight lipid droplets, cells were fixed and stained with Oil Red O (Sigma-Aldrich, Milan, Italy).

Moreover, since it happens that some types of NPs can dissolve into the culture medium, the experiment was carried out in parallel by using the same concentration of the corresponding Cobalt salt ($CoCl_2$). This helped to discriminate if the differentiation effect was due to CoNPs instead of $CoCl_2$.

The employed concentration of CoNPs was assumed by the result of the cytotoxicity assay also keeping in consideration that each of the used NPs tends to precipitate to the bottom of the well plate. Consequently, the final CoNPs concentration used for this test was calculated by normalizing the amount of μg NPs on the total surface area of the well (0.32 cm^2 per well in a 96-well plate and 9.4 cm^2 per well in a 6-well plate). Hence, the 2 mL of CoNPs 4.6 μg/mL resulted in about 0.94 μg of CoNPs per cm^2 of well surface that correspond to the lowest amount of CoNPs tested in the cell viability assay.

IV.II RESULTS AND DISCUSSION

hASCs characterization

After hASCs isolation from adipose tissue, their phenotype was assessed firstly by their morphological aspects and secondly by the presence of specific cell surface markers with flow cytometry.

The picture of hASCs acquired by ICPM (Fig. 27) shows the typical spindle-shaped fibroblast-like morphology as also observed in some previous studies[174–176].

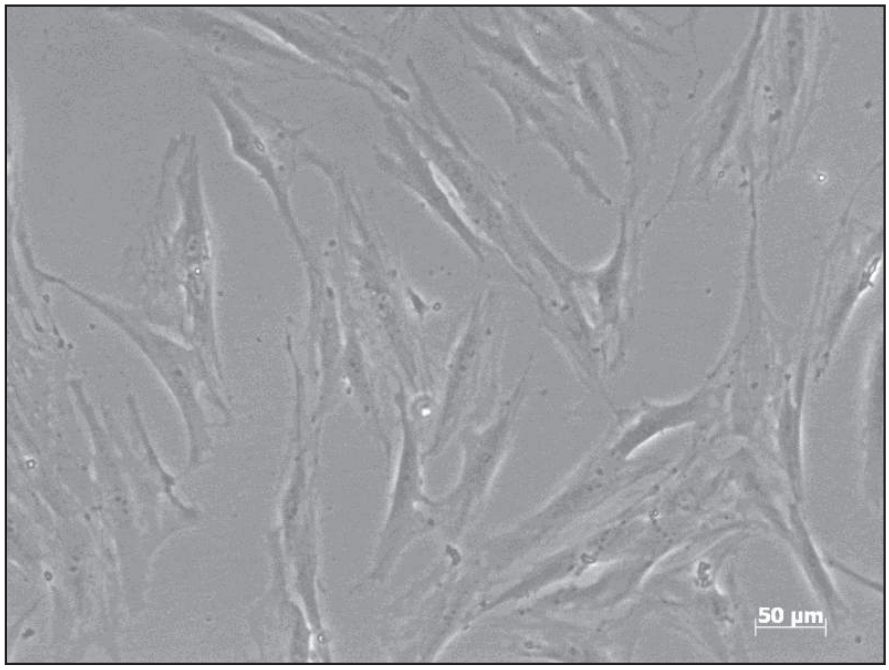

Fig. 27: hASCs morphology with the typical spindle-shaped fibroblast-like aspect. The picture was acquired by an Inverted Contrast-Phase Microscope (ICPM)

The flow cytometry analysis (Fig. 28) reports that hASCs, similarly to the mesenchymal stem cells (MSCs) isolated from other tissues, expressed the CD44, CD90 and CD105 surface markers but not the CD45 that, indeed, is expressed on endothelium as well as on leukocytes. Moreover, the hASCs

population positively expressed the HLA-A,B,C surface molecules but not the HLA-DR one.

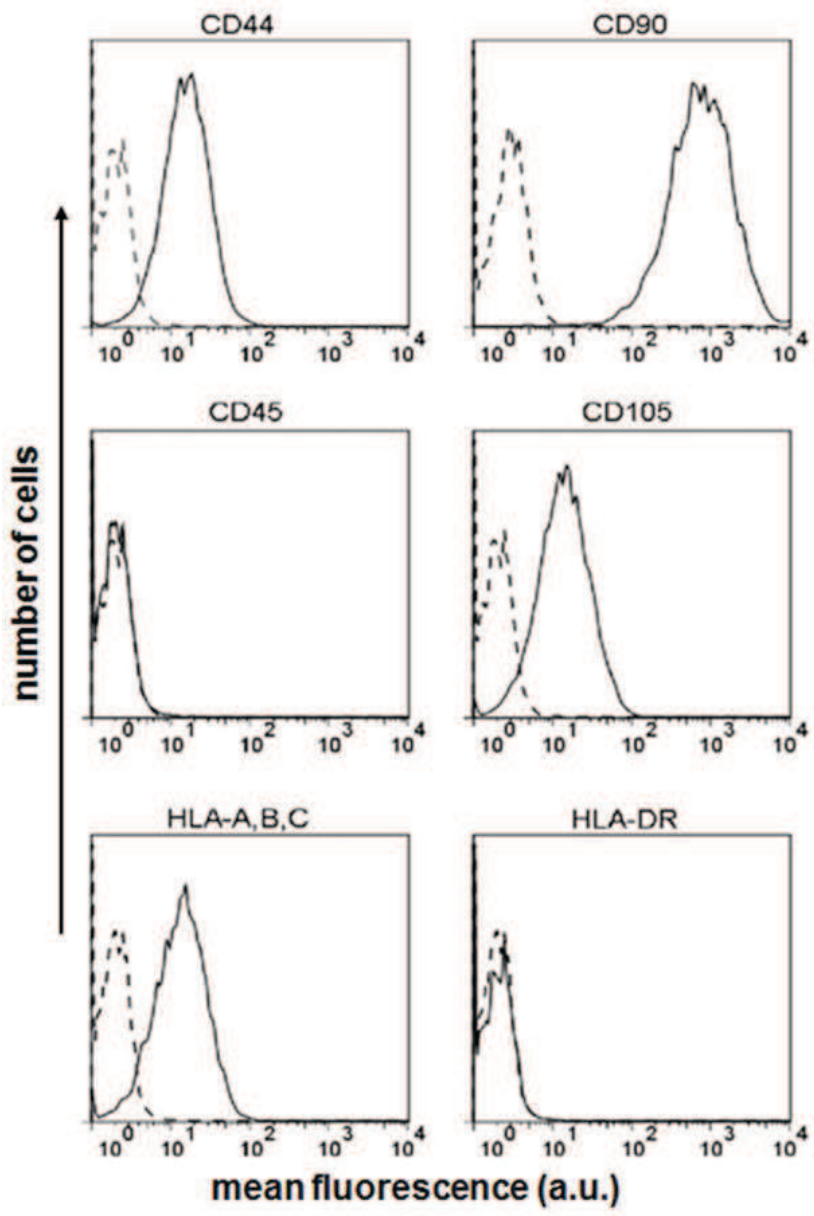

Fig. 28: hASCs immunophenotype from flow cytometry assays. The specific fluorescence is represented by the bold histogram; the dashed histogram is the negative control of the unlabelled isotypes. In the abscissa the mean fluorescence in arbitrary unit (a.u.) is reported whilst in the ordinate the number of analyzed cells.

This peculiar cellular immunophenotype, where the CD44, CD90, CD105 and HLA-A,B,C are positively expressed whilst the CD-45 and HLA-DR are not, confirmed the stemness of the isolated hASCs population utilized in this study. Furthermore, this immunophenotype is observed in many studies[174–178].

Cell viability

The cell viability assay was performed on hASCs exposed to an increasing amount (0.3125 – 100 μg) of CoNPs, FeNPs and NiNPs for up to 96 h. The cell viability results (Fig. 29) show a dose and time dependent toxicity for both CoNPs and NiNPs whilst only dose dependent for FeNPs: the more cytotoxic NPs were the NiNPs followed by CoNPs and lastly by FeNPs. The cytotoxicity of NiNPs and CoNPs at between 20 – 100 μg was very similar even though at the lower range (0.3125 – 10 μg) it appeared to be slightly different. Although the toxicity exerted by FeNPs on hASCs was more due to the dose instead of the time of exposure, they did not report a complete cell death also at the highest dose tested. These results partially fit with those of literature[179] conducted on different cell lines.

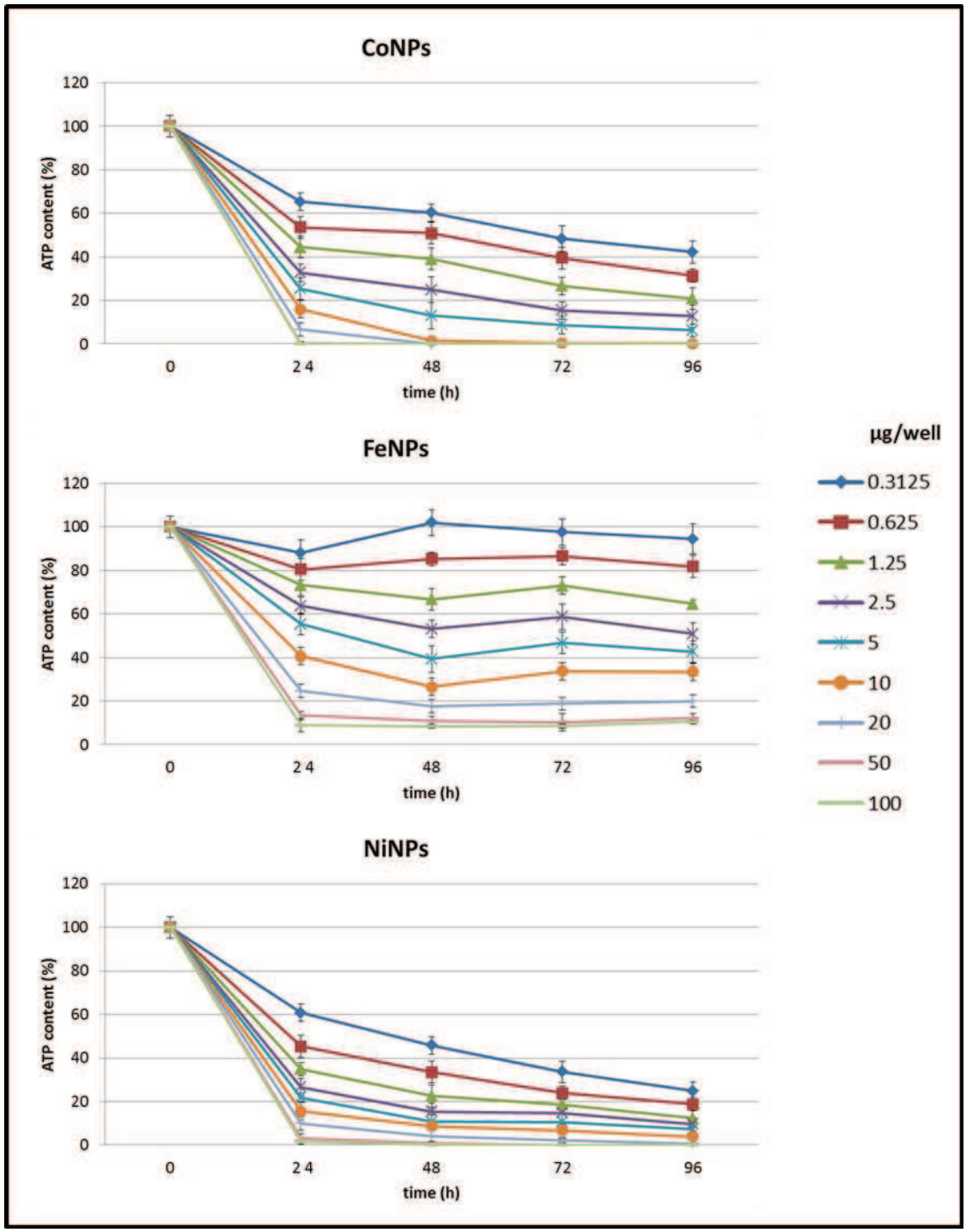

Fig. 29: Viability assay shows that cell viability is dose and time dependent for both CoNPs and NiNPs whilst only dose dependent for FeNPs. Error bars refer to the standard deviation among three tests.

Adipogenic differentiation after hASCs exposure to CoNPs and $CoCl_2$

The results obtained from cell viability assay with CoNPs were used to get the suitable concentration to perform the first of the hASCs Adipogenic differentiation test. Thus, it was chosen the concentration of 4.6 μg/mL (see "Material and Methods"), that correspond to the lowest amount of CoNPs tested in the cell viability assay, to lead hASCs up to 10 days without an excessive cell death.

Since it has been proved that CoNPs can dissolve into the culture media releasing ions[179,180], in parallel with the NPs treatment, it was also assayed the differentiation potential of $CoCl_2$ at the same concentration.

After 4 days of cell exposure to Cobalt, both NPs and ions revealed a low cytotoxicity accompanied by the beginning of the Adipogenic differentiation process as shown by the lipid droplets (Fig. 30a) highlighted after the ORO staining. These lipid droplets, always absent in the control hASCs, increased from day 4 to day 10 in the treated hASCs (Fig. 30b-c). However, after 10 days of exposure to Cobalt, the cell viability was greatly reduced and the presence of several vacuoles suggested the activation of the apoptotic processes.

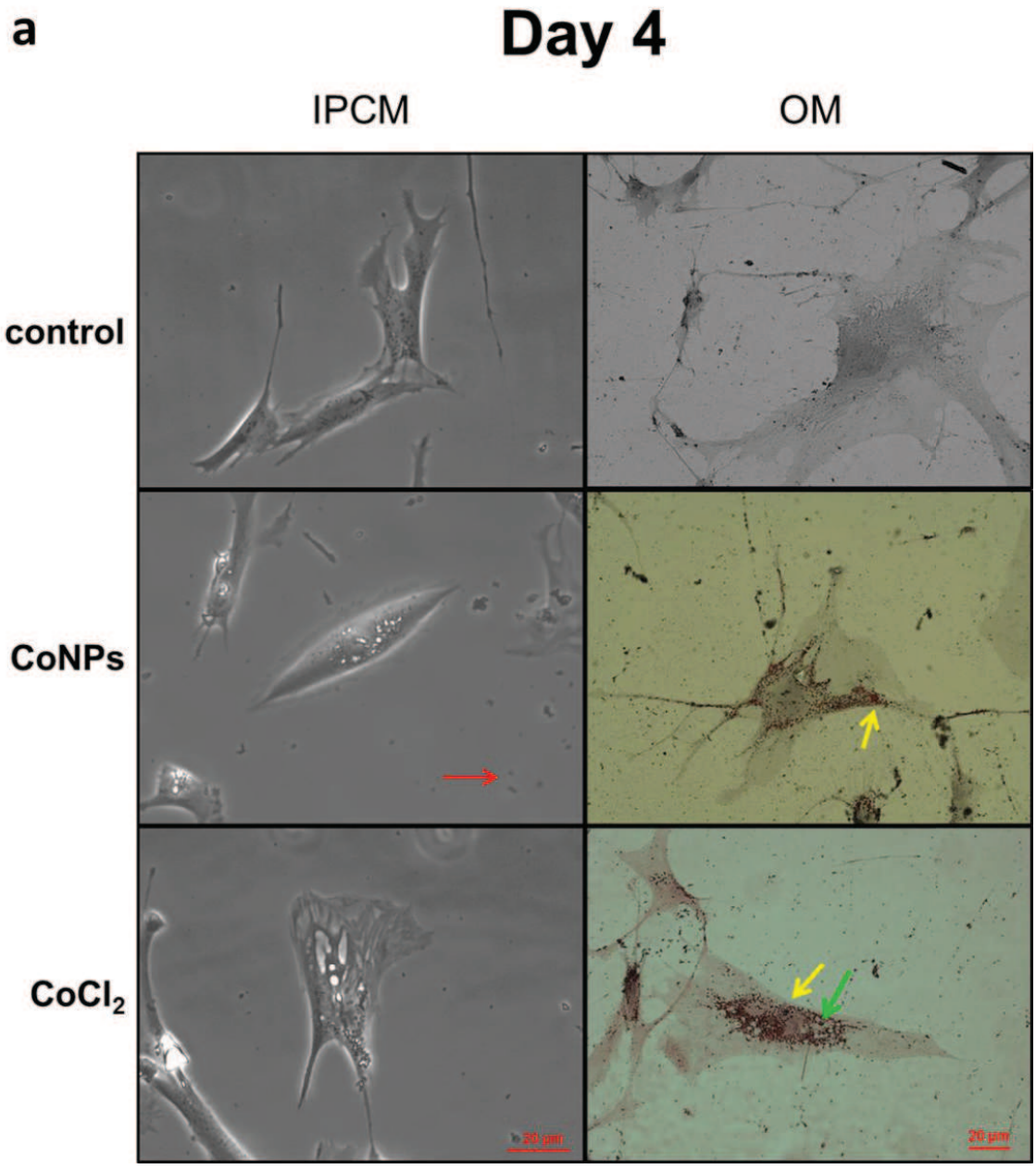
a
Day 4
IPCM
OM
control
CoNPs
CoCl2
50 µm
20 µm

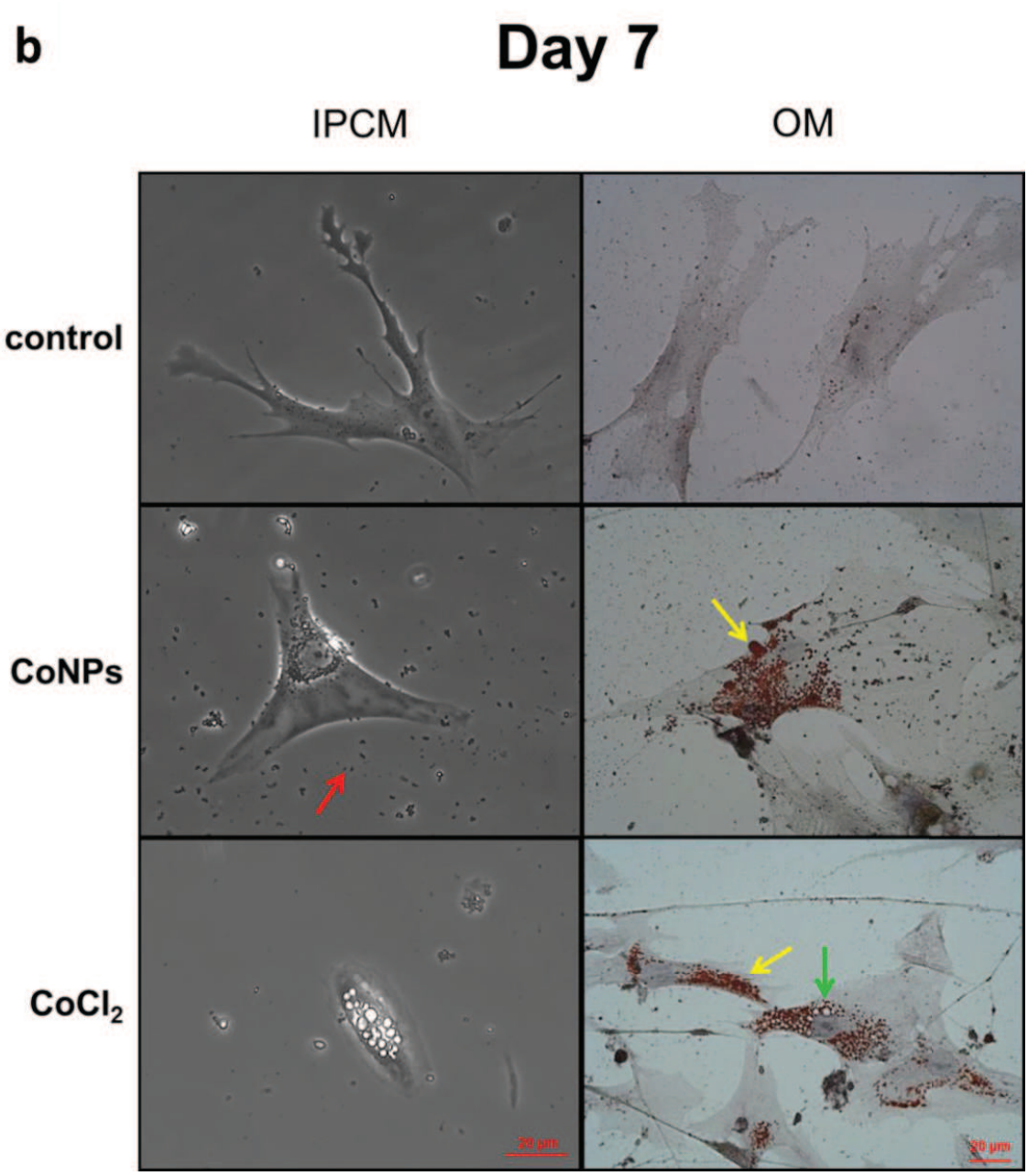
b
Day 7
IPCM
OM
control
CoNPs
$CoCl_2$

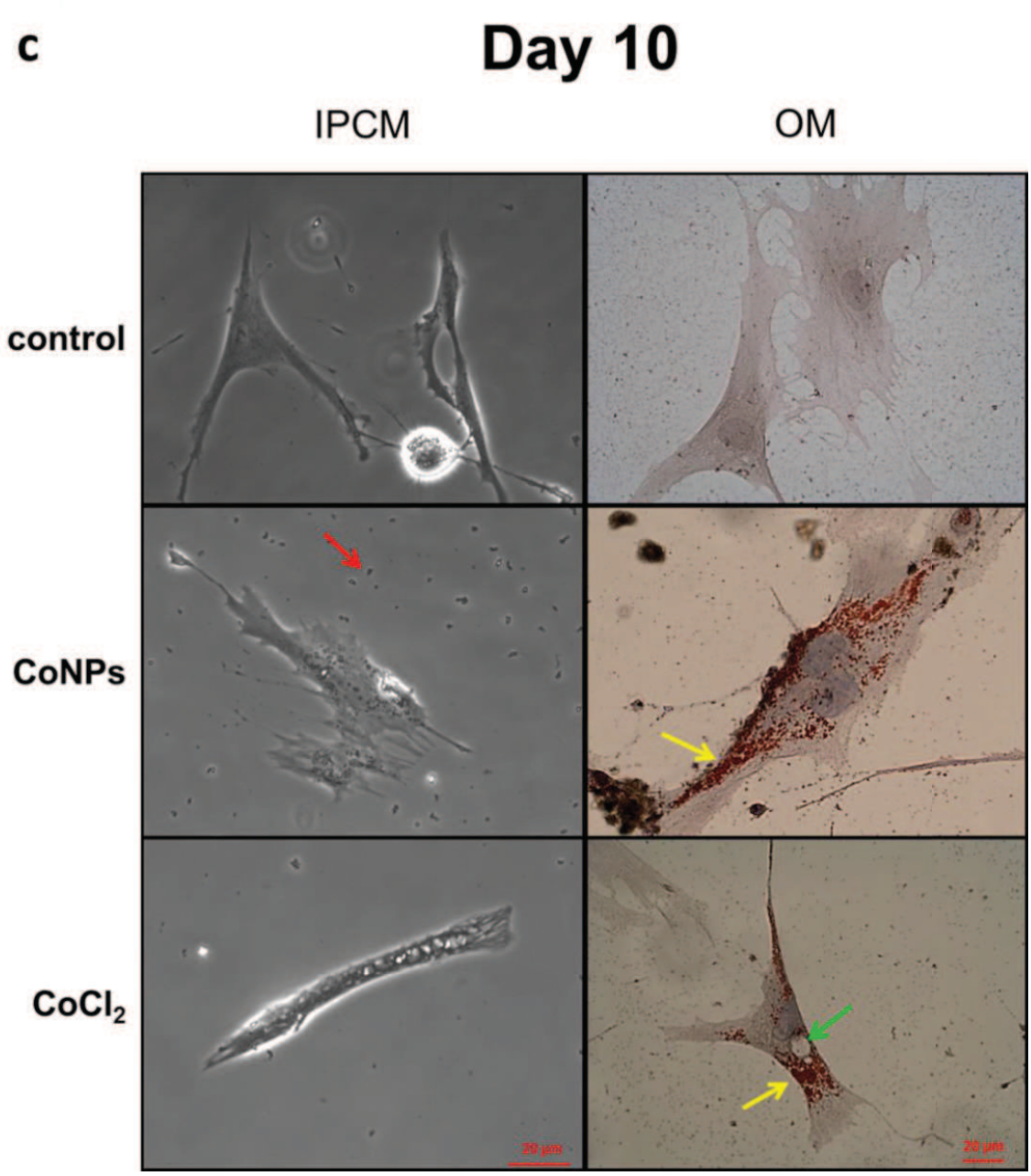

Fig. 30: hASCs Adipogenic differentiation after 4(**a**), 7(**b**) and 10(**c**) days of Cobalt exposure. Red arrows indicate the CoNPs while the yellow ones the lipid droplets, clearly visible after Oil Red O staining. The presence of several vacuoles (green arrows) is probably a sign of an apoptotic process. Inverted phase-contrast microscope (IPCM); optic microscope (OM).

These preliminary results demonstrate the Cobalt capability, without distinction among CoNPs and $CoCl_2$, to differentiate hASCs into preadipocytes. Nevertheless, the concentration of Cobalt used was too high inducing an extensive cell death.

IV.III CONCLUSIONS

Since the NP applications are exponentially growing, we have to be aware about their safety or not. We chose to perform the experiments with stem cells because they play a key role in our life and the possible perturbation of their homeostasis could be very harmful. Hence, in the last part of this work we started to investigate the *in vitro* NP toxicity using a subgroup of MSCs extracted from human adipose tissue, named hASCs, as a cell-line model because of their many advantages compared to other stem cell (see the "Adipose Stem Cell (ASCs)" section in "Chapter I").

In this study a hASCs population was effectively isolated, as shown by the morphological and the flow cytometry characterization. The *in vitro* stemness of this MSCs population was proved by the positivity to CD44, CD90, CD105 and HLA-A,B,C and negativity to CD45 and HLA-DR.

Furthermore, the cytotoxicity of CoNPs, FeNPs and NiNPs was assayed on hASCs: CoNPs and NiNPs exert a higher cytotoxic effect, which is also dose and time dependent, than FeNPs, only dose dependent.

Finally, the possible hASCs adipogenic differentiation induced by CoNPs was evaluated. The morphological analysis pointed out that both CoNPs and $CoCl_2$ were able to speed up the differentiation process even though in this experimental condition the mortality was rather high. These are preliminary results and we need to investigate in more detail if this process is due to CoNPs or Co^{2+} ions or both these components.

Future aims will be to assess deeper each experimental step carried out in this study:

1. We have to verify the *in vivo* hASCs stemness by exposing them to an appropriate growing media added with hormones/molecules able to differentiate them toward the different cellular lineages. Each step will be investigated through both Real-time PCR and differential staining by using specific molecular markers.
2. We will perform the NPs dissolution assays also in hASCs plating medium (DMEM:DMEM-F12) to know whether and how many ions can be released into the medium. Later on we will assay how this process is relevant for the overall toxicity and differentiation processes; then we will compare the NPs toxicity to that of their corresponding salts.
3. We will set up differentiation tests also for NiNPs and FeNPs and their relative salts. During NPs-induced differentiation process each passage will be followed by the analysis of the telomerase activity, the length of telomeres and the eventual mutation of P53.

BIBLIOGRAPHY

1. Union PO of the E. Commission Recommendation of 18 October 2011 on the definition of nanomaterial Text with EEA relevance. 2011.

2. Di Gioacchino M, Verna N, Gornati R, Sabbioni E, Bernardini G. Metal Nanoparticle Health Risk Assessment. In: *Nanotoxicity*. Chichester, UK: John Wiley & Sons, Ltd; :519-541. doi:10.1002/9780470747803.ch24.

3. Oberdörster G, Oberdörster E, Oberdörster J. Nanotoxicology: an emerging discipline evolving from studies of ultrafine particles. *Environ Health Perspect*. 2005;113(7):823-839. doi:10.1289/ehp.7339.

4. Nasrollahzadeh M, Bagherzadeh M, Karimi H. Preparation, characterization and catalytic activity of CoFe2O4 nanoparticles as a magnetically recoverable catalyst for selective oxidation of benzyl alcohol to benzaldehyde and reduction of organic dyes. *J Colloid Interface Sci*. 2016;465:271-278. doi:10.1016/j.jcis.2015.11.074.

5. Saha K, Agasti SS, Kim C, Li X, Rotello VM. Gold Nanoparticles in Chemical and Biological Sensing. *Chem Rev*. 2012;112(5):2739-2779. doi:10.1021/cr2001178.

6. Stratakis E, Kymakis E. Nanoparticle-based plasmonic organic photovoltaic devices. *Mater Today*. 2013;16(4):133-146. doi:10.1016/j.mattod.2013.04.006.

7. Zhang X, Wang X, Sun M, et al. A Magnetic Nanoparticle Based Enzyme-Linked Immunosorbent Assay for Sensitive Quantification of Zearalenone in Cereal and Feed Samples. *Toxins (Basel)*. 2015;7(10):4216-4231. doi:10.3390/toxins7104216.

8. Burke DJ, Pietrasiak N, Situ SF, et al. Iron Oxide and Titanium Dioxide Nanoparticle Effects on Plant Performance and Root Associated Microbes. *Int J Mol Sci*. 2015;16(10):23630-23650. doi:10.3390/ijms161023630.

9. Pyrgiotakis G, Vedantam P, Cirenza C, et al. Optimization of a nanotechnology based antimicrobial platform for food safety applications using Engineered Water Nanostructures (EWNS). *Sci Rep*. 2016;6(21073):21073.

doi:10.1038/srep21073.

10. Bülbül G, Hayat A, Andreescu S. Portable Nanoparticle-Based Sensors for Food Safety Assessment. *Sensors (Basel)*. 2015;15(12):30736-30758. doi:10.3390/s151229826.

11. Lohani A, Verma A, Joshi H, et al. Nanotechnology-based cosmeceuticals. *ISRN Dermatol*. 2014;2014:843687. doi:10.1155/2014/843687.

12. Tichota DM, Silva AC, Sousa Lobo JM, Amaral MH. Design, characterization, and clinical evaluation of argan oil nanostructured lipid carriers to improve skin hydration. *Int J Nanomedicine*. 2014;9:3855-3864. doi:10.2147/IJN.S64008.

13. Tsuzuki T. Commercial scale production of inorganic nanoparticles. *Int J Nanotechnol*. 2009;6(5/6):567. doi:10.1504/IJNT.2009.024647.

14. Crespo P, De La Presa P, Marín P, et al. Magnetism in nanoparticles: tuning properties with coatings. *J Phys Condens Matter*. 2013;25(25):484006-484021. doi:10.1088/0953-8984/25/48/484006.

15. Sun S, Murray CB, Weller D, et al. Monodisperse FePt nanoparticles and ferromagnetic FePt nanocrystal superlattices. *Science*. 2000;287(5460):1989-1992. doi:10.1126/science.287.5460.1989.

16. Wang Y, Yang M, Xu B, et al. Controlled assembly of FePt nanoparticles monolayer on solid substrates. *J Colloid Interface Sci*. 2014;417:100-108. doi:10.1016/j.jcis.2013.11.027.

17. Ivanov YP, Chuvilin A, Lopatin S, Kosel J. Modulated Magnetic Nanowires for Controlling Domain Wall Motion: Toward 3D Magnetic Memories. doi:10.1021/acsnano.6b01337.

18. Lux F, Sancey L, Bianchi A, Yannick, Crémillieux SR, Tillement & O. Gadolinium-based nanoparticles for theranostic MRI-radiosensitization. *Nanomedicine (Lond)*. 2015;10(11):1801-1815.

19. Mishra SK, Kumar BSH, Khushu S, Tripathi RP, Gangenahalli G. Increased transverse relaxivity in ultrasmall superparamagnetic iron oxide nanoparticles used as MRI contrast agent for biomedical imaging. *Contrast Media Mol Imaging*. 2016. doi:10.1002/cmmi.1698.

20. Gobbo OL, Sjaastad K, Radomski MW, Volkov Y, Prina-Mello A. Magnetic Nanoparticles in Cancer Theranostics. *Theranostics*. 2015;5(11):1249-1263. doi:10.7150/thno.11544.

21. Nandwana V, De M, Chu S, et al. Theranostic Magnetic Nanostructures (MNS) for Cancer. *Cancer Treat Res*. 2015;166:51-83. doi:10.1007/978-3-319-16555-4_3.

22. Hajba L, Guttman A. The use of magnetic nanoparticles in cancer theranostics: Toward handheld diagnostic devices. *Biotechnol Adv*. 2016;34(4):354-361. doi:10.1016/j.biotechadv.2016.02.001.

23. Tombácz E, Turcu R, Socoliuc V, Vékás L. Magnetic iron oxide nanoparticles: Recent trends in design and synthesis of magnetoresponsive nanosystems. *Biochem Biophys Res Commun*. 2015;468(3):442-453. doi:10.1016/j.bbrc.2015.08.030.

24. Hola K, Markova Z, Zoppellaro G, Tucek J, Zboril R. Tailored functionalization of iron oxide nanoparticles for MRI, drug delivery, magnetic separation and immobilization of biosubstances. *Biotechnol Adv*. 2015;33(6 Pt 2):1162-1176. doi:10.1016/j.biotechadv.2015.02.003.

25. Hofmann-Amtenbrink M, Von Rechenberg B, Hofmann H. Superparamagnetic nanoparticles for biomedical applications. *Transw Res Netw*. 37661(2):695-23.

26. Wu W, He Q, Jiang C. Magnetic iron oxide nanoparticles: synthesis and surface functionalization strategies. *Nanoscale Res Lett*. 2008;3(11):397-415. doi:10.1007/s11671-008-9174-9.

27. del Campo A, Sen T, Lellouche J-P, Bruce IJ. Multifunctional magnetite and silica–magnetite nanoparticles: Synthesis, surface activation and applications in life sciences. *J Magn Magn Mater*. 2005;293(1):33-40. doi:10.1016/j.jmmm.2005.01.040.

28. Feng B, Hong RY, Wang LS, et al. Synthesis of Fe3O4/APTES/PEG diacid functionalized magnetic nanoparticles for MR imaging. *Colloids Surfaces A Physicochem Eng Asp*. 2008;328(1):52-59. doi:10.1016/j.colsurfa.2008.06.024.

29. Conde J, Dias JT, Grazù V, Moros M, Baptista P V., de la Fuente JM. Revisiting 30 years of biofunctionalization and surface chemistry of inorganic

nanoparticles for nanomedicine. *Front Chem*. 2014;2:48. doi:10.3389/fchem.2014.00048.

30. Grillo R, Rosa AH, Fraceto LF. Engineered nanoparticles and organic matter: A review of the state-of-the-art. *Chemosphere*. 2015;119:608-619. doi:10.1016/j.chemosphere.2014.07.049.

31. Stark WJ. Nanoparticles in Biological Systems. *Angew Chemie Int Ed*. 2011;50(6):1242-1258. doi:10.1002/anie.200906684.

32. Rahman M, Laurent S, Tawil N, Yahia L, Mahmoudi M. Nanoparticle and Protein Corona. In: ; 2013:21-44. doi:10.1007/978-3-642-37555-2_2.

33. Verma A, Stellacci F. Effect of Surface Properties on Nanoparticle-Cell Interactions. *Small*. 2010;6(1):12-21. doi:10.1002/smll.200901158.

34. Mogoșanu GD, Grumezescu AM, Bejenaru C, Bejenaru LE. Polymeric protective agents for nanoparticles in drug delivery and targeting. *Int J Pharm*. 2016. doi:10.1016/j.ijpharm.2016.03.014.

35. Oldenborg PA, Zheleznyak A, Fang YF, et al. Role of CD47 as a marker of self on red blood cells. *Science*. 2000;288(5473):2051-2054. doi:10.1126/science.288.5473.2051.

36. Huang C, Yang G, Ha Q, Meng J, Wang S. Multifunctional "Smart" Particles Engineered from Live Immunocytes: Toward Capture and Release of Cancer Cells. *Adv Mater*. 2015;27(2):310-313. doi:10.1002/adma.201402213.

37. Hu C-MJ, Zhang L, Aryal S, Cheung C, Fang RH, Zhang L. Erythrocyte membrane-camouflaged polymeric nanoparticles as a biomimetic delivery platform. *Proc Natl Acad Sci*. 2011;108(27):10980-10985. doi:10.1073/pnas.1106634108.

38. Li L-L, Xu J-H, Qi G-B, Zhao X, Yu F, Wang H. Core-Shell Supramolecular Gelatin Nanoparticles for Adaptive and "On-Demand" Antibiotic Delivery. 2014;8(5):4975-4983. doi:10.1021/nn501040h.

39. Hu C-MJ, Fang RH, Copp J, Luk BT, Zhang L. A biomimetic nanosponge that absorbs pore-forming toxins. 2013. doi:10.1038/NNANO.2013.54.

40. Gao W, Hu C-MJ, Fang RH, Luk BT, Su J, Zhang L. Surface Functionalization of Gold Nanoparticles with Red Blood Cell Membranes. *Adv Mater*. 2013;25(26):3549-3553. doi:10.1002/adma.201300638.

41. Rao L, Xu J-H, Cai B, et al. Synthetic nanoparticles camouflaged with biomimetic erythrocyte membranes for reduced reticuloendothelial system uptake. *Nanotechnology*. 2016;27(8):85106. doi:10.1088/0957-4484/27/8/085106.

42. Oh N, Park J-H. Endocytosis and exocytosis of nanoparticles in mammalian cells. *Int J Nanomedicine*. 2014;9 Suppl 1(Suppl 1):51-63. doi:10.2147/IJN.S26592.

43. Pelkmans L, Helenius A. Endocytosis Via Caveolae. *Traffic*. 2002;3(5):311-320. doi:10.1034/j.1600-0854.2002.30501.x.

44. Pratten MK, Lloyd JB. Pinocytosis and phagocytosis: the effect of size of a particulate substrate on its mode of capture by rat peritoneal macrophages cultured in vitro. *Biochim Biophys Acta*. 1986;881(3):307-313. http://www.ncbi.nlm.nih.gov/pubmed/3008849. Accessed July 8, 2016.

45. Meng H, Yang S, Li Z, et al. Aspect Ratio Determines the Quantity of Mesoporous Silica Nanoparticle Uptake by a Small GTPase-Dependent Macropinocytosis Mechanism. 2011;5(6):4434-4447. doi:10.1021/nn103344k.

46. Taylor U, Klein S, Petersen S, Kues W, Barcikowski S, Rath D. Nonendosomal cellular uptake of ligand-free, positively charged gold nanoparticles. *Cytometry A*. 2010;77(5):439-446. doi:10.1002/cyto.a.20846.

47. Bossi E, Zanella D, Gornati R, Bernardini G. Cobalt oxide nanoparticles can enter inside the cells by crossing plasma membranes. *Sci Rep*. 2016;6:22254. doi:10.1038/srep22254.

48. Yanes RE, Tarn D, Hwang AA, et al. Involvement of Lysosomal Exocytosis in the Excretion of Mesoporous Silica Nanoparticles and Enhancement of the Drug Delivery Effect by Exocytosis Inhibition. *Small*. 2013;9(5):697-704. doi:10.1002/smll.201201811.

49. Strobel C, Oehring H, Herrmann R, Förster M, Reller A, Hilger I. Fate of cerium dioxide nanoparticles in endothelial cells: exocytosis. *J Nanoparticle Res*. 2015;17(5):206. doi:10.1007/s11051-015-3007-4.

50. Mahmoudi M, Saeedi-Eslami SN, Shokrgozar MA, et al. Cell vision": complementary factor of protein corona in nanotoxicology. doi:10.1039/c2nr31185b.

51. Nel A, Xia T, Mädler L, Li N. Toxic potential of materials at the nanolevel. *Science*. 2006;311(5761):622-627. doi:10.1126/science.1114397.

52. Shang L, Nienhaus K, Nienhaus GU. Engineered nanoparticles interacting with cells: size matters. *J Nanobiotechnology*. 2014;12:5. doi:10.1186/1477-3155-12-5.

53. Wilhelm S, Tavares AJ, Dai Q, et al. Analysis of nanoparticle delivery to tumours. *Nat Rev Mater*. 2016;1(5):16014. doi:10.1038/natrevmats.2016.14.

54. Gatoo MA, Naseem S, Arfat MY, Mahmood Dar A, Qasim K, Zubair S. Physicochemical properties of nanomaterials: Implication in associated toxic manifestations. *Biomed Res Int*. 2014;2014. doi:10.1155/2014/498420.

55. Sajid M, Ilyas M, Basheer C, et al. Impact of nanoparticles on human and environment: review of toxicity factors, exposures, control strategies, and future prospects. *Environ Sci Pollut Res*. 2015;22(6):4122-4143. doi:10.1007/s11356-014-3994-1.

56. Blanco E, Shen H, Ferrari M. Principles of nanoparticle design for overcoming biological barriers to drug delivery. *Nat Biotechnol*. 2015;33(9). doi:10.1038/nbt.3330.

57. Park J, Lim D-H, Lim H-J, et al. Size dependent macrophage responses and toxicological effects of Ag nanoparticlesw. *Chem Commun Chem Commun*. 2011;47(47):4382-4384. doi:10.1039/c1cc10357a.

58. Misra SK, Dybowska A, Berhanu D, Luoma SN, Valsami-Jones E. The complexity of nanoparticle dissolution and its importance in nanotoxicological studies. doi:10.1016/j.scitotenv.2012.08.066.

59. Chompoosor A, Saha K, Ghosh PS, et al. The Role of Surface Functionality on Acute Cytotoxicity, ROS Generation and DNA Damage by Cationic Gold Nanoparticles. *Small*. 2010;6(20):2246-2249. doi:10.1002/smll.201000463.

60. Pan Y, Leifert A, Ruau D, et al. Gold Nanoparticles of Diameter 1.4 nm Trigger Necrosis by Oxidative Stress and Mitochondrial Damage. *Small*.

2009;5(18):2067-2076. doi:10.1002/smll.200900466.

61. Singh N, Jenkins GJS, Nelson BC, et al. The role of iron redox state in the genotoxicity of ultrafine superparamagnetic iron oxide nanoparticles. *Biomaterials*. 2012;33(1):163-170. doi:10.1016/j.biomaterials.2011.09.087.

62. Kunzmann A, Andersson B, Vogt C, et al. Efficient internalization of silica-coated iron oxide nanoparticles of different sizes by primary human macrophages and dendritic cells. *Toxicol Appl Pharmacol*. 2011;253(2):81-93. doi:10.1016/j.taap.2011.03.011.

63. Paik S-Y-R, Kim J-S, Shin S, Ko S. Characterization, Quantification, and Determination of the Toxicity of Iron Oxide Nanoparticles to the Bone Marrow Cells. *Int J Mol Sci*. 2015;16(9):22243-22257. doi:10.3390/ijms160922243.

64. Ivask A, Titma T, Visnapuu M, et al. Toxicity of 11 Metal Oxide Nanoparticles to Three Mammalian Cell Types In Vitro. *Curr Top Med Chem*. 2015;15(18):1914-1929. http://www.ncbi.nlm.nih.gov/pubmed/25961521. Accessed July 11, 2016.

65. Karlsson HL, Gustafsson J, Cronholm P, Möller L. Size-dependent toxicity of metal oxide particles--a comparison between nano- and micrometer size. *Toxicol Lett*. 2009;188(2):112-118. doi:10.1016/j.toxlet.2009.03.014.

66. Kumar Gupta A, Gupta M. Cytotoxicity suppression and cellular uptake enhancement of surface modified magnetic nanoparticles. *Biomaterials*. 2005;26:1565-1573. doi:10.1016/j.biomaterials.2004.05.022.

67. Malvindi MA, De Matteis V, Galeone A, et al. Toxicity assessment of silica coated iron oxide nanoparticles and biocompatibility improvement by surface engineering. *PLoS One*. 2014;9(1):e85835. doi:10.1371/journal.pone.0085835.

68. Valdiglesias V, Kiliç G, Costa C, et al. Effects of iron oxide nanoparticles: Cytotoxicity, genotoxicity, developmental toxicity, and neurotoxicity. *Environ Mol Mutagen*. 2015;56(2):125-148. doi:10.1002/em.21909.

69. Valdiglesias V, Fernández-Bertólez N, Kiliç G, et al. Are iron oxide nanoparticles safe? Current knowledge and future perspectives. *J Trace Elem Med Biol*. 2016. doi:10.1016/j.jtemb.2016.03.017.

70. Dissanayake N, Current K, Obare S. Mutagenic Effects of Iron Oxide

Nanoparticles on Biological Cells. *Int J Mol Sci*. 2015;16(10):23482-23516. doi:10.3390/ijms161023482.

71. Carlson C, Hussain SM, Schrand AM, et al. Unique Cellular Interaction of Silver Nanoparticles: Size-Dependent Generation of Reactive Oxygen Species. 2008.

72. Gliga AR, Skoglund S, Odnevall Wallinder I, et al. Size-dependent cytotoxicity of silver nanoparticles in human lung cells: the role of cellular uptake, agglomeration and Ag release. *Part Fibre Toxicol*. 2014;11(1):11. doi:10.1186/1743-8977-11-11.

73. Sabella S, Carney RP, Brunetti V, et al. A general mechanism for intracellular toxicity of metal-containing nanoparticles. *Nanoscale*. 2014;6(12):7052. doi:10.1039/c4nr01234h.

74. Stoehr LC, Gonzalez E, Stampfl A, et al. Shape matters: effects of silver nanospheres and wires on human alveolar epithelial cells. *Part Fibre Toxicol*. 2011;8:36. doi:10.1186/1743-8977-8-36.

75. Luther W. Technological Analysis: Industrial application of nanomaterials - chances and risks. *Futur Technol*. 2004;54:119.

76. Lee J, Mahendra S, Alvarez PJJ. Nanomaterials in the Construction Industry: A Review of Their Applications and Environmental Health and Safety Considerations. *ACS Nano*. 2010;4(7):3580-3590. doi:10.1021/nn100866w.

77. Liu W, Wang L, Jiang R. Specific Enzyme Immobilization Approaches and Their Application with Nanomaterials. *Top Catal*. 2012;55(16-18):1146-1156. doi:10.1007/s11244-012-9893-0.

78. Koeller KM, Wong C-H. Enzymes for chemical synthesis. *Nature*. 2001;409(6817):232-240. doi:10.1038/35051706.

79. Wohlgemuth R, Holliger P, Jaeger KE. Biocatalysis — key to sustainable industrial chemistry. *Curr Opin Biotechnol*. 2010;21:713-724. doi:10.1016/j.copbio.2010.09.016.

80. Nestl BM, Nebel BA, Hauer B. Recent progress in industrial biocatalysis. *Curr Opin Chem Biol*. 2011;15(2):187-193. doi:10.1016/j.cbpa.2010.11.019.

81. Choi J-M, Han S-S, Kim H-S. Industrial applications of enzyme biocatalysis: Current status and future aspects. 2015. doi:10.1016/j.biotechadv.2015.02.014.

82. Grange RD, Thompson JP, Lambert DG. Radioimmunoassay, enzyme and non-enzyme-based immunoassays. *Br J Anaesth*. 2014;112(2):213-216. doi:10.1093/bja/aet293.

83. Mehta J, Bhardwaj SK, Bhardwaj N, et al. Progress in the biosensing techniques for trace-level heavy metals. *Biotechnol Adv*. 2016;34(1):47-60. doi:10.1016/j.biotechadv.2015.12.001.

84. Dinçer A, Telefoncu A. Improving the stability of cellulase by immobilization on modified polyvinyl alcohol coated chitosan beads. *J Mol Catal B Enzym*. 2007;45:10-14. doi:10.1016/j.molcatb.2006.10.005.

85. Elleuche S, Schrö Der C, Sahm K, Antranikian G. Extremozymes — biocatalysts with unique properties from extremophilic microorganisms. *Curr Opin Biotechnol*. 2014;29:116-123. doi:10.1016/j.copbio.2014.04.003.

86. Sheldon RA, Van Pelt S. Enzyme immobilisation in biocatalysis: why, what and how. *Chem Soc Rev Chem Soc Rev*. 2013;42(42):6223-6235. doi:10.1039/c3cs60075k.

87. Liese A, Hilterhaus L. Evaluation of immobilized enzymes for industrial applications Motivation and recent developments. *Chem Soc Rev Chem Soc Rev*. 2013;42(42):6236-6249. doi:10.1039/c3cs35511j.

88. Dicosimo R, Mcauliffe J, Poulose AJ, Bohlmann G. Industrial use of immobilized enzymes. *Chem Soc Rev Chem Soc Rev*. 2013;42(42):6437-6474. doi:10.1039/c3cs35506c.

89. Johnson BJ, Russ Algar W, Malanoski AP, Ancona MG, Medintz IL. Understanding enzymatic acceleration at nanoparticle interfaces: Approaches and challenges. *Nano Today*. 2014;9(1):102-131. doi:10.1016/j.nantod.2014.02.005.

90. Meridor D, Gedanken A. Preparation of enzyme nanoparticles and studying the catalytic activity of the immobilized nanoparticles on polyethylene films. *Ultrason Sonochem*. 2013;20(1):425-431. doi:10.1016/j.ultsonch.2012.06.005.

91. Liu Y, Wang S, Zhang C, Su X, Huang S, Zhao M. Enhancing the selectivity of

enzyme detection by using tailor-made nanoparticles. *Anal Chem*. 2013;85(10):4853-4857. doi:10.1021/ac4007914.

92. Wu C-S, Lee C-C, Wu C-T, Yang Y-S, Ko F-H. Size-modulated catalytic activity of enzyme-nanoparticle conjugates: a combined kinetic and theoretical study. *Chem Commun (Camb)*. 2011;47(26):7446-7448. doi:10.1039/c1cc11020a.

93. Wang W, Xu Y, Wang DIC, Li Z. Recyclable nanobiocatalyst for enantioselective sulfoxidation: facile fabrication and high performance of chloroperoxidase-coated magnetic nanoparticles with iron oxide core and polymer shell. *J Am Chem Soc*. 2009;131(36):12892-12893. doi:10.1021/ja905477j.

94. Yu C-C, Kuo Y-Y, Liang C-F, et al. Site-Specific Immobilization of Enzymes on Magnetic Nanoparticles and Their Use in Organic Synthesis. doi:10.1021/bc200396r.

95. Garcia J, Zhang Y, Taylor H, et al. Multilayer enzyme-coupled magnetic nanoparticles as efficient, reusable biocatalysts and biosensors. *Nanoscale*. 2011;3(9):3721. doi:10.1039/c1nr10411j.

96. Mukherjee J, Gupta MN. Lipase coated clusters of iron oxide nanoparticles for biodiesel synthesis in a solvent free medium. *Bioresour Technol*. 2016;209:166-171. doi:10.1016/j.biortech.2016.02.134.

97. Shahrestani H, Taheri-Kafrani A, Soozanipour A, Tavakoli O. Enzymatic clarification of fruit juices using xylanase immobilized on 1,3,5-triazine-functionalized silica-encapsulated magnetic nanoparticles. *Biochem Eng J*. 2016;109:51-58. doi:10.1016/j.bej.2015.12.013.

98. Bobo D, Robinson KJ, Islam J, Thurecht KJ, Corrie SR. Nanoparticle-Based Medicines: A Review of FDA-Approved Materials and Clinical Trials to Date. *Pharm Res*. June 2016:1-15. doi:10.1007/s11095-016-1958-5.

99. Subbiah R, Veerapandian M, Yun KS. Nanoparticles: functionalization and multifunctional applications in biomedical sciences. *Curr Med Chem*. 2010;17(36):4559-4577. http://www.ncbi.nlm.nih.gov/pubmed/21062250. Accessed June 16, 2016.

100. Onoue S, Yamada S, Chan H-K. Nanodrugs: pharmacokinetics and safety. *Int J*

Nanomedicine. 2014;9:1025-1037. doi:10.2147/IJN.S38378.

101. Masserini M. Nanoparticles for Brain Drug Delivery. *ISRN Biochem*. 2013;2013:1-8. doi:http://dx.doi.org/10.1155/2013/238428.

102. Mangraviti A, Gullotti D, Tyler B, Brem H. Nanobiotechnology-based delivery strategies: New frontiers in brain tumor targeted therapies. *J Control Release*. March 2016. doi:10.1016/j.jconrel.2016.03.031.

103. Huang Y, Zhang B, Xie S, Yang B, Xu Q, Tan J. Superparamagnetic Iron Oxide Nanoparticles Modified with Tween 80 Pass through the Intact Blood–Brain Barrier in Rats under Magnetic Field. *ACS Appl Mater Interfaces*. 2016;8(18):11336-11341. doi:10.1021/acsami.6b02838.

104. Cheon J, Lee J-H. Synergistically Integrated Nanoparticles as Multimodal Probes for Nanobiotechnology. 2008. doi:10.1021/ar800045c.

105. Zhu Y, Fang Y, Kaskel S. Folate-Conjugated Fe3O4@SiO2 Hollow Mesoporous Spheres for Targeted Anticancer Drug Delivery. *J Phys Chem C*. 2010;114(39):16382-16388. doi:10.1021/jp106685q.

106. Kelkar SS, Reineke TM. Theranostics: Combining Imaging and Therapy. *Bioconjug Chem*. 2011;22(10):1879-1903. doi:10.1021/bc200151q.

107. Wu W, Wu Z, Yu T, Jiang C, Kim W-S. Recent progress on magnetic iron oxide nanoparticles: synthesis, surface functional strategies and biomedical applications. *Sci Technol Adv Mater*. 2015;16. http://iopscience.iop.org/1468-6996/16/2/023501. Accessed July 5, 2016.

108. Banerjee SS, Chen D-H. Grafting of 2-Hydroxypropyl-beta-Cyclodextrin on Gum Arabic-Modified Iron Oxide Nanoparticles as a Magnetic Carrier for Targeted Delivery of Hydrophobic Anticancer Drug. *Int J Appl Ceram Technol*. 2010;7(1):111-118. doi:10.1111/j.1744-7402.2008.02332.x.

109. Talelli M, Rijcken CJF, Lammers T, et al. Superparamagnetic iron oxide nanoparticles encapsulated in biodegradable thermosensitive polymeric micelles: toward a targeted nanomedicine suitable for image-guided drug delivery. *Langmuir*. 2009;25(4):2060-2067. doi:10.1021/la8036499.

110. Beik J, Abed Z, Ghoreishi FS, et al. Nanotechnology in hyperthermia cancer

therapy: From fundamental principles to advanced applications. *J Control Release*. 2016;235:205-221. doi:10.1016/j.jconrel.2016.05.062.

111. Zhou Z, Sun Y, Shen J, et al. Iron/iron oxide core/shell nanoparticles for magnetic targeting MRI and near-infrared photothermal therapy. *Biomaterials*. 2014;35(26):7470-7478. doi:10.1016/j.biomaterials.2014.04.063.

112. Ren X, Chen H, Yang V, Sun D. Iron oxide nanoparticle-based theranostics for cancer imaging and therapy. *Front Chem Sci Eng*. 2014;8(3):253-264. doi:10.1007/s11705-014-1425-y.

113. Toporkiewicz M, Meissner J, Matusewicz L, Czogalla A, Sikorski AF. Toward a magic or imaginary bullet? Ligands for drug targeting to cancer cells: principles, hopes, and challenges. *Int J Nanomedicine*. 2015;10:1399-1414. doi:10.2147/IJN.S74514.

114. Kuan Yen S, Padmanabhan P, Tamil Selvan S. Multifunctional Iron Oxide Nanoparticles for Diagnostics, Therapy and Macromolecule Delivery. *Theranostics*. 2013;3(312):986-1003. doi:10.7150/thno.4827.

115. Bava A, Gornati R, Cappellini F, Caldinelli L, Pollegioni L, Bernardini G. D-amino acid oxidase–nanoparticle system: a potential novel approach for cancer enzymatic therapy. *http://dx.doi.org/102217/nnm12187*. 2013.

116. Cappellini F, Recordati C, Maglie M De, et al. New synthesis and biodistribution of the D-amino acid oxidase-magnetic nanoparticle system. *http://dx.doi.org/104155/fso1567*. 2015.

117. Pollegioni L, Piubelli L, Sacchi S, Pilone MS, Molla G. Physiological functions of D-amino acid oxidases: from yeast to humans. *Cell Mol Life Sci*. 2007;64(11):1373-1394. doi:10.1007/s00018-007-6558-4.

118. D'Aniello A, D'Onofrio G, Pischetola M, et al. Biological role of D-amino acid oxidase and D-aspartate oxidase. Effects of D-amino acids. *J Biol Chem*. 1993;268(36):26941-26949. http://www.ncbi.nlm.nih.gov/pubmed/7903300. Accessed September 27, 2016.

119. Tishkov VI, Khoronenkova S V. D-amino acid oxidase: structure, catalytic mechanism, and practical application. *Biochem*. 2005;70(1):40-54.

doi:10.1007/s10541-005-0050-2.

120. Hsieh HC, Kuan IC, Lee SL, Tien GY, Wang YJ, Yu CY. Stabilization of d-amino acid oxidase from Rhodosporidium toruloides by immobilization onto magnetic nanoparticles. *Biotechnol Lett*. 2009;31(4):557-563. doi:10.1007/s10529-008-9894-z.

121. Pollegioni L, Diederichs K, Molla G, et al. Yeast D-amino acid oxidase: structural basis of its catalytic properties. *J Mol Biol*. 2002;324(3):535-546. http://www.ncbi.nlm.nih.gov/pubmed/12445787. Accessed September 27, 2016.

122. Pilone MS, Pollegioni L. D-amino Acid Oxidase as an Industrial Biocatalyst. *Biocatal Biotransformation*. 2002;20(3):145-159. doi:10.1080/10242420290020679.

123. Pollegioni L, Molla G. New biotech applications from evolved D-amino acid oxidases. *Trends Biotechnol*. 2011;29(6):276-283. doi:10.1016/j.tibtech.2011.01.010.

124. Fernández-Lafuente R, Rodríguez V, Mateo C, et al. Stabilization of enzymes (d-amino acid oxidase) against hydrogen peroxide via immobilization and post-immobilization techniques. *J Mol Catal B Enzym*. 1999;7(1-4):173-179. doi:10.1016/S1381-1177(99)00040-5.

125. Divakaran SA, Sreekanth KM, Rao K V., Nair CKK. D-Aminoacid Oxidase-Fe2O3 Nanoparticle Complex Mediated Antitumor Activity in Swiss Albino Mice. *J Cancer Ther*. 2011;2(5):666-674. doi:10.4236/jct.2011.25089.

126. Fang J, Sawa T, Akaike T, Maeda H. Tumor-targeted Delivery of Polyethylene Glycol-conjugated D-Amino Acid Oxidase for Antitumor Therapy via Enzymatic Generation of Hydrogen Peroxide. *CANCER Res*. 2002;62:3138-3143.

127. Stegman LD, Zheng H, Neal ER, et al. Induction of Cytotoxic Oxidative Stress by d-Alanine in Brain Tumor Cells Expressing Rhodotorula gracilis D-Amino Acid Oxidase: A Cancer Gene Therapy Strategy. *Hum Gene Ther*. 1998;9:185-193.

128. Pollegioni L, Motta P, Molla G. l-Amino acid oxidase as biocatalyst: a dream too far? *Appl Microbiol Biotechnol*. 2013;97(21):9323-9341. doi:10.1007/s00253-013-5230-1.

129. Sakuraba H, Yoneda K, Asai I, Tsuge H, Katunuma N, Ohshima T. Structure of l-aspartate oxidase from the hyperthermophilic archaeon Sulfolobus tokodaii. *Biochim Biophys Acta - Proteins Proteomics*. 2008;1784(3):563-571. doi:10.1016/j.bbapap.2007.12.012.

130. Bifulco D, Pollegioni L, Tessaro D, Servi S, Molla G. A thermostable L-aspartate oxidase: a new tool for biotechnological applications. *Appl Microbiol Biotechnol*. 2013;97(16):7285-7295. doi:10.1007/s00253-013-4688-1.

131. D'Arrigo P, Allegretti C, Fiorati A, et al. Immobilization of l -aspartate oxidase from Sulfolobus tokodaii as a biocatalyst for resolution of aspartate solutions. *Catal Sci Technol*. 2015;5(2):1106-1114. doi:10.1039/C4CY00968A.

132. Zuk PA, Zhu M, Mizuno H, et al. Multilineage cells from human adipose tissue: implications for cell-based therapies. *Tissue Eng*. 2001;7(2):211-228. doi:10.1089/107632701300062859.

133. Zuk PA, Zhu M, Ashjian P, et al. Human adipose tissue is a source of multipotent stem cells. *Mol Biol Cell*. 2002;13(12):4279-4295. doi:10.1091/mbc.E02-02-0105.

134. Mizuno H. Adipose-derived stem cells for tissue repair and regeneration: ten years of research and a literature review. *J Nippon Med Sch*. 2009;76(2):56-66. http://www.ncbi.nlm.nih.gov/pubmed/19443990. Accessed August 2, 2016.

135. Zuk P. Adipose-Derived Stem Cells in Tissue Regeneration: A Review. *Int Sch Res Not*. 2013;2013(1):e713959. doi:10.1155/2013/713959.

136. Cherubino M, Valdatta L, Balzaretti R, et al. Human adipose-derived stem cells promote vascularization of collagen-based scaffolds transplanted into nude mice. *Regen Med*. 2016;11(3):261-271. doi:10.2217/rme-2015-0010.

137. Colazzo F, Chester AH, Taylor PM, Yacoub MH. Induction of mesenchymal to endothelial transformation of adipose-derived stem cells. *J Heart Valve Dis*. 2010;19(6):736-744. http://www.ncbi.nlm.nih.gov/pubmed/21214098. Accessed September 27, 2016.

138. Gonzalez-Rey E, Gonzalez MA, Varela N, et al. Human adipose-derived mesenchymal stem cells reduce inflammatory and T cell responses and induce

regulatory T cells in vitro in rheumatoid arthritis. *Ann Rheum Dis*. 2010;69(1):241-248. doi:10.1136/ard.2008.101881.

139. Gimble JM, Grayson W, Guilak F, Lopez MJ, Vunjak-Novakovic G. Adipose tissue as a stem cell source for musculoskeletal regeneration. *Front Biosci (Schol Ed)*. 2011;3:69-81. http://www.ncbi.nlm.nih.gov/pubmed/21196358. Accessed August 2, 2016.

140. Yañez R, Lamana ML, García-Castro J, Colmenero I, Ramírez M, Bueren JA. Adipose tissue-derived mesenchymal stem cells have in vivo immunosuppressive properties applicable for the control of the graft-versus-host disease. *Stem Cells*. 2006;24(11):2582-2591. doi:10.1634/stemcells.2006-0228.

141. Feisst V, Meidinger S, Locke MB. From bench to bedside: use of human adipose-derived stem cells. *Stem Cells Cloning*. 2015;8:149-162. doi:10.2147/SCCAA.S64373.

142. Fraser JK, Wulur I, Alfonso Z, Hedrick MH. Fat tissue: an underappreciated source of stem cells for biotechnology. *Trends Biotechnol*. 2006;24(4):150-154. doi:10.1016/j.tibtech.2006.01.010.

143. Locke M, Windsor J, Rod Dunbar P. Human adipose-derived stem cells: isolation, characterization and applications in surgery. *ANZ J Surg*. 2009;79:235-244. doi:10.1111/j.1445-2197.2009.04852.x.

144. Puntes VF, Krishnan KM, Alivisatos AP. Colloidal nanocrystal shape and size control: the case of cobalt. *Science*. 2001;291(5511):2115-2117. doi:10.1126/science.1057553.

145. Skumryev V, Stoyanov S, Zhang Y, Hadjipanayis G, Givord D, Nogués J. Beating the superparamagnetic limit with exchange bias. *Nature*. 2003;423(6942):850-853. doi:10.1038/nature01687.

146. Liu TY, Zhao L, Tan X, et al. Effects of physicochemical factors on Cr(VI) removal from leachate by zero-valent iron and α-Fe2O3 nanoparticles. *Water Sci Technol*. 2010;61(11):2759-2767. doi:10.2166/WST.2010.167.

147. Bouchard L-S, Anwar MS, Liu GL, et al. Picomolar sensitivity MRI and

photoacoustic imaging of cobalt nanoparticles. *Proc Natl Acad Sci U S A*. 2009;106(11):4085-4089. doi:10.1073/pnas.0813019106.

148. Lacroix L-M, Delpech F, Nayral C, Lachaize S, Chaudret B. New generation of magnetic and luminescent nanoparticles for in vivo real-time imaging. *Interface Focus*. 2013;3(3):20120103. doi:10.1098/rsfs.2012.0103.

149. Horev-Azaria L, Kirkpatrick CJ, Korenstein R, et al. Predictive toxicology of cobalt nanoparticles and ions: comparative in vitro study of different cellular models using methods of knowledge discovery from data. *Toxicol Sci*. 2011;122(2):489-501. doi:10.1093/toxsci/kfr124.

150. Bernardini G, Cattaneo AG, Sabbioni E, et al. Toxicology of Engineered Metal Nanoparticles. In: *General, Applied and Systems Toxicology*. Chichester, UK: John Wiley & Sons, Ltd; 2011. doi:10.1002/9780470744307.gat240.

151. Wang W, Hua Y, Li S, Yan W, Zhang W. Removal of Pb(II) and Zn(II) using lime and nanoscale zero-valent iron (nZVI): A comparative study. *Chem Eng J*. 2016;304:79-88. doi:10.1016/j.cej.2016.06.069.

152. Cundy AB, Hopkinson L, Whitby RLD. Use of iron-based technologies in contaminated land and groundwater remediation: A review. *Sci Total Environ*. 2008;400(1):42-51. doi:10.1016/j.scitotenv.2008.07.002.

153. Adeleye AS, Keller AA, Miller RJ, Lenihan HS. Persistence of commercial nanoscaled zero-valent iron (nZVI) and by-products. *J Nanoparticle Res*. 2013;15(1):1418. doi:10.1007/s11051-013-1418-7.

154. Ma X, Gurung A, Deng Y. Phytotoxicity and uptake of nanoscale zero-valent iron (nZVI) by two plant species. *Sci Total Environ*. 2013;443:844-849. doi:10.1016/j.scitotenv.2012.11.073.

155. Morozov YG, Belousova O V., Kuznetsov M V. Preparation of nickel nanoparticles for catalytic applications. *Inorg Mater*. 2011;47(1):36-40. doi:10.1134/S0020168510121027.

156. Wessells CD, Peddada S V., Huggins RA, Cui Y. Nickel Hexacyanoferrate Nanoparticle Electrodes For Aqueous Sodium and Potassium Ion Batteries. *Nano Lett*. 2011;11(12):5421-5425. doi:10.1021/nl2031934q.

157. Kasprzak KS, Sunderman FW, Salnikow K. Nickel carcinogenesis. *Mutat Res*. 2003;533(1-2):67-97. http://www.ncbi.nlm.nih.gov/pubmed/14643413. Accessed September 27, 2016.

158. Ahamed M. Toxic response of nickel nanoparticles in human lung epithelial A549 cells. *Toxicol In Vitro*. 2011;25(4):930-936. doi:10.1016/j.tiv.2011.02.015.

159. Phillips JI, Green FY, Davies JCA, Murray J. Pulmonary and systemic toxicity following exposure to nickel nanoparticles. *Am J Ind Med*. 2010;53(8):763-767. doi:10.1002/ajim.20855.

160. Ispas C, Andreescu D, Patel A, Goia D V, Andreescu S, Wallace KN. Toxicity and developmental defects of different sizes and shape nickel nanoparticles in zebrafish. *Environ Sci Technol*. 2009;43(16):6349-6356. http://www.ncbi.nlm.nih.gov/pubmed/19746736. Accessed September 27, 2016.

161. Gallo A, Boni R, Buttino I, Tosti E. Spermiotoxicity of nickel nanoparticles in the marine invertebrate *Ciona intestinalis* (ascidians). *Nanotoxicology*. 2016;10(8):1096-1104. doi:10.1080/17435390.2016.1177743.

162. Sonia F, Loredano P, Mirella PS. Engineering, expression and purification of a His-tagged chimeric D-amino acid oxidase from Rhodotorula gracilis. *Enzyme Microb Technol*. 2001;29(6-7):407-412. doi:10.1016/S0141-0229(01)00400-8.

163. Bee A, Massart R, Neveu S. Synthesis of very fine maghemite particles. *J Magn Magn Mater*. 1995;149(1-2):6-9. doi:10.1016/0304-8853(95)00317-7.

164. Geppert M, Hohnholt M, Gaetjen L, Grunwald I, Bäumer M, Dringen R. Accumulation of Iron Oxide Nanoparticles by Cultured Brain Astrocytes. 2009;5(3):285-293. doi:10.1166/JBN.2009.1033.

165. Monopoli MP, Walczyk D, Campbell A, et al. Physical–Chemical Aspects of Protein Corona: Relevance to *in Vitro* and *in Vivo* Biological Impacts of Nanoparticles. *J Am Chem Soc*. 2011;133(8):2525-2534. doi:10.1021/ja107583h.

166. Krpetić Ž, Davidson AM, Volk M, Lévy R, Brust M, Cooper DL. High-Resolution Sizing of Monolayer-Protected Gold Clusters by Differential Centrifugal Sedimentation. *ACS Nano*. 2013;7(10):8881-8890.

doi:10.1021/nn403350v.

167. Xiao K, Li Y, Luo J, et al. The effect of surface charge on in vivo biodistribution of PEG-oligocholic acid based micellar nanoparticles. *Biomaterials*. 2011;32(13):3435-3446. doi:10.1016/j.biomaterials.2011.01.021.

168. Kim W-S, Park B-S, Kim H-K, et al. Evidence supporting antioxidant action of adipose-derived stem cells: Protection of human dermal fibroblasts from oxidative stress. *J Dermatol Sci*. 2008;49:133-142. doi:10.1016/j.jdermsci.2007.08.004.

169. Dayem AA, Choi H-Y, Kim J-H, Cho S-G. Role of Oxidative Stress in Stem, Cancer, and Cancer Stem Cells. *Cancers (Basel)*. 2010;2(2):859-884. doi:10.3390/cancers2020859.

170. Kolhatkar AG, Jamison AC, Litvinov D, Willson RC, Lee TR, Edu A. Tuning the Magnetic Properties of Nanoparticles. *Int J Mol Sci Int J Mol Sci*. 2013;14:15977-16009. doi:10.3390/ijms140815977.

171. Ansari SA, Husain Q. Potential applications of enzymes immobilized on/in nano materials: A review. 2012. doi:10.1016/j.biotechadv.2011.09.005.

172. Ding S, Cargill AA, Medintz IL, Claussen JC. Increasing the activity of immobilized enzymes with nanoparticle conjugation. *Curr Opin Biotechnol*. 2015;34:242-250. doi:10.1016/j.copbio.2015.04.005.

173. Gronthos S, Zannettino ACW. Methods for the purification and characterization of human adipose-derived stem cells. *Methods Mol Biol*. 2011;702:109-120. doi:10.1007/978-1-61737-960-4_9.

174. Musina RA, Bekchanova ES, Sukhikh GT. Comparison of Mesenchymal Stem Cells Obtained from Different Human Tissues. *Cell Technol Biol Med*. 2005;1(2):89-94.

175. Wagner W, Wein F, Seckinger A, et al. Comparative characteristics of mesenchymal stem cells from human bone marrow, adipose tissue, and umbilical cord blood. *Exp Hematol*. 2005;33(11):1402-1416. doi:10.1016/j.exphem.2005.07.003.

176. Vishnubalaji R, Al-Nbaheen M, Kadalmani B, Aldahmash A, Ramesh T.

Comparative investigation of the differentiation capability of bone-marrow- and adipose-derived mesenchymal stem cells by qualitative and quantitative analysis. *Cell Tissue Res*. 2012;347(2):419-427. doi:10.1007/s00441-011-1306-3.

177. Lee RH, Kim B, Choi I, et al. Characterization and expression analysis of mesenchymal stem cells from human bone marrow and adipose tissue. *Cell Physiol Biochem*. 2004;14(4-6):311-324. doi:10.1159/000080341.

178. Schäffler A, Büchler C. Concise review: adipose tissue-derived stromal cells--basic and clinical implications for novel cell-based therapies. *Stem Cells*. 2007;25(4):818-827. doi:10.1634/stemcells.2006-0589.

179. Gornati R, Pedretti E, Rossi F, et al. Zerovalent Fe, Co and Ni nanoparticle toxicity evaluated on SKOV-3 and U87 cell lines. *J Appl Toxicol*. 2016;36(3):385-393. doi:10.1002/jat.3220.

180. Wang S, Liu F, Zeng Z, Yang H, Jiang H. The Protective Effect of Bafilomycin A1 Against Cobalt Nanoparticle-Induced Cytotoxicity and Aseptic Inflammation in Macrophages In Vitro. *Biol Trace Elem Res*. 2016;169(1):94-105. doi:10.1007/s12011-015-0381-9.

PAPERS